UNIVERSITE DE MONTREAL

NATURAL CONVECTION HEAT TRANSFER IN A SHALLOW RECTANGULAR CAVITY WITH UNIFORM HEAT FLUX

par

Chong Huai WANG
DEPARTEMENT DE GENIE MECANIQUE
ECOLE POLYTECHNIQUE DE MONTREAL

THESE PRESENTEE EN VUE DE L'OBTENTION
DU GRADE DE PHILOSOPHIAE DOCTOR (Ph.D.)

Décembre 1990

© Chong Huai WANG 1990

lational Library
f Canada

Bibliothèque nationale
du Canada

:anadian Theses Service

Service des thèses canadiennes

ttawa, Canada
1A 0N4

The author has granted an irrevocable non-exclusive licence allowing the National Library of Canada to reproduce, loan, distribute or sell copies of his/her thesis by any means and in any form or format, making this thesis available to interested persons.

L'auteur a accordé une licence irrévocable et non exclusive permettant à la Bibliothèque nationale du Canada de reproduire, prêter, distribuer ou vendre des copies de sa thèse de quelque manière et sous quelque forme que ce soit pour mettre des exemplaires de cette thèse à la disposition des personnes intéressées.

The author retains ownership of the copyright in his/her thesis. Neither the thesis nor substantial extracts from it may be printed or otherwise reproduced without his/her permission.

L'auteur conserve la propriété du droit d'auteur qui protège sa thèse. Ni la thèse ni des extraits substantiels de celle-ci ne doivent être imprimés ou autrement reproduits sans son autorisation.

ISBN 0-315-69599-4

Canada

UNIVERSITE DE MONTREAL

ECOLE POLYTECHNIQUE

Cette thèse intitulée:

NATURAL CONVECTION HEAT TRANSFER IN A SHALLOW RECTANGULAR CAVITY WITH UNIFORM HEAT FLUX

présentée par: Chong Huai WANG

en vue de l'obtention du grade de: PHILOSOPHIAE DOCTOR (Ph.D.)

a été dûment acceptée par le jury d'examen constitué de:

M. Ricardo Camarero ..... Ph.D., président

M. Patrick Vasseur ..... Ph.D., directeur de recherche

M. Adrian Bejan ..... Ph.D.

M. Michel Prud'homme ..... Ph.D.

Dedicated to my parents and my wife

ABSTRACT

An analytical and numerical study has been performed on natural convection heat transfer through fluids and saturated porous media with uniform heating and cooling through opposite walls. An approximate solution is obtained by assuming a parallel flow in the core region of the cavity. A numerical solution of the complete governing equations is also conducted. This technique is applicable to a large variety of problems and a few examples described below will be illustrated in this thesis.

The case of an inclined porous layer is first examined. The model used to describe the flow in the cavity accounts for Brinkman friction. It is shown that the boundary effect, though not important in low-porosity media, becomes significant in high-porosity media. The flow and heat transfer variables are obtained in terms of the Darcy-Rayleigh number R and the Darcy number Da. The critical Darcy-Rayleigh number for the onset of convection in a bottom-heated cavity is predicted. The results for a viscous fluid ($Da \to \infty$) and the Darcy porous medium ($Da \to 0$) emerge from the present analysis as limiting cases.

The influence of multiple diathermal partitions on the laminar natural convection heat transfer in inclined porous layers is studied next. On the basis of the Darcy-Oberbeck-Boussinesq equations, the governing equations are solved analytically in the limit of a thin layer. The relationship between Nusselt number Nu and the number of partitions, their relative positions and the angle of inclination of the system is determined. The critical Darcy-Rayleigh number for the onset of convection in a bottom-heated horizontal system is predicted. The influence of a thermal barrier which is sandwiched between two porous layers is also discussed.

The stability and natural convection in a system consisting of a horizontal fluid layer over a saturated porous medium , with heating from below, have also been considered. The upper surface is either rigid or dynamically free with surface-tension effects allowed for. The critical Rayleigh number and Nusselt number are found to depend on the depth ratio, the Darcy number, the viscosity ratio, the thermal conductivity ratio, and the Marangoni number. Results are given for a range of values of each of the governing parameters. The results are compared with limiting cases of the problem for standard terrestrial conditions or microgravity, and are found to be in agreement.

Finally, the mechanism of natural and Marangoni convection in systems with two stratified fluid layers without mass transfer at the interface is investigated. It is demonstrated that four different patterns of convection can be observed in the present system. The zone of occurrence of these flow patterns are specified in terms of non-dimensional parameters. Velocity and temperature distributions, stream function and Nusselt number are presented over a wide range of the governing parameters. The results obtained are explained in terms of the basic physical mechanisms that govern these flows showing many interesting aspects of the complex interaction between the buoyant and surface tension mechanisms.

SOMMAIRE

Une étude analytique et numérique du transfert de chaleur par convection naturelle au sein de milieux fluides ou poreux chauffés par des flux de chaleur constants, a été effectuée. La solution analytique est obtenue en supposant l'existence d'un écoulement parallèle dans le coeur de la cavité alors que dans la méthode numérique on résoud le système complet d'équations de base gouvernant le problème. Cette technique est applicable à de nombreuses situations et les quelques exemples décrits ci dessous servent d'illustration.

Le cas d'une couche poreuse inclinée est d'abord examiné. Le modèle de Brinkman est utilisé pour décrire le mouvement du fluide dans la cavité. Il est montré que les effets dus à la frontière, bien que négligeables pour des milieux poreux ayant une faible porosité, deviennent importants pour des milieux ayant une porosité importante. L'écoulement et le transfert de chaleur sont obtenus en termes du nombre de Darcy-Rayleigh R et du nombre de Darcy Da. Le nombre de Darcy-Rayleigh critique pour un système chauffé par le bas est prédit par la présente théorie. Les résultats pour un milieu fluide ($Da \to \infty$) et pour un milieu de Darcy pur ($Da \to 0$) sont également prédits par la présente théorie.

Dans une deuxiéme phase on étudie le transfert de chaleur au sein de couches poreuses inclinées. Le système est résolu, sur la base des équations de Darcy-Oberbeck, dans le cas limite d'une couche mince. La relation entre le nombre de Nusselt Nu et le nombre de partitions, leurs positions relatives et l'angle d'inclinaison du système est déterminée. Le nombre de Rayleigh critique pour un système chauffé par le bas est prédit. L'influence d'une barrière thermique comprise entre deux couches poreuses est également étudiée.

La stabilité et la convection naturelle dans un système constitué d'une couche fluide horizontale au dessus d'une couche poreuse ont également été considérées. La surface supérieure est soit rigide soit dynamiquement libre avec des effets de tension de surface. Le nombre de Rayleigh critique et le nombre de Nusselt dépendent du rapport des profondeurs, du nombre de Darcy, du rapport des viscosités, du rapport des conductivités thermiques et du nombre de Marangoni. Les résultats sont présentés de façon à refléter l'influence des paramètres de base.

Finalement, le mécanisme de la convection naturelle et de Marangoni dans un système constitué de deux couches de fluide horizontales est étudié. Il est montré que quatre régimes

d'écoulements différents peuvent être observés dans le présent système. La zone d'apparition de ces différents régimes d'écoulements est déterminée en terme des paramètres de base du problème. Les champs de vitesse et de température et le nombre de Nusselt sont présentés pour diverses valeurs des paramètres de base. Les résultats obtenus sont expliqués en termes des mécanismes de base physiques qui gouvernent ces écoulements.

ACKNOWLEDGEMENTS

I wish to gratefully thank Professor P. Vasseur; my advisor, and Professor L. Robillard, my co-advisor, for their counseling in the various phases of my graduate study at The Ecole Polytechnique and for introducing me to the present area of research. Special thanks are given to the member of my reading committee, Professor A. Bejan, Professor R. Camarero and Professor M. Prud'homme.

The author also wishes to thank the National Sciences and Engineering Research Council of Canada, whose financial assistance permitted the author to devote full time to this work.

My most sincere and great appreciation, of course, goes to my parents who have given to my education since its beginning.

TABLE OF CONTENTS

	Page
Abstract	v
Sommaire	viii
Acknowledgements	xi
Table of Contents	xii
List of Figures	xvii
List of Tables	xxi
List of Symbols	xxiii
Chapter 1	
INTRODUCTION	1
Chapter 2	
THE PARALLEL FLOW APPROXIMATION FOR SHALLOW CAVITIES ...	6
2.1 Literature Review	6

Page

2.2 Natural Convection in a Porous Enclosure 8

2.3 Analytical Solution for Small Aspect Ratios 10

Chapter 3

AN INCLINED SHALLOW POROUS CAVITY WITH UNIFORM FLUX: THE BRINKMAN MODEL 18

3.1 Literature Review 18

3.2 Problem Statement and Solution Procedure 23

3.3 Analytical Solution 26

3.3.1 Natural Solution: $C \sin\varphi > 0$ 28

3.3.2 Antinatural Solution: $C \sin\varphi < 0$ 32

3.3.3 Horizontal Layer: $C \sin\varphi = 0$ 34

3.3.3.1 All Boundaries Rigid 36

i) Darcy Porous Medium Limit 39

ii) Viscous Fluid Limit 40

3.3.3.2 Upper Surface Free 41

Viscous Fluid Limit 43

page

3.3.3.3 Both Horizontal Surfaces Free 44

Viscous Fluid Limit 45

3.4 Numerical Solution 45

3.5 Results and Discussion 48

3.6 Summary 65

Chapter 4

A POROUS LAYER WITH MULTIPLE PARTITIONS 70

4.1 Literature Review 70

4.2 Statement of the Problem 72

4.3 Numerical Method 75

4.4 Approximate Analytical Solution 76

4.4.1 The Horizontal Cavity Heated from the Bottom 80

4.4.2 The Vertical Cavity Heated from the Side 82

4.5 Two Porous Layers Separated by a Thermal Barrier 84

4.6 Analytical and Numerical Results 88

page

4.7 Summary 95

Chapter 5

THERMAL INSTABILITY AND NATURAL CONVECTION IN A FLUID LAYER OVER A POROUS SUBSTRATE 98

5.1 Literature Review 98

5.2 Formulation of the Problem 99

5.2.1 Porous Layer 100

5.2.2 Fluid Layer 102

5.2.3 Boundary Conditions 103

5.2.4 Approximate Solution 105

5.3 All boundaries rigid 107

5.4 Upper Surface Free 114

5.5 Critical Rayleigh and Marangoni Number Results .. 118

5.5.1 Composite System with a Rigid Upper Surface . 118

5.5.2 Composite System with a Free Upper Surface .. 121

5.6 Flow and Heat Transfer Results 123

5.7 Summary 126

page

Chapter 6

A SHALLOW CAVITY FILLED WITH TWO IMMISCIBLE FLUIDS 128

6.1 Literature Review 128

6.2 Formulation of the Problem 129

6.3 Approximate Solution 133

6.4 Results and Discussion 136

6.5 Summary 148

Chapter 7

CONCLUSIONS 150

REFERENCES 156

LIST OF FIGURES

Page

2.1: Schematic diagram of the two-dimensional porous layer 165

3.1: Flow configuration considered 166

3.2: Isotherms and streamlines for R=400, Da=10^{-2}, (a) $\varphi=20^0$, (b) $\varphi=35^0$, (c) $\varphi=50^0$ R=250, $\varphi=90^0$, (d) Da=10^{-4}, (e) Da=10^{-2}, (f) Da=1 Da=10^{-3}, $\varphi=80^0$, (g) R=50, (h) R=250, (i) R=500 . 167

3.3: Numerical solutions for the flow and temperature field 170

3.4(a): Stream function at center of layer Ψ_c as a function of Darcy number Da and Darcy-Rayleigh number R for bottom heating 172

3.4(b): Stream function at center of layer Ψ_c as a function of Darcy number Da and Darcy-Rayleigh number R for side wall heating 173

3.5: Nusselt number Nu as a function of Darcy-Rayleigh number R for selected values of Darcy number Da for bottom heating 174

3.6: Nusselt number Nu as a function of Darcy number Da for selected values of Darcy-Rayleigh number R for bottom heating 175

3.7: Temperature difference ΔT as a function of Darcy number Da for selected values of Darcy-Rayleigh number R for side wall heating 176

3.8: Comparison of Brinkman (present) and Darcy models for R=100 for bottom heating 177

3.9: Critical Darcy-Rayleigh number R_c as a function of Darcy number Da for bottom heating 178

3.10: Stream function at center of layer Ψ_c as a function of Rayleigh number R and Darcy number Da 179

page

3.11: Nusselt number Nu as a function of Rayleigh number R and Darcy number Da 180

3.12: Velocity profile at mid-height of the enclosure, y=0, as a function of Darcy number Da for R=100 and (a) $\varphi=30^0$, (b) $\varphi=90^0$, $\varphi=120^0$ 181

3.13: Temperature profile at mid-height of the enclosure, y=0, as a function of Darcy number Da for R=100 and (a) $\varphi=30^0$, (b) $\varphi=90^0$, $\varphi=120^0$ .. 184

3.14: Variation of stream function at center of layer, Ψ_c, as a function of tilt angle φ for various values of Da for R=500 187

3.15: Variation of Nusselt number, Nu, as a function tilt angle φ for various values of Da for R=500 188

3.16: Tilt angle for maximum Nusselt number, φ_N, as a function of Rayleigh number R and Darcy number Da 189

4.1: Schematic diagram of the partitioned inclined porous layer 190

4.2: Isotherms and streamlines for
(a) R=50, $\eta=0.5$, $\varphi=90^0$
(b) R=300, $\eta=0.5$, $\varphi=90^0$
(c) R=500, $\eta=0.5$, $\varphi=90^0$
(d) R=500, $\eta=0.2$, $\varphi=90^0$
(e) R=500, $\eta=0.5$, $\varphi=60^0$
(f) R=500, $\eta=0.5$, $\varphi=0^0$ 191

4.3: Heat transfer through a vertical porous layer with a single partition: effect of the partition position 193

4.4: Heat transfer through a vertical porous layer with N equally spaced partitions 194

4.5: Heat transfer through a horizontal porous layer with a single partition: effect of the partition position 195

page

4.6: Heat transfer through a horizontal porous layer with N equally spaced partitions 196

4.7: Effects of inclination angle φ on heat transfer through a porous layer with N equally spaced partitions, R=1000 197

4.8: Isotherms and streamlines for a vertical porous layer borded by a solid slab
(a) R=800, η=0.7, K^*=1
(b) R=800, η=0.3, K^*=1
(c) R=800, η=0.3, K^*=5 198

4.9: Heat transfer through a vertical porous layer of extension η borded by a solid slab: effect of K, R=800 199

5.1: Physical model and coordinate system 200

5.2: The effect of Da and η on the critical Rayleigh number Ra_c for a fluid-porous bed system with rigid upper surface (G=1, γ=1) 201

5.3: The effect of G and η on the critical Rayleigh number Ra_c for a fluid-fluid system with rigid upper surface (γ=1) 202

5.4(a): The effect of Da on the temperature distribution for a fluid-porous bed system with rigid upper surface (G=1, γ=1, η=0.5, Ra=10^4) 203

5.4(b): The effect of Da on the temperature distribution for a fluid-porous bed system with rigid upper surface (G=1, γ=1, η=0.5, Ra=10^4) 204

5.5(a): The effect of Ma on the velocity distribution for a fluid-porous bed system with free upper surface (G=1, γ=1, η=0.5, Ra=10^4) 205

5.5(b): The effect of Ma on the temperature distribution for a fluid-porous bed system with free upper surface (G=1, γ=1, η=0.5, Ra=10^4) 206

5.6(a): The effect of η and Ra on the Nusselt number for a fluid-porous bed system with rigid upper surface (G=1, γ=1, Da=10^{-3}) 207

page

5.6(b): The effect of η and Ra on the Nusselt number for a fluid-porous bed system with free upper surface (G=1, γ=1, Ma=0, Da=10^{-3}) 208

6.1: Schematic representation of two-layer geometry . 209

6.2: Flow structures in the two layers 210

6.3: Effect on the flow structures in a two-layer system of (a) K with G=0, μ^*=1; (b) G with K=1, μ^*=1; (c) μ^* with G=0, K=1 211

6.4: Distribution of horizontal velocity. Effect of (a) K with η=0.5, μ^*=1, G=0; (b) G with η=0.5, μ^*=1, K=1; (c) μ^* with η=0.5, G=0, K=1 214

6.5: Vertical temperature distributions for a system heated from the side. Effect of (a) K with η=0.5, G=0, μ^*=1; (b) G with η=0.5, K=1, μ^*=1; (c) μ^* with η=0.5, G=0, K=1 217

6.6: Maximum stream function Ψ_m in each fluid layer for a system heated from the bottom as a function of G with Ra_1=4x10^4, μ^*=1, K=1 and (a) η=0.5; (b) η=0.45; (c) η=0.55 220

6.7: The effect of G and η on the critical Rayleigh number Ra_c for bottom heating with μ^*=1, K=1 ... 223

6.8: The effect on the Nusselt number Nu for bottom heating with μ^*=1, K=1 and (a) Ra_1=4x10^4; (b) η= 0.5 224

6.9: The effect of G on the Nusselt number Nu for a single layer of fluid with an upper free surface and bottom heating 226

LIST OF TABLES

page

3.1: Analytical and numerical (in parentheses) Nusselt number and streamfunction at center for a cavity with a free upper surface and bottom heating 227

3.2: Analytical and numerical (in parentheses) Nusselt number and streamfunction at center for a cavity with a free upper surface and side wall heating 227

3.3: Analytical and numerical in parentheses) temperature difference and streamfunction at center for a cavity with both boundaries free and bottom heating 228

3.4: Analytical and numerical (in parentheses) temperature difference and streamfunction at center for a cavity with both boundaries free and side wall heating 228

4.1: Analytical and numerical Nusselt number for a vertical layer ($\varphi=90^0$) with a central partition 229

4.2: Analytical and numerical Nusselt number for an horizontal porous layer ($\varphi=0^0$) with a central partition 229

4.3: Analytical and numerical Nusselt number for an inclined porous layer with a central partition, R=300 230

5.1: The effect of G and Da on the critical Rayleigh number Ra_c for a fluid-porous bed system with rigid upper surface: $\gamma=1$, $\eta=0.5$ 231

5.2: The effect of Da and η on the critical Rayleigh Ra_c and Marangoni Ma_c numbers for a fluid-porous bed system with free upper surface, $G=\gamma=1$ 232

5.3: The effect of G and η on the critical Rayleigh Ra_c and Marangoni Ma_c numbers for a fluid-fluid system with free upper surface, $\gamma=1$ 233

Page

6.1: The effect of Rayleigh number Ra_1 on axial temperature gradient C, with η=0.5, K=1, G=0, μ^*=1 234

6.2: The effect of parameter K on axial temperature gradient C, with η=0.5, G=0, μ^*=1, $Ra_1=10^5$ 234

6.3: The effect of parameter G on axial temperature gradient C, with η=0.5, K=1, μ^*=1, $Ra_1=10^5$ 235

6.4: The effect of parameter μ^* on axial temperature gradient C, with η=0.5, K=1, G=0, μ^*=1, $Ra_1=10^5$ 235

LIST OF SYMBOLS

A	: aspect ratio of the system, H'/L'
C	: temperature gradient along y direction
Da	: Darcy number
g	: gravitational acceleration
G	: parameter, μ_f/μ_p
h'_i	: height of layer i
h'_f	: thickness of fluid layer
h'_p	: thickness of porous layer
H'	: thickness of the system
k	: thermal conductivity of fluid-saturated porous medium
k_b	: thermal conductivity of thermal barrier
K	: permeability of porous medium
K^*	: solid to porous conductivity ratio
L'	: length of the system
Ma	: Marangoni number, $SL^2q'/k_f\mu_f\alpha_f$
Pr	: Prandtl number, ν/α
Nu	: Nusselt number
N	: number of partitions
q'	: constant heat flux
R	: Rayleigh number for the porous medium, $g\beta k'L'^2q'/k\alpha\nu$
R_c	: critical Rayleigh number for zero inclination

Ra : Rayleigh number for the fluid, Ra=R/Da

S : surface tension gradient with respect to temperature

T : dimensionless temperature

T'_r : reference temperature at $x=\eta$, $y=0$

T'_0 : reference temperature at $x=y=0$

ΔT : dimensionless temperature difference at $y=0$

u,v : dimensionless velocities

x,y : dimensionless coordinate system

Greek symbols

α : thermal diffusivity

α_f : thermal diffusivity of the fluid

α_p : effective thermal diffusivity of the porous medium

β : coefficient of thermal expansion of the fluid

η : dimensionless position of the interface, h_f/L

θ : temperature variation with x

μ : dynamic viscosity

ν : kinematic viscosity

γ : dimensionless parameter, k_p/k_f

ρ : density

σ : surface tension

Ψ : dimensionless stream function

ω : dimensionless vorticity

φ : angle of inclination of the enclosure

Superscript

′ : dimensional quantities

Subscript

f : fluid

p : porous

c : critical conditions

- : refers to porous medium

i : in the fluid layer (i=1, 2)

* : ratio of ...

CHAPTER 1

INTRODUCTION

Natural convection heat transfer is becoming an increasingly important subject for experimental and theoretical studies. Some form of natural convection occurs in most processes where fluids are heated or cooled in a gravitational force field. Often this is combined with forced convection. In situations where forced cooling is not practical or possible, natural convection alone is an important mechanism for heat transfer.

Early work on natural convection considered heat transfer from a body immersed in an isothermal stagnant fluid of infinite extent. Geometries studied include a vertical flat plate, horizontal and vertical cylinders and spheres. Boundary layer solutions were obtained for each of these valid for laminar flow at large values of the Rayleigh number. More recently considerable research efforts have been devoted to the study of heat transfer in cavities filled with a fluid-saturated, porous medium. To a large extent, this interest is stimulated by the fact that thermally driven flows in porous media are of considerable engineering interest. These problems arise in the design of pebble bed nuclear reactors, catalytic reactors, compact heat exchangers, solar power

collectors, geothermal energy conversion, use of fibrous materials in the thermal insulation of buildings and geophysical flows. Another important area of application is heat transfer from the storage of agricultural products which generate heat as a result of metabolism. An excellent review of existing experimental and numerical results have been presented by Combarnous and Bories (1975) and Catton (1978).

The purpose of the present thesis is to examine the effects of natural convection in inclined, rectangular, porous layers when a constant heat flux is applied on two opposing walls, while the other two walls are maintained adiabatic. The layer is referred to as being horizontal, vertical or tilted, depending on the orientation of its thermally active walls with respect to the gravity acceleration vector. A review of the literature shows that most previous theoretical publications deal with vertical (Burns et al. (1976), Weber, (1979) and Shiralkar et al. (1983)) or horizontal (Elder, (1974) and Rudraiah et al. (1982)) cases. For situations involving inclined layers, available studies are relatively limited. The problem of a sloped porous layer, heated isothermally from below, has been considered theoretically and experimentally by Bories and Combarnous (1973). Depending on the values of the slope of the layer and the Rayleigh number R, different shapes of free convection move-

ments have been observed. Hence, a two-dimensional stable unicellular flow takes place in the layer if $R<4\pi^2/\cos\varphi$, where φ is the angle between the heated wall and the horizontal plane. On the other hand, when the Rayleigh number is higher than a critical value a transition from unicellular flow to stable three-dimensional flow is observed. The resulting convective movement take then the form of polyhedral cells for φ lower than about 15^0 while for higher values of φ it consists of adjacent longitudinal coils climbing up along the direction of the slope. Finally for very high Rayleigh numbers it was found that, depending on the slope of the layer, a fluctuating regime or a wavy coil regime could be observed. Convection in a tilted, porous box -with two parallel isothermal planes and the other limits insulated -has been studied numerically by Vlasuk (1972) for the range $A=1$, $-90^0<\varphi<90^0$ and $R\lesssim 350$. It was found that the tilt angle, for maximum heat transfer, is approximately 50^0.

Holst and Aziz (1972), considering temperature-dependent physical properties, investigated the heat transfer of a tilted square of porous material. Steady natural convection in a slightly inclined, rectangular, porous box has been studied by Walch and Dulieu (1979) using the Galerkin method. A correlation for the Nusselt number as a function of Rayleigh number, aspect ratio and tilt angle has been obtained by

these authors. More recently, the existence of multiple solutions, in a slightly inclined, porous cavity heated from the bottom, has been studied numerically by Walch and Dulieu (1979), Moya et al. (1987) and analytically by Caltagirone and Bories (1985) who determined their stability. It was demonstrated that, for small angles of inclination, three different real solutions may exist for a given Rayleigh number and aspect ratio.

All the above studies have considered cavities with isothermal walls despite the fact that in many engineering applications the temperature of a wall is not uniform but, rather, is a result of the imposition of a constant heat flux. Results available for the situation where a constant heat flux is applied on one (Prasad, et al., (1984)) or two (Bejan, (1983)) walls have been reported only for the case of a vertical cavity.

The objective of the present work is to analyze the behavior of natural convection flows in rectangular, tilted, porous systems heated and cooled by constant heat fluxes. The organization of this thesis is the following. In Chapter 2 the parallel flow approximation is developed for the simple case of a horizontal Darcy layer. The control volume approach introduced in the past by Bejan (1983) is described. The

problem of an inclined Brinkman-extended Darcy porous layer is studied in Chapter 3. The critical Darcy-Rayleigh number for the onset of convection in a bottom-heated horizontal cavity is also discussed in this chapter. The influence of multiple diathermal partitions in inclined porous layers is studied in Chapter 4. The stability and natural convection in a system consisting of a horizontal fluid layer over a layer of porous medium saturated with the same fluid, with heating from below, are considered in Chapter 5. The mechanism of natural and Marangoni convection in a system with two stratified fluid layers is investigated in Chapter 6. The thesis concludes with Chapter 7.

CHAPTER 2

THE PARALLEL FLOW APPROXIMATION FOR SHALLOW CAVITIES

2.1 LITERATURE REVIEW

Though the published results for the convection heat transfer in a rectangular cavity cover wide ranges of Rayleigh number and aspect ratio, most of them have been limited to large aspect ratios A (A=height/width$\geq$1). For low aspect ratios, A<1, the relative scarcity of published work has been noted by Ostrach (1980). In a series of papers, Cormack et al. (1974a,b) and Imberger (1974) investigated the case of the gravity induced flow in slender horizontal fluid enclosures with differentially heated end walls. The problem was solved by means of an asymptotic theory for very small aspect ratios A<<1 and arbitrary but fixed values of the Grashof and Prandtl numbers. It was shown by these authors 7

that the flow inside the cavity consists of two distinct regimes: a parallel flow in the core region and a second, non-parallel flow near the ends of the cavity. A solution valid at all orders in the aspect ratio A was found for the core region, while the first several terms of the asymptotic expansion were obtained for the end regions. The same problem was also considered by Bejan and Tien (1978a) who have devel

oped an approximate solution, valid for small but finite aspect ratios, to cover the three regimes of $Ra \to 0$, intermediate Ra and large Ra.

The Nusselt number prediction, based on the three-regimes theory, was found to agree very well with available numerical and experimental heat transfer data. The case of a porous layer confined in a horizontal space with the two ends maintained at different temperatures and the long horizontal walls being adiabatic was also considered by Bejan and Tien (1978b). The results demonstrated the dependence of the Nusselt number for axial heat transfer on the Rayleigh number and the aspect ratio of the horizontal porous medium. A numerical solution for the above problem was obtained by Hickox and Gartling (1981) and regions of validity for the analytical results were delineated. A more formal treatment of the limit case considered by Bejan and Tien (1978b), with Ra fixed and $A \to 0$, has been given by Walker and Homsy (1978), where there is also a discussion of the limit $Ra \to 0$ and A fixed, i.e. the conduction dominated regime. Solutions for the flow field and the Nusselt number were obtained up to $O(Ra^4)$. A classification of the limiting behaviours of the thermal convection in a cavity filled with a porous medium, when the applied temperature gradient is perpendicular to the gravity vector, was presented recently by Blythe et al.

(1983). In particular the case of the shallow cavity, was considered. A discussion of the relationship between the different possible flow regimes was given in terms of a new scaling law. Existing theories for the Nusselt number were reviewed and shown to be consistent with their scaling law. All these works have considered exclusively cavities having isothermal vertical walls. However, in many applications, the temperature of the heated wall is not maintained uniform but is rather the consequence of the heat flux imposed on the wall. For instance, the temperature of the great majority of walls encountered in architectural and solar applications results directly from the imposition of a constant heat flux through these walls. Thus the study of the natural convection in a shallow cavity, induced by a constant heat flux, is certainly of practical importance.

2.2 NATURAL CONVECTION IN A POROUS ENCLOSURE

In order to illustrate the type of approximation that will be utilized in the present thesis we will now consider the simple case of natural convection in a horizontal rectangular cavity containing a Darcy medium. The porous material is isotropic and homogeneous and the fluid is incompressible. All properties of the fluid and porous medium are considered constant, except the density of the fluid which gives rise to

the buoyancy force. This so-called Boussinesq approximation is practically valid for small temperature and pressure variations within the flow region. As shown in Fig. 2.1, the cavity is taken to be of height H′ and length L′ with a coordinate system (x′,y′) fixed at the geometric center of the slot. The two horizontal surfaces are taken to be perfectly insulated and a uniform heat flux is imposed along both side walls. The momentum boundary conditions are no mass flux through the boundaries. Invoking Darcy's law along with the Boussinesq approximation and neglecting thermal dispersion, the dimensionless form of the governing equations using the streamfunction formulation are:

$$\nabla^2 \Psi = -R \frac{\partial T}{\partial x} \tag{2.1}$$

$$\nabla^2 T = u \frac{\partial T}{\partial x} + v \frac{\partial T}{\partial y} \tag{2.2}$$

$$u = \frac{\partial \Psi}{\partial y} \; ; \qquad v = - \frac{\partial \Psi}{\partial x} \tag{2.3}$$

with the conditions:

$$\begin{aligned} &\Psi = 0 \quad \frac{\partial T}{\partial x} = 1 \qquad \text{on} \quad x = \pm 1/2 \\ &\Psi = 0 \quad \frac{\partial T}{\partial y} = 0 \qquad \text{on} \quad y = \pm A^*/2 \end{aligned} \tag{2.4}$$

In the above equations the variables have been reduced to dimensionless form by introducing the following scales:

$$x,y = (x',y')/L' \qquad u,v = (u',v')L'/\alpha$$

$$\Psi = \Psi'/\alpha \qquad T = (T'-T'_0)/\Delta T' \qquad (2.5)$$

$$\Delta T' = q'L'/k \qquad R = g\beta KL'^2 q'/\alpha\nu k$$

$$A^* = H'/L'$$

where primes denote dimensional variables, u' and v' are the velocity components in the x' and y' directions, T' the temperature, T'_0 the temperature in the geometric center of the slot, R the Darcy-Rayleigh number, q' the heat flux applied to both side walls, and A^* the aspect ratio of the cavity. The symbols α, β, g, K, k and ν denote the effective thermal diffusivity, the coefficient of thermal expansion, the gravitational acceleration, the permeability, the thermal conductivity and the kinematic viscosity respectively.

2.3 ANALYTICAL SOLUTION FOR SMALL ASPECT RATIOS

In this section an approximate analytical solution to the full governing Eqs. (2.1) to (2.4) is sought for the case with R fixed and $A^* \ll 1$. The problem of natural convection in a porous cavity of small aspect ratio with differentially

heated isothermal end walls has been considered in the past by Walker and Homsy (1978). It was shown by the use of matched asymptotic expansions, that the flow inside the cavity may be decomposed into three parts; a core region of extent $O(A^{*-1})$ in the center of the cavity, and two end regions within an $O(1)$ distance from the end walls. The solutions in the three regions are coupled by the matching requirements in the regions of overlap. As the aspect ratio approaches zero, the disparity in the length scales increases and it is expected that the resistance forces in the core region eventually dominate the flow structure over most of the cavity. Physically, the basic flow consists of a buoyancy driven parallel flow which is moderated by viscous effects over a length L'. The flow then turns through 180^0 in the end regions.

In order to find out the asymptotic solution, it is first appropriate to rescale the governing equations in a way which reflects the existence of two different regions with different characteristic horizontal length scales, $O(L'))$ in the core and $O(H')$ at the ends. Thus the solution in the core region is obtained by scaling y' with H', x' with L' and Ψ' with $\alpha A^{*2} R^*$. It is furthermore advantageous to introduce a new Rayleigh number based on the height $R^* = (g\beta K H'^2 q'/k\nu\alpha) = R A^{*2}$. With these scalings, the core field equations become:

$$A^{*2}\frac{\partial^2\Psi^*}{\partial x^{*2}} + \frac{\partial^2\Psi^*}{\partial y^{*2}} = -\frac{\partial T^*}{\partial x^*} \tag{2.6}$$

$$A^{*2}\frac{\partial^2 T^*}{\partial x^{*2}} + \frac{\partial^2 T^*}{\partial y^{*2}} = A^* R^* \left[\frac{\partial\Psi^*}{\partial y^*}\frac{\partial T^*}{\partial x^*} - \frac{\partial\Psi^*}{\partial x^*}\frac{\partial T^*}{\partial y^*} \right] \tag{2.7}$$

where $T^* = (T - T'_0)/\Delta T'$, $u^* = \partial\Psi^*/\partial y^*$, $v^* = -\partial\Psi^*/\partial x^*$ and $*$ refers to the variables in the core region. The boundary conditions are:

$$\Psi^* = 0 \quad \partial T^*/\partial x^* = 1 \quad \text{on} \quad x^* = \pm 1/2 \tag{2.8a}$$

$$\Psi^* = 0 \quad \partial T^*/\partial y^* = 0 \quad \text{on} \quad y^* = \pm 1/2 \tag{2.8b}$$

Expanding the stream function and temperature as a regular series in the small parameter A^*:

$$\Psi^* = \Psi^*_0 + A^*\Psi^*_1 + A^{*2}\Psi^*_2 + \ldots$$

$$T^* = T^*_0 + A^* T^*_1 + A^{*2} T^*_2 + \ldots \tag{2.9}$$

substituting in Eqs. (2.6) to (2.8) and solving the resulting equations the solution is:

$$\Psi^* = -\frac{C}{2}(y^{*2} - 1/4) \tag{2.10}$$

$$T^* = Cx^* - \frac{C^2}{2} R^* A^* (y^{*3}/3 - y^*/4) \tag{2.11}$$

$$u^* = -Cy^* \tag{2.12}$$

where the constant C, the axial temperature gradient, has to be determined from the thermal boundary conditions imposed on the vertical walls (Eq. 2.8a)

The constant C may be obtained by matching the core solution with solutions valid in the end regions. In the case of a porous cavity with isothermal end walls, such a solution has been developed formally by Walker and Homsy (1978) and a first order description of the entire flow field, including the corner interaction regions was obtained. However it was shown by Bejan and Tien (1978a) that, in order to determine the constant C, which defines the core flow, a detailed analysis of the end regions is not absolutely necessary. In fact the constant C may be evaluated simply by matching the core region with an integral solution for the flow and temperature field in the end region. In the case of a cavity with isothermal vertical walls this was done by selecting reasonable profiles for the velocity and temperature distributions inside the end regions. In the present problem, due to the fact that a constant heat flux is imposed on the vertical walls, a guess of the velocity and temperature profiles inside the end regions is not even required to solve the core region.

As discussed by Bejan (1983) the value of the constant C may be obtained simply by considering the arbitrary control volume of Fig. 2.1. Integration of the energy Eq. (2.7) over this control volume yields:

$$\int_V \nabla^{*2} T^* \, dV = A^* R^* \int_V \vec{v}^* . \nabla^* T^* \, dV \tag{2.13}$$

such that

$$\int_S \nabla^* T^* . \overrightarrow{dS} = A^* R^* \int_S \vec{v}^* T^* . \overrightarrow{dS} \tag{2.14}$$

where

$$\nabla^{*2} = A^{*2} \frac{\partial^2}{\partial x^{*2}} + \frac{\partial^2}{\partial y^{*2}}$$

and

$$\nabla^* = A^* \frac{\partial}{\partial x^*} + \frac{\partial}{\partial y^*}$$

By making use of the fact that both horizontal boundaries are adiabatic ($\partial T^* / \partial y^* = 0$), a constant heat flux is applied on the vertical walls ($\partial T^* / \partial x^* = 1$) and the solid boundaries are impermeable ($\vec{V} . \overrightarrow{dS} = 0$) it may be shown that Eq. (2.14) yields

$$\int_{-1/2}^{1/2} \frac{\partial T^*}{\partial x^*} \Big|_{x^*} dy^* - \frac{R^*}{A^*} \int_{-1/2}^{1/2} T^* u^* \Big|_{x^*} dy^* = 1 \tag{2.15}$$

at any value of x^*.

The above equation expresses the fact that the constant heat flux entering through the left wall flows undiminished through the right one owing to the adiabatic conditions imposed on both horizontal walls. The constant horizontal heat flux inside the cavity is the sum of the horizontal heat conduction through the vertical section of the layer and the enthalpy convected by the horizontal counterflow.

Substituting Eqs. (2.11) and (2.12) into Eq. (2.15) and integrating yields:

$$C^3 R^{*2} + 120C - 120 = 0 \tag{2.16}$$

The value of the axial temperature gradient C may thus be obtained, for a given Rayleigh number R^*, from Eq. (2.16).

Solutions (2.10), (2.11) and (2.16) indicate that the core flow is essentially parallel to the horizontal boundaries for all orders of magnitude in A, while, for the first order in A, the temperature is linear in x^* and independent of y^*. It follows from this result that

$$\Psi^*(x^*, y^*) \simeq \Psi^*(y^*) \tag{2.17}$$

and

$$T^*(x^*, y^*) \simeq Cx^* + \theta(y^*) \tag{2.18}$$

In the past, the above technique has been applied to various problems. For instance, Vasseur et al. (1986) have considered natural convection in an inclined, porous layer when a constant heat flux is applied on two opposing walls, while the other two walls are maintained adiabatic. Solutions for the flow fields, temperature distributions and Nusselt numbers were obtained explicitly in terms of the Rayleigh number and the angle of inclination of the cavity. For the same problem, Sen et al. (1987) have demonstrated analyti17

cally, on the basis of the parallel flow approximation, that for small angles of inclination, three different real solutions may exist for a given Rayleigh number. A similar phenomenon has also been reported by Vasseur et al. (1987) for the case of an inclined fluid layer. Also, multiple steady states have been reported by Sen et al. (1988) for the case of parallel flow convection in a tilted two dimensional porous layer heated from all sides.

In the following chapters the parallel flow approximation will be used to solve various problems of natural convection in shallow enclosures. Although the parallel flow approximation is independent per se of the thermal boundary conditions applied on the system, it happens that, when a constant heat flux is considered, the solutions become particularly straightforward. Also, the resulting solution is found to be

valid for any Rayleigh number. Moreover, in the case of bottom heated systems, it is possible to deduce in a direct way the resulting critical Rayleigh number for the onset of convective motion. In this way, it has been possible to determine the limit stability of relatively complex systems. In fact many of the critical Rayleigh numbers predicted in the past by the linear stability analysis have been recovered in the present thesis as limit cases of the problems considered.

In the following chapters we will illustrate the use of the above method by considering a large variety of situations such as inclined fluid or porous cavities and combined layers of different nature (fluid-fluid or fluid-saturated porous media). It will also be shown that it is possible to include various hydrodynamic boundary conditions such as free surfaces with or without surface tension effects.

CHAPTER 3

AN INCLINED SHALLOW POROUS CAVITY WITH UNIFORM FLUX -- THE BRINKMAN MODEL

3.1 LITERATURE REVIEW

The phenomenon of convective heat transfer in a fluid-saturated porous cavity has received considerable attention in the past because of numerous applications in geophysics and energy related engineering problems. Applications include geothermal reservoirs, porous insulation, packed-bed catalytic reactors heat storage bed, nuclear waste disposal systems, sensible heat storage beds, and enhanced recovery of petroleum resources (Cheng, (1978); Combarnous, (1975); Denloye, (1977); Bejan, (1981); Beavers, (1967); Saffman, (1971); Brinkman, (1948); Tam, (1969); and Lundgren, (1972)). The many possible configurations in which the flow and heat transfer processes in such systems have been examined include a rectangular enclosure with differentially heated vertical side walls, an annular cavity with radial heating and an infinitely long horizontal porous layers heated from below.

Most analytical studies for natural convection in porous media are based on Darcy flow model which is empirically

given by

$$\frac{\mu \vec{\mathbf{v}}}{K} = - (\nabla p + \rho g \vec{\mathbf{k}}) \tag{3.1}$$

where μ, $\vec{\mathbf{v}}$, p, K, ρ, g, and $\vec{\mathbf{k}}$ represent the viscosity of the liquid, the velocity vector, pressure, the permeability of the porous medium, the density of the liquid, the acceleration due to gravity and a unit vector pointed vertically upward, respectively.

One of the main advantages of Darcy's law is that it linearizes the momentum equation, thus removing a considerable amount of difficulty in solving the governing equations. Darcy's law is found to give satisfactory results for flow velocities and heat transfer rate when the porous medium is closely packed i.e. it has a low permeability. On the other hand, since Darcy's law is of order one less than the Navier-Stokes equations it cannot account for the no-slip boundary condition on rigid boundaries. In order to take into consideration the boundary effect, which may become important in porous media with high porosities such as foam metals and fibrous materials, other laws should be used.

An alternate and more appropriate approach was proposed by Brinkman (1948) who extended the Darcy model by adding a

viscous-like term in Eq. (3.1) thereby making it a second-order equation. This extended-Darcy equation can be written in the form

$$\frac{\mu\vec{\mathbf{v}}}{K} = -(\nabla p + \rho g\vec{\mathbf{k}}) + \mu_p \nabla^2 \vec{\mathbf{v}} \tag{3.2}$$

where μ_p is the effective viscosity.

The Brinkman equation removes the deficiencies of Darcy's law in the sense that it is applicable to media with high permeability and can account for all boundary conditions at a solid surface or a fluid interface .

Although the effective viscosity μ_p appearing in Eq. (3.2) was recently shown (Koplik, (1983)) to be less than μ, the pore fluid value, it has been a common practice to take these two viscosities to be equal.(Howells, (1974); Hinch, (1977)). So in the present Chapter we will take $\mu_p = \mu$.

The first theoretical investigation of natural convection in a porous enclosure using the Brinkman model, was made by Chan et al. (1970) who studied the flow and heat transfer rate in a rectangular box with solid (impermeable) walls. The box was differentially heated in the horizontal direction. Chan et al. considered enclosures with aspect ratios

(depth/width) greater than or equal to one. Their numerical computation indicate that when the Darcy number based on the width of the enclosure is less than 10^{-3}, Darcy's law and the Brinkman equation give virtually the same result for the heat transfer rate. Within the past few years there has been a renewed interest in the use of the Brinkman equation for analyzing flows through porous media. Rudraiah et al. (1980) used this model to investigate convective instabilities of a fluid-saturated porous layer heated from below. In a different context, the Brinkman equation was used by Nandakumar and Masliyah (1982) to determine the flow of a newtonian fluid past a permeable sphere and by Haber and Mauri (1983) in their study of flow around a porous sphere with a solid core. More recently, Tong and Subramanian (1985) examined the boundary layer region for natural convection in a Brinkman medium inside an enclosure with an aspect ratio of 0(1). The same problem was considered recently by Vasseur and Robillard (1987) for the case of a vertical cavity heated by constant heat fluxes.

Several investigators (see for instance Bejan, (1978)) analyzed in the past the shallow cavity problem using Darcy's law. Among them, Hickox and Gartling (1981) applied the Galerkin form of the finite element method and numerically computed the heat transfer rate through the cavity in terms

of a Nusselt number. Approximate analytical expressions for the Nusselt number have been derived by Walker and Homsy (1978) and Bejan and Tien (1978) A comparison of heat transfer results obtained from the present study and from those using Darcy's law will be made here.

In the original form, neither Darcy's law, Eq. (3.1) nor Brinkman Eq. (3.2), incorporate inertial effects. Muskat (1946) accounted for fluid inertia by introducing a velocity-squared term in the equation Among others, Whitaker (1969) and Slattery (1968) and more recently Vafai and Tien (1981) developed equations for fluid motion through a porous medium, including inertial effects. However, in this analysis, the effects of inertia will actually be ignored.

The present study proceeds as follows. First, we examine buoyancy-driven convection in a shallow inclined porous cavity with all rigid boundaries. Our mathematical treatment parallels that of Cormack et al.(who consider natural convection in a shallow cavity filled with a newtonian liquid, (1974a,b)) and is based on the asymptotic limit that the aspect ratio of the cavity goes to infinity (A>>1). This is followed by an analysis of natural convection in a shallow porous cavity with rigid and free horizontal surfaces. The primary objective is to determine the heat transfer rate

though the cavity in terms of a Nusselt number.

3.2 PROBLEM STATEMENT AND SOLUTION PROCEDURE

Consider a two-dimensional cavity filled with an isotropic, homogeneous, fluid-saturated porous medium confined on all sides by an impermeable rectanguar box. The enclosure, shown in Fig.3.1, is of height H′, width L′ and tilted at an angle φ with respect to the horizontal plane. An adiabatic condition is imposed on the two end walls while a uniform heat flux $q'=-k\partial T'/\partial x'$ is applied along both side walls. Here, k is the thermal conductivity of the porous medium, T′ the temperature and primes denote dimensional variables. It is assumed that the flow is laminar and steady and that the Boussinesq approximation applies. The usual Darcy assumptions are adopted in the porous medium, except that the viscous Brinkman term is retained.

Under these conditions, the governing equation for the porous medium are:

$$\frac{\partial u'}{\partial x'} + \frac{\partial v'}{\partial y'} = 0 \tag{3.3}$$

$$u' = -\frac{K}{\mu}\left[\frac{\partial p'}{\partial x'} - \mu\left(\frac{\partial^2 u'}{\partial x'^2} + \frac{\partial^2 u'}{\partial y'^2}\right)\right] - \rho g\beta\cos\varphi(T'-T_0') \tag{3.4}$$

$$v' = -\frac{K}{\mu}\left[\frac{\partial p'}{\partial y'} - \mu\left(\frac{\partial^2 v'}{\partial x'^2} + \frac{\partial^2 v'}{\partial y'^2}\right)\right] - \rho g\beta\sin\varphi(T'-T_0') \tag{3.5}$$

$$u'\frac{\partial T'}{\partial x'} + v'\frac{\partial T'}{\partial y'} = \alpha\left[\frac{\partial^2 T'}{\partial x'^2} + \frac{\partial^2 T'}{\partial y'^2}\right] \tag{3.6}$$

where u', v', p', T_0', g, K, μ and α stand for the velocity components in x' and y' direction, pressure, temperature at the geometric center of the cavity, gravitational acceleration, medium permeability, viscosity and thermal diffusivity respectively.

The solution is obtained in terms of the stream function and vorticity defined, as usual, by

$$u' = \frac{\partial \Psi'}{\partial y'}, \qquad v' = -\frac{\partial \Psi'}{\partial x'} \tag{3.7a}$$

$$\omega' = \frac{\partial v'}{\partial x'} - \frac{\partial u'}{\partial y'} \tag{3.7b}$$

With the use of appropriate scales for length, velocity temperature and stream function, the following dimensionless variables are used:

$$(x,y) = \frac{(x',y')}{L'}, \qquad (u,v) = \frac{(u',v')}{\alpha_f/L'}, \qquad T = \frac{T' - T_0'}{\Delta T'}$$

$$\Delta T' = \frac{q'L'}{k}, \qquad \Psi = \frac{\Psi'}{\alpha_f}$$

The nondimensional governing equations for the porous medium are,

$$\nabla^2 \Psi = -\omega \tag{3.8}$$

$$\nabla^2 \omega = Da^{-1}\left[\omega - R\left(\frac{\partial T}{\partial x}\sin\varphi + \frac{\partial T}{\partial y}\cos\varphi\right)\right] \tag{3.9}$$

$$\nabla^2 T = \frac{\partial \Psi}{\partial y}\frac{\partial T}{\partial x} - \frac{\partial \Psi}{\partial x}\frac{\partial T}{\partial y} \tag{3.10}$$

where $Da=K/L'^2$ is the Darcy number and $R=g\beta KL'^2q'/k\alpha\nu$ the Darcy-Rayleigh number based on the constant heat flux q' and the permeability K of the medium.

The boundary conditions on Ψ and T are

$$\Psi = 0, \quad \frac{\partial T}{\partial x} = 1 \qquad \text{at } x = \pm\frac{1}{2} \tag{3.11a}$$

$$\Psi = 0, \quad \frac{\partial T}{\partial y} = 0, \qquad \text{at } y = \pm\frac{A}{2} \tag{3.11b}$$

where $A=H'/L'$ is the aspect ratio of the cavity.

In the present problem, a representative Nusselt number reflecting the convective heat transfer is defined as

$$Nu = \frac{q'L'}{k\Delta T'} = \frac{1}{\Delta T} \tag{3.12}$$

where $\Delta T=T(1/2,0)-T(-1/2,0)$ is the wall-to-wall dimensionless temperature difference, taken arbitrarily at the position $(x=0,\ y=0)$.

3.3 ANALYTICAL SOLUTION

In this section we proceed to search for an analytical solution for large aspect ratio of the cavity ($A>>1$). As discussed in Chapter 2, the main features of the solution are: (1) a core region in the centre of the cavity in which the flow is essentially parallel ($u=0$, $v=v(x)$) and the temperature distribution linear in the y-direction, and (2) two regions near each end wall where the flow turns around and recirculates. This behavior, in the context of the present problem, suggests the following transformation for the temperature field in the core region (see Eqs. 2.17 and 2.18),

$$\begin{aligned} T(x,y) &= \theta(x) + Cy \\ \Psi(x,y) &= \Psi(x) \end{aligned} \tag{3.13}$$

where C is the unknown constant temperature gradient measured in the core region along the y-direction. The value of C is obtained from Eqs. (2.14), (3.11) and (3.13) as

$$C = 2 \int_0^{1/2} vT|_y \, dx \tag{3.14}$$

Substituting Eq. (3.13) into the governing Eqs. (3.8) to (3.10) and using the fact that, in the core region, $\Psi(x,y)=\Psi(x)$, we get

$$\frac{d^2\Psi}{dx^2} = Da \frac{d^4\Psi}{dx^4} - R\left[\frac{d\theta}{dx} \sin\varphi + C \cos\varphi \right] \tag{3.15}$$

and

$$\frac{d^2\theta}{dx^2} = - C \frac{d\Psi}{dx} \tag{3.16}$$

Substitution of (3.16) into (3.15) readily gives

$$\frac{d^5\Psi}{dx^5} - \frac{1}{Da}\frac{d^3\Psi}{dx^3} + \frac{RC}{Da} \sin\varphi \frac{d\Psi}{dx} = 0 \tag{3.17}$$

The solution of Eq. (3.17) may be written as a sum of exponentials

$$\Psi = \sum_{n=1}^{4} a_n \exp(-\lambda_n x) \tag{3.18}$$

where λ_n are the roots of the quartic equation

$$\lambda^2 \left(\lambda^2 - \frac{1}{Da} \right) + \frac{RC}{Da} \sin\varphi = 0 \tag{3.19}$$

as follows from substitution of (3.18) into (3.17).

The behavior of the roots λ in (3.19) depends on the sign of $C \sin\varphi$, so the three cases $C \sin\varphi$ positive, negative and zero will be considered in turn.

3.3.1 $C \sin\varphi > 0$

This corresponds to a stable temperature gradient in the core region, and C in temperature distribution (3.13) would be positive (negative) for $\sin\varphi$ positive (negative). This situation corresponds to "natural" or "preferred" (Ehrhard and Mueller (1990)) flow. This is the motion that would start from rest and from a conductive temperature field (i.e. counterclockwise (clockwise) motion for $\sin\varphi$ positive (negative)).

Solutions to Eqs. (3.16) and (3.17) satisfying boundary condition (3.11a) are

$$\Psi = - \frac{B}{a^2+b^2} \left[\alpha_1 \cosh(ax)\cos(bx) + \alpha_2 \sinh(ax)\sin(bx) - D \right]$$

and (3.20)

$$\theta = B\beta_0\left[\alpha_0 \sinh(ax)\cos(bx) + \cosh(ax)\sin(bx)\right] + \frac{v}{2R\sin\varphi} - Cx\cot\varphi \tag{3.21}$$

where v is the velocity component, given by

$$v = B\left[\sinh(ax)\cos(bx) - \alpha_0\cosh(ax)\sin(bx)\right] \tag{3.22}$$

and

$$a = \sqrt{\frac{\gamma+1}{4Da}}, \quad b = \sqrt{\frac{\gamma-1}{4Da}}, \quad \gamma = \sqrt{4RC\ Da\ \sin\varphi}$$

$$B = \frac{\gamma(1+C\cot\varphi)}{2C\ D\ Da}, \quad \beta_0 = \sqrt{\frac{\gamma^2-1}{2R\ \sin\varphi}}$$

$$D = \alpha_1\cosh(a/2)\cos(b/2) + \alpha_2\sinh(a/2)\sin(b/2) \tag{3.23}$$

$$\alpha_0 = \cot(b/2)\tanh(a/2), \quad \alpha_1 = a + b\alpha_0, \quad \alpha_2 = b - a\alpha_0$$

The Nusselt number Nu is obtained, by substituting (3.20) into (3.12), as

$$Nu = \frac{1}{2E\ B\ \beta_0 - C\cot\varphi} \tag{3.24}$$

where $E = \alpha_0\sinh(a/2)\cos(b/2) + \cosh(a/2)\sin(b/2)$

The next task is to determine C. Substituting (3.20) and (3.21) into (3.14) yields

$$\frac{B\cot\varphi}{a^2+b^2}\left[D - \frac{4ab}{a^2+b^2}E\right] - \frac{B^2}{8RC}\left[\{G(1+F)+M\}\right.$$

$$\left. + (\alpha_0{}^2-F)(M+2-G) + \frac{H}{\alpha_0}\{F(1-\alpha_0{}^2)-2\alpha_0{}^2\}\right] + 1 = 0 \quad (3.25)$$

where

$$F = \alpha_0\sqrt{4RC\ Da - 1}$$

$$M = \frac{\sin a}{a} - \frac{\sin b}{b} - 1$$

$$G = (b\cosh a\sin b + a\sinh a\cos b)/(a^2+b^2)$$

$$H = (a\cosh a\sin b - b\sinh a\cos b)/(a^2+b^2)$$

Equation (3.25) can readily be solved numerically to obtain C as a function of R and Da. The temperature and velocity distributions and Nusselt number are then given by Eqs. (3.20) to (3.24) respectively.

At this stage it should be noted that the present analysis, based solely on the assumption of parallel flow, is valid even at relatively low Rayleigh numbers. These results must be valid for the boundary layer regime. This regime,in a vertical cavity with uniform heat flux from the side, has been studied in the past by Bejan (1983) for a Darcy medium ,

and by Kimura and Bejan (1984) for a viscous fluid. The boundary layer equation were solved analytically using a modified Oseen linearization method (Gill, (1966)). Since the Brinkman equation reduces to the Darcy equation as the permeability $K \to 0$ and to the Stokes equation as $K \to \infty$ we can check the previous results in these two pecial cases.

a) Da<<1: the Darcy medium

Taking the limit of Eqs. (3.20-3.25) when $\varphi=90^0$ for $Da \to 0$ and $R \to \infty$ it is readily found that

$$v = -\alpha^{3/2}\exp(-\alpha x^*)$$

$$\text{for } x^* = 0$$

$$T = \frac{y}{\alpha^{1/2}} - \frac{1}{\alpha}\exp(-\alpha x^*) \qquad (3.26)$$

$$Nu = \frac{\alpha}{2}$$

where $\alpha=R^{2/5}$ and $x^*=(1/2 - x)$.

The above equations, when translated into corresponding notations, are the same as those obtained by Bejan (1983).

b) Da >> 1: the viscous fluid

Taking the limit of Eqs. (3.20-3.25) when $\varphi=90^0$ for $Da \to \infty$ and $R \to \infty$ it is readily found that

$$v = -\frac{Ra}{2a^3}\exp(-ax^*)\sin(ax^*)$$

$$T = \frac{4a^4}{Ra}y - \frac{1}{a}\exp(-ax^*)\cos(ax^*) \qquad (3.27)$$

$$Nu = a/2$$

where $a^9 = Ra^2/32$, $Ra = R/Da$, and $x^* = (1/2 - x)$. The above equations are similar to the results obtained by Kimura and Bejan (1984).

3.3.2 C sinφ < 0

This corresponds to an unstable temperature gradient in the core region so that C in temperature distribution (3.13), would be negative (positive) for sinφ positive (negative). For positive inclination the motion is clockwise, while it is counterclockwise for negative inclination. In either case this motion, which cannot be started from rest condition with conductive temperature field, will be referred to as "anti-natural" since it is opposite in direction to the natural motion (see for instance Moya et al. (1987)). It may be also termed as "isolated" since its forms a separate branch on the bifurcation diagram (Ehrhard and Mueller (1990)).

An analysis similar to the above can be carried out such that we obtain

$$\Psi = -B_1 \left[\frac{\cosh(a^* x) - \cosh(a^*/2)}{a^*} + \alpha_3 \frac{\cos(b^* x) - \cos(b^*/2)}{b^*} \right] \tag{3.28}$$

$$\theta = B_1 C \left[\frac{\sinh(a^* x)}{a^{*2}} + \alpha_3 \frac{\sin(b^* x)}{b^{*2}} \right] - Cx \cot\varphi \tag{3.29}$$

$$v = B_1 \left[\sinh(a^* x) - \alpha_3 \sin(b^* x) \right] \tag{3.30}$$

$$Nu = \frac{1}{2 B_1 C F - C \cot\varphi} \tag{3.31}$$

where

$$a^* = \sqrt{(\beta+1)/2Da}, \qquad b^* = \sqrt{(\beta-1)/2Da}$$

$$\beta = \sqrt{1 - 4RCDa \sin\varphi}, \qquad \alpha_3 = \frac{\sinh(a^*/2)}{\sin(b^*/2)}$$

$$F = \frac{\sinh(a^*/2)}{a^{*2}} + \alpha_3 \frac{\sin(b^*/2)}{b^{*2}}$$

$$G = \frac{\cosh(a^*/2)}{a^*} + \alpha_3 \frac{\cos(b^*/2)}{b^*}$$

$$B_1 = \frac{1 + C \cot\varphi}{GC}$$

The value of C is given by:

$$B_1 \cot\varphi \; P - B_1{}^2 \left[Q + \frac{\alpha_3}{a^{*2} b^{*2}} \left(\frac{a^{*2} - b^{*2}}{a^{*2} + b^{*2}} \right) S \right] + \frac{1}{2} = 0 \qquad (3.32)$$

where

$$P = \frac{1}{2a^{*2}} \left[a^* \cosh(a^*/2) - 2 \sinh(a^*/2) \right]$$

$$+ \frac{\alpha^3}{2b^{*2}} \left[b^* \cos(b^*/2) - 2 \sin(b^*/2) \right]$$

$$Q = \frac{1}{4a^{*3}} (\sinh a^* - a^*) + \frac{\alpha_3{}^2}{4b^{*3}} (\sin b^* - b^*)$$

$$S = a^* \sin(b^*/2) \cosh(a^*/2) - b^* \cos(b^*/2) \sinh(a^*/2)$$

Here again a numerical procedure can be used to solve Eq. (3.32) in order to obtain C as a function of R and Da. The temperature and velocity distributions and Nusselt number are then given by Eqs. (3.28) to (3.31) respectively.

3.3.3 C.sinφ = 0, (φ = 0)

This corresponds to a horizontal porous layer. For this particular situation we will consider the case where the layer is heated either by the bottom or either from the sides. Also the cases with either rigid or free horizontal surfaces will be studied.

With $\varphi = 0$ the governing Eqs. (3.8)-(3.10) reduce to

$$\nabla^2 \Psi = Da\ \nabla^4 \Psi - R \frac{\partial T}{\partial y} \tag{3.33}$$

$$\nabla^2 T = \frac{\partial \Psi}{\partial y} \frac{\partial T}{\partial x} - \frac{\partial \Psi}{\partial x} \frac{\partial T}{\partial y} \tag{3.34}$$

The governing Eqs. (3.33) and (3.34) together with the approximation, Eqs. 3.13, yield the following differential equations

$$\frac{d^4 \Psi}{dx^4} - \alpha^2 \frac{d^2 \Psi}{dx^2} = RC\alpha^2 \tag{3.35}$$

and

$$\frac{d^2 \theta}{dx^2} = C \frac{d\Psi}{dx}$$

where $\alpha^2 = Da^{-1}$. The constant C depends upon R and Da and the thermal boundary conditions imposed on the end regions of the cavity.

The thermal boundary conditions are

$$\frac{\partial T}{\partial x} = a \qquad \text{at} \quad x = \pm\ 1/2 \tag{3.36a}$$

$$\frac{\partial T}{\partial y} = b \qquad \text{at} \quad y = \pm A/2 \tag{3.36b}$$

The constants a and b for bottom heating are a=1, b=0, while for sidewall heating they are a=0, b=1.

Integration of Eq. (3.34) over the control volume illustrated in Fig. 3.1, together with the thermal boundary conditions, yield

$$\int_{-1/2}^{1/2} \left(vT - \frac{\partial T}{\partial y}\right)\Big|_y dx = -b \tag{3.37}$$

at any y position.

3.3.3.1 All boundaries rigid

The hydrodynamical boundary conditions over the whole perimeter of the enclosure are the no-slip condition. Both Ψ and its normal derivative are zero at all boundaries. The solutions to Eqs. (3.35) are

$$\Psi = \frac{RC}{2\alpha}\left[\left(\frac{\cosh(\alpha x)}{\sinh(\alpha/2)} - \coth(\alpha/2)\right) - \alpha(x^2 - 1/4)\right] \tag{3.38a}$$

$$T = Cy+x\left[a + \frac{RC^2}{24}(4x^2-3)\right] - \frac{RC^2}{2\alpha^2}\left[\frac{\sinh(\alpha x)}{\sinh(\alpha/2)} - \alpha x \coth(\alpha/2)\right] \tag{3.38b}$$

To obtain an expression for the constant C, condition (3.37) can be used to give

$$R^2 C^2 \left[\frac{\coth(\alpha/2)}{12\alpha^3}(\alpha^2-6) - \frac{\coth^2(\alpha/2)}{8\alpha^2}\left[\frac{1}{\cosh^2 \alpha/2} + 2\right] - \frac{1}{120} + \frac{2}{\alpha^4} + \frac{\sinh\alpha}{8\alpha^3 \sinh^2(\alpha/2)}\right] + aR\left[\frac{1}{12} - \frac{\coth(\alpha/2)}{2\alpha} + \frac{1}{\alpha^2}\right] - 1 - \frac{b}{C} = 0 \tag{3.39}$$

The value of the axial temperature gradient C may be evaluated numerically from the above equation, for a given Darcy-Rayleigh number R and Darcy number Da, using a Newton-Raphson scheme. On taking the appropriate values of a and b, Eqs. (3.38) and (3.39) can be applied to both botton and side wall heating.

In the particular case of a cavity heated from the bottom (a=1, b=0), Eq. (3.39) gives

$$C = 0 \tag{3.40a}$$

or

$$C = \pm \sqrt{\left[1 - R\left(\frac{1}{12} + \frac{1}{\alpha^2} - \frac{\coth(\alpha/2)}{2\alpha}\right)\right]/A} \qquad (3.40b)$$

where

$$A = R^2 \left[\frac{\coth(\alpha/2)}{12\alpha^3}(\alpha^2-6) - \frac{\coth^2(\alpha/2)}{8\alpha^2}\left[\frac{1}{\cosh^2(\alpha/2)} + 2\right] \right. \qquad (3.41)$$

$$\left. - \frac{1}{120} + \frac{2}{\alpha^4} + \frac{\sinh\alpha}{8\alpha^3 \sinh^2(\alpha/2)}\right]$$

When the Darcy-Rayleigh number R is below a critical value R_c, there is no convective flow possible and the only value of C is zero. Heat transfer is through conduction alone. However, when R is above R_c, there are two additional convective solutions representing symmetrical clockwise and counterclockwise circulation. Substituting $R=R_c$ and $C=0$ into Eq. (3.40b), it is found that

$$R_c = \frac{1}{(Da+1/12)-(Da/2)\coth(1/2\,Da)} \qquad (3.42)$$

This prediction of the critical Darcy-Rayleigh number is correctly obtained from the present parallel-flow analysis because the convection that occurs when a constant heat flux or a constant pressure is applied on the boundaries of a horizontal layer is at zero wave number. Using linear stabil-

ity analysis Nield (1968), in the case of a porous layer, and Sparrow et al. (1964), for a fluid layer, found zero wave numbers for the onset of convection.

From the temperature distribution, the Nusselt number is

$$Nu = \frac{1}{1-(RC^2/12)[1+(6/\alpha^2)(2-\alpha \coth(\alpha/2))]} \tag{3.43}$$

i) Darcy porous medium limit

As Da→0, the Brinkman equation reduces to Darcy's law. In this limit, we obtain

$$\Psi = \frac{RC}{2}\left[\frac{1}{\alpha}(e^{\alpha(x-1/2)} + e^{-\alpha(x+1/2)} - 1)-(x^2 - 1/4)\right] \tag{3.44a}$$

$$T = Cy + x\left[a + \frac{RC^2}{24}(4x^2 - 3)\right] \tag{3.44b}$$

$$R^2C^3 + 10C(12 - aR) - 120b = 0 \tag{3.45}$$

Also, for bottom heating we can get

$$Nu = \frac{1}{(1/6) + (10/R)} \tag{3.46a}$$

and

$$R_c = 12 \tag{3.46b}$$

which have been obtained by Vasseur et al. (1987) and Nield (1968) , respectively.

ii) Viscous fluid limit

For $Da \to \infty$, the governing equations are those for a viscous fluid. In this case

$$\Psi = \frac{Ra\ C}{24}\left[x^4 - x^2/2 + 1/16\right] \tag{3.47a}$$

$$T = Cy + x\left[a - \frac{Ra\ C^2}{120}(x^4 - 5x^2/6 + 5/16)\right] \tag{3.47b}$$

$$Ra^2 C^3 + 504C(720 - a\ Ra) - 362{,}880b = 0 \tag{3.48}$$

where Ra=R/Da is the Rayleigh number for a viscous fluid. This Rayleigh number does not depend on the permeability of the porous medium and should not be confused here with the Darcy-Rayleigh number R used for a porous medium.

For a bottom-heated cavity,

$$Nu = \frac{1}{(3/10)+(504/Ra)} \tag{3.49a}$$

and

$$Ra_c = 720 \tag{3.49b}$$

respectively. These results have been obtained by Vasseur et al. (1987) in a study of the natural convection in an inclined fluid layer with uniform heat flux. The critical Rayleigh number was given by Sparrow et al. (1964)

3.3.3.2 Upper surface free, lower rigid

We assume that surface tension is negligible and that the free surface remains horizontal everywhere. Since there is no shear stress at the free surface, Ψ and its second normal derivative are both zero. Applying the same procedure as before, it is found that the streamfunction and temperature field are given by

$$\Psi = -\frac{A}{\alpha} e^{\alpha x} + \frac{B}{\alpha} e^{-\alpha x} - RC\frac{x^2}{2} - Dx + F \tag{3.50a}$$

and

$$T = Cy + C\left[\frac{A}{\alpha^2} e^{\alpha x} + \frac{B}{\alpha^2} e^{-\alpha x} + RC\left(\frac{x^3}{6} + \frac{Dx^2}{2} - Fx\right)\right] + ax + G \tag{3.50b}$$

where

$$A = \frac{RC}{H}\left[\frac{\alpha e^{\alpha/2}}{2} + e^{-\alpha/2} - \frac{2}{\alpha}\sinh(\alpha/2)\right]$$

$$B = \frac{RC}{H}\left[\frac{\alpha e^{-\alpha/2}}{2} - e^{\alpha/2} + \frac{2}{\alpha}\sinh(\alpha/2)\right]$$

$$D = \frac{RC}{H}\left[\frac{4\ \sinh^2\ \alpha/2}{\alpha} - \sinh\ \alpha\right]$$

$$F = -\frac{RC}{8} + \frac{RC}{H\alpha}\left[1 + (2-\alpha^2)\left(\frac{\cosh\ \alpha}{2} - \frac{\sinh\ \alpha}{\alpha}\right)\right]$$

$$G = -\frac{RC^2}{H\alpha^2}\left[\alpha\ \cosh(\alpha/2) + \frac{2(1-\alpha)}{\alpha}\ \sinh(\alpha/2)\right]$$

$$H = 2\ (\sinh\ \alpha - \alpha\ \cosh\ \alpha) \tag{3.51}$$

From condition (3.37), the value of C is given by

$$\sinh\ \alpha\left(\frac{A^2+B^2}{\alpha^3}\right) - \cosh(\alpha/2)D\left(\frac{A+B}{\alpha}\right) + \left(\frac{2AB}{\alpha^2}\right)$$

$$+\sinh(\alpha/2)D\left[\frac{4}{\alpha^2} + \frac{1}{4}\right]\left[\frac{A+B}{\alpha}\right] + \frac{R^2C^2}{480}$$

$$+\ 2\ \sinh(\alpha/2)\left[F - \frac{a}{C} - \frac{2RC}{\alpha^2} - \frac{RC}{8}\right](A-B)/\alpha^2$$

$$+\ \cosh(\alpha/2)\left[-F + \frac{a}{C} + \frac{2RC}{\alpha^2} + \frac{RC}{24}\right](A-B)/\alpha$$

$$+\ \frac{1}{12}\left(aR - FRC + \frac{D^2}{2}\right) - 1 - \frac{b}{C} = 0 \tag{3.52}$$

It is also possible to obtain explicit expressions for and Nu for a bottom-heated cavity. However, since the algebra is straightforward and the expressions lengthy, they will not be presented here. Of particular interest is the critical Darcy-Rayleigh number R_c, which is given by

$$R_c = \frac{1}{1/12+[(\cosh^2(\alpha/2))/\alpha^2 H](\alpha-2\tanh(\alpha/2))[2+(\alpha-4/\alpha)\tanh(\alpha/2)]} \tag{3.53}$$

Viscous fluid limit

For $Da\to\infty$, it is readily shown that

$$\Psi = \frac{Ra\ C}{24}\left[x^4 - \frac{x^3}{2} - \frac{3}{4}x^2 + \frac{x}{8} + \frac{1}{8}\right] \tag{3.54a}$$

$$T = Cy + x\left[a - \frac{RaC^2}{120}\left(x^4 - \frac{5}{8}x^3 - \frac{5}{4}x^2 + \frac{5}{16}x + \frac{5}{8}\right)\right] \tag{3.54b}$$

$$Ra^2 C^3 + \frac{4536}{19}C(320 - a\ Ra) - \frac{1,451,520}{19}b = 0 \tag{3.55}$$

while, in the particular case of a bottom-heated cavity, the Nusselt number and critical Rayleigh number are

$$Nu = \frac{1}{(193/760)+(4536/19Ra)} \tag{3.56a}$$

and

$$Ra_c = 320 \tag{3.56b}$$

3.3.3.3 Both horizontal surfaces free

If both upper and lower surfaces are free, the resulting streamfunction and temperature fields are

$$\Psi = \frac{RC}{\alpha^2}\left[\left(\frac{\cosh(\alpha x)}{\cosh(\alpha/2)} - 1\right) - \frac{\alpha^2}{2}\left(x^2 - \frac{1}{4}\right)\right] \tag{3.57a}$$

and

$$T = Cy + x\left[a + RC^2\left(\frac{x^2}{6} - \frac{1}{8} + \frac{1}{\alpha^2}\right)\right] - \frac{RC^2}{\alpha^3}\frac{\sinh(\alpha x)}{\cosh(\alpha/2)} \tag{3.57b}$$

The axial temperature gradient C is determened from

$$2R^2C^2\left[\frac{\sinh(\alpha) - \alpha}{4\alpha^5\cosh^2(\alpha/2)} + \frac{1}{960} + \frac{1}{24}\left(\frac{a}{RC^2} + \frac{1}{\alpha^2} - \frac{1}{8}\right)\right.$$

$$- \frac{1}{6\alpha^5\cosh(\alpha/2)}\left[\cosh(\alpha/2)\left(3\alpha + \frac{\alpha^3}{8}\right) - 3\left(\frac{\alpha^2}{4} + 2\right)\sinh(\alpha/2)\right] \tag{3.58}$$

$$\left. - \frac{1}{\alpha^3\cosh(\alpha/2)}\left[\frac{2}{\alpha^2} + \frac{a}{RC^2} - \frac{1}{8}\right]\left[\frac{\alpha}{2}\cosh(\alpha/2) - \sinh(\alpha/2)\right]\right] - 1 - \frac{b}{C} = 0$$

For a bottom-heated cavity, the Nusselt number is given by

$$Nu = \frac{1}{1 + (RC^2/\alpha^2)[1 - (\alpha^2/12) - (2/\alpha)\tanh(\alpha/2)]} \tag{3.59}$$

The critical Darcy-Rayleigh number is

$$R_c = \frac{1}{2Da^{3/2}\ \tanh[1/(2Da^{1/2})] + (1/12) - Da} \tag{3.60}$$

Viscous fluid limit

For $Da \to \infty$, the above equations reduce to

$$\Psi = \frac{Ra\ C}{8}\left[\frac{x^4}{3} - \frac{x^2}{2} + \frac{5}{48}\right] \tag{3.61a}$$

$$T = Cy + x\left[a - \frac{Ra\ C^2}{120}\left(x^4 - \frac{5}{2}x^3 + \frac{25}{16}\right)\right] \tag{3.61b}$$

$$Ra^2 C^3 + \frac{3024}{31} C(120 - a\ Ra) - \frac{362{,}880}{31} b = 0 \tag{3.62}$$

and, for a bottom-heated cavity, we have

$$Nu = \frac{1}{(29/155) + [3024/(31\ Ra)]} \tag{3.63a}$$

and

$$Ra_c = 120 \tag{3.63b}$$

3.4 NUMERICAL SOLUTION

Solution for the flow field and the temperature distribution within the cavity may be found by standard numerical

methods. The governing equation for stream function (3.8), vorticity (3.9), and temperature (3.10) are first discretized according to a central difference scheme. The discretized equations for Ψ, ω and T are then solved twice at each time step, using the latest available field values, until convergence to a steady solution is achieved. Boundary conditions (3.11a) and (3.11b) are used for T and Ψ respectively. For the vorticity equation, the latest values of ω from Eq. (3.8) on the boundaries are used to obtain the new field values.

The discretized Poisson equation for ψ is solved explicitly with a successive over-relaxation method whereas the T and ω equations are solved using an alternating directions implicit method. The resultant set of finite-difference equations is tridiagonal in form and therefore both easy and economical to solve on a computer. In order to achieve both the desirable accuracy and the dominance of the principal diagonal of the tridiagonal systems of the finite difference equations, very small time steps are used.

The adiabatic boundary condition for the temperature equation is implemented at the strip wall using image points. A first-order formulation for the vorticity boundary condition is used since second-order formulations have been

reported to generate unstable solutions at low Darcy numbers. It is believed that this is due to the velocity profiles associated with the Brinkman-extended Darcy model, which display a peak very close to the wall (Lauriat and Prasad (1987)).

Convergence of the solution is based on the criterion

$$\frac{\Sigma|f_{k+1}-f_k|}{\Sigma|f_k|} < R_{es} \tag{3.64}$$

where f stands for Ψ, T or ω and the subscript k indicates the iteration order. The summation is over all mesh points. In most cases the residue, R_{es}, was set equal to 10^{-4} for Ψ and 10^{-5} for both T and ω. The converged results were stored on disk after each run to be used as initial condition for the next calculations.

The numerical results exhibited in this chapter were all obtained using uniform grids. A grid of 51 x 51 was found to model accurately the flow fields described in the results. Increasing the number of grid points further had no visible effect on the numerical results. For example , for $Da=10^{-6}$ (Darcy medium) and R=250, increasing the number of grid points from 2601 to 6561 yielded an increase in the value of

the Nusselt number of only 1.35%. in order to check the accuracy of the results, an energy balance was used for the system. For this the heat transfer through each x=constant plane was evaluated at each location for $-1/2 \leq x \leq 1/2$, and compared with the heat input at x=1/2. For most of the results reported here, the energy balance was satisfied to within 1-2%.

3.5 RESULTS AND DISCUSSION

It has been shown that the problem is dependent upon Rayleigh number R, Darcy number Da, angle of inclination φ and aspect ratio A. However, the flow structure and heat transfer over the central part of the cavity become independent of A provided that the aspect ratio is made large enough for the parallel flow assumption to be valid. In fact, with the thermal boundary conditions considered here, parallel flow can be easily established if the end effects are not very strong, i.e., if the aspect ratio and/or the Rayleigh number are large enough. For a Darcy medium (Da=0), it has been demonstrated numerically by Vasseur et al. (1987) that, for $R \leq 500$, this is indeed the case when $A \geq 2$. All the numerical results presented in this study were obtained for cavities with an aspect ratio A=3 and 4. It is worthwhile mentioning here that this behavior cannot be generalized to the

case of cavity with isothermal walls for which the solution does depend upon the aspect ratio of the cavity no matter how large is the aspect ratio (see for instance Prasad and Kulacki, (1983)).

Numerical results were obtained for a wide range of Rayleigh numbers extending from the pseudo-conduction to the boundary layer regimes, and for various values of Da and φ. Some typical results are presented in Figs. 3.2(a) to 3.2(i) which clearly illustrate the fact that, in the core of the cavity, the flow can be considered as parallel, i.e. with u = 0. At each end of the cavity the flow is turned around in regions that are approximately square. This is to be expected since, as demonstrated analytically among others by Sen (1987), the length scale characterizing the flow in the end regions is comparable to the depth of the cavity.

Effects of the Darcy number are illustrated in Figs. 3.2(d) to 3.2(f) corresponding to R=250 and $\varphi=90^{\circ}$. The streamlines of Fig. 3.2(d), with $Da=10^{-4}$, are closely spaced near the solid boundaries, this result indicating that the fluid velocity is a maximum in this region. This is expected since when Da is small enough, i.e., when the viscous term which is responsible for the boundary effects becomes negligible, the Brinkman model predicts results qualitatively

similar to Darcy's law which allows fluid to slip on a solid boundary. However, as the Darcy number is increased the viscous Brinkman term becomes gradually more important and slows down the flow in the neighborhood of the walls as can be seen by comparing Figs. 3.2(d)-3.2(f). In particular, the isotherms and streamlines of Figs. 3.2(f), with Da=1, are characteristic of a pseudo-conduction regime. Effects of increasing Rayleigh number can be observed from Figs. 3.2(g)-3.2(i) with $\varphi=80^0$ and $Da=10^{-3}$. The development of the boundary flow regime with an increasing Rayleigh number is clearly illustrated by the formation of a plateau in the core region as well as by the steepness of the temperature and velocity profiles near the thermally active walls.

The isotherms and streamlines for $Da=10^{-4}$, 5×10^{-2} and 10^{-1} and R=250 are presented in Figs. 3.3(a) to 3.3(c) for the case of a horizontal cavity with all rigid boundaries, heated from the bottom. It is seen from these figures that the flow rate within the cavity decreases significantly as Da increases. The streamlines become relatively more and more sparsely spaced near the solid boundaries, and the strong flow circulation depicted in Fig. 3.3(a) decreases as Da increases. This indicates that the viscous Brinkman term becomes gradually more important and slows down the fluid in the neighborhood of the walls. Consequently, the maximum

horizontal velocity drifts gradually from the solid wall toward the horizontal middle plane. The sequence of Figs. 3.3(a) to 3.3(c) also illustrates the effect of Da on the temperature field. When Da is small, the extreme contortion of the isotherms in Fig. 3.3(a) provides some indication of the velocity of the fluid. As Da increases, the flow is gradually inhibited by the viscous forces; the temperature field indicates that heat transfer by conduction becomes relatively more important than that due to convection. Figure 3.3(d) shows the results obtained for $Da=5x10^{-2}$ and R=250 in the case of a cavity, with all rigid boundaries, heated from the side. It is evident from Figs. 3.3(b) and 3.3(d) that, for the same values of R and Da, the magnitude of the convection with bottom heating is higher than that with side wall heating.

Typical streamlines and isotherms for a cavity with an upper free surface are presented in Figs. 3.3(e) and 3.3(f) with bottom heating and side wall heating respectively. The absence of shear at the free surface of the cavity results in larger horizontal velocities at the top than at the bottom of the cavity. Consequently, the center of the eddy is displaced upwards. Dimensionless temperature distributions are nearly anti-symmetrical, with deviations from anti-symmetry due to higher velocities at the free surface. As in the case of a

cavity with all rigid boundaries, the convective heat transfer for a given set of R and Da is greater for a cavity heated from the bottom than for a cavity heated from the side.

The dependence of the stream function at the center Ψ_c on the Darcy number Da and Darcy-Rayleigh number R is presented in Figs. 3.4a and b for bottom heating and side wall heating, respectively. The convection becomes less and less vigorous as the Darcy number (i.e., viscous effects) is increased. The limits for Darcy's law ($Da \to 0$) and viscous fluid ($Da \to \infty$) are also presented on these graphs as dashed lines for comparison. When Da is sufficiently small, the prediction of the Brinkman model is in agreement with Darcy's law. As R is increased, a smaller Da is required to obtain such an agreement.

Figures 3.5 and 3.6 show the dependence of the Nusselt number Nu on R and Da for a cavity with all rigid boundaries, heated from the bottom. For a given Da there is a critical Darcy-Rayleigh number R_c, below which convection is not possible. Thus, for each of the Darcy numbers considered in Fig. 3.5, the Nusselt number approaches the conduction solution, $Nu \to 1$ and $\Psi_c \to 0$ as $R \to R_c$. The limits are $R_c = 12$ for Darcy's law ($Da \to 0$) and $Ra_c = R_c / Da = 720$ for a viscous fluid

($Da \to \infty$) . From Fig. 3.6 it is seen that, as usual, the Nusselt number increases with R, but the effect of the Darcy number is just the reverse. Thus, for a given value of R, the Nusselt number decreases toward unity as the Darcy number increases. For example, the heat transfer is by conduction alone up to R=500 when Da=0.6. Although in general the Nusselt number increases with R, it is clear from Fig. 3.5 that Nu tends asymptotically toward a constant value that depends on Da. For instance, according to Eqs. (3.46a) and (3.39a), $Nu \to 6$ for a Darcy medium ($Da \to 0$), while $Nu \to 10/3$ for a viscous fluid ($Da \to \infty$), respectively. This surprising result has not been observed for a cavity heated from the side, where Nu always increases with R. However, the flow structure in the two cases is quite different. For instance, with side wall heating the horizontal surfaces are insulated and the x dependence of the temperature field is characterized by a slightly stable stratification. On the other hand, with bottom heating the lower horizontal surface is heated while the upper one is cooled, this situation resulting in a strongly unstable stratification of the layer.

From the numerical results it was observed that, when R is relatively small, the flow structure consists simply of a layer of hot fluid in the lower half of the cavity, below a layer of cold fluid in the upper half. As R is increased,

convective motion gradually brings more and more hot fluid into the upper layer and cold fluid into the lower layer, giving rise to the formation of two new layers of fluid in the central part of the cavity. The flow structure is then made up of a thin layer of cold fluid below a thin layer of hot fluid, near the center of the cavity, these two layers being sandwiched between two thick layers of cold and hot fluid located respectively near the upper and lower horizontal boundaries. As R is further increased, the thickness of the two centrally located layers increases while that of the layers adjacent to the boundaries decreases. However, this process cannot continue indefinitely since it would result in the disappearance of the two layers of fluid adjacent of the boundaries, which is impossible because of the thermal boundary conditions applied there. Ultimately, an equilibrium has to be reached where the thickness of the fluid layers and the Nusselt number remain constant even if the Darcy-Rayleigh number is increased further.

Good agreement between the numerical results and the analytical solution is observed in Figs. 3.5 and 3.6. In Fig. 3.5 it was not possible to obtain numerical results beyond the Darcy-Rayleigh numbers depicted on the graph, since the flow was found to become oscillatory. Hence there should be a certain limit for the Darcy-Rayleigh number over which the

analytical solution is also not valid. This limit could be determined from a stability analysis of the parallel flow in the core region. It should also be mentioned that, in the case of a cavity heated from the bottom by a constant heat flux, the unicellular flow discussed in this study is not the only mode of convection possible since, as already discussed by Vasseur et al. (1987), this situation may also lead to Bénard-type multicellular convective motion, for which the present theory is naturally not valid.

The prediction of Nu for the case of a cavity heated from the side by a constant heat flux requires a knowledge of the temperature distribution on the vertical walls. This necessitates a detailed analysis of the flow and temperature patterns in the end regions as carried out, for instance, by Cormack et al. (1974) for a shallow cavity with differentially heated end walls. Since, in the present study, the end regions have been considered only through a control volume analysis, it is not possible to obtain an analytical expression for Nu. As a substitute, the temperature difference $\Delta T=T(1/2,0)-T(-1/2,0)$ at the $y=0$ section is used in Fig. 3.7 to characterize the temperature field. Since the heat transfer is globally in the y direction, ΔT is relatively small and varies little with R. All the curves in Fig. 3.7 are observed to pass through a maximum at a value of Da that

depends on R. The peaks are also predicted by the viscous limit of Eqs. 3.47b and 3.48 with a=0 and b=1, and occur at Da=R/1205. They result from the fact that, for a given value of R, ΔT goes from zero as $Da \to \infty$ (that is, $Ra=R/Da \to 0$; pure conduction state) to a maximum value and then back to zero in the other limit $Da \to 0$ (that is, $Ra \to \infty$, where the vertical heat diffusion contributes to the reduction in T).

The variation of the Nusselt number with α^2 (Da^{-1}), for a typical value of R=100 is presented in Fig. 3.8 for a cavity heated from the bottom. In the same figure, the Nusselt number obtained from Darcy's law is also shown as a horizontal dashed line. It is clear from Fig. 3.8 that with R fixed, the Nusselt number increases as α^2 increases (that is, Da decreases) for the three hydrodynamic boundary conditions considered in this study. As expected, all the curves are seen to approach the Darcy value asymptotically as $Da \to 0$. Furthermore, it is apparent from Fig. 3.8 that the heat transfer rate for a cavity with all rigid boundaries is smaller that for a cavity with either one or two free surfaces. This result is reasonable on physical grounds since, when a surface is rigid (that is, with no slip) heat transfer through this surface must be by conduction. However, the tangential velocity permitted by a zero-shear free surface allows convection to play a role in the heat transfer pro-

cess. As can be seen from Fig. 3.8, the analytical and numerical results, although quite close, do not match as well for the free-free case as compared to the rigid-rigid case. Numerically it is easier to approximate a rigid surface than a free surface . The numerical results for the free-free case could have been improved by using a finer mesh size in the vicinity of the free surfaces. However, because of the additional computational expense, this was not considered necessary.

Tables 3.1 to 3.4 show the analytically predicted heat transfer and stream function at the center (Ψ_c) as a function of R and Da for a cavity with one and two free surfaces, and for a cavity heated from the bottom and by the side. In these tables the values in brackets were obtained numerically. The results clearly indicate that for all the cases considered, both the heat transfer and convective motion decrease as Da increases for the same value of R. The same trend is observed as R decreases with Da fixed. With a given set of R and Da, it is observed that the heat transfer for a cavity with two free surfaces is always greater than that for a cavity with a single free surface, especially when the permeability of the medium is large. For instance, the percentage increase in the heat transfer rate is about 7.5% when R=300 and Da=5×10^{-4} and 27.5% when R=300 and Da=5×10^{-2} (see Tables 3.1 and 3.3).

The critical Darcy-Rayleigh number R_c for the onset of convection in a Brinkman layer heated from the bottom by a constant heat flux is plotted in Fig. 3.9 as a function of Da for the three hydrodynamical boundary conditions considered in this study. The solid curves are the results of Eqs. (3.42), (3.53) and (3.60), respectively. As mentioned earlier, the critical Darcy-Rayleigh number $R_c=12$ for a Darcy medium has been obtained by Nield (1968). On the other hand, the value $Ra_c=120$, for the case of a fluid layer with both boundaries free, has been obtained independently by Hurle et al. (1967) and Nield (1967). All these results are presented as broken lines in Fig. 3.9. When the Darcy number is small ($\approx 10^{-4}$), the three curves are seen to approach the Darcy value as an asymptote. This is to be expected, since in the limit $Da \to 0$ the Brinkman model reduces to Darcy's law and, except in a very thin layer near the boundaries, the velocity profile is the same in both models. However, when Da is large (≈ 1), each of the curves tends asymptotically toward the particular critical Rayleigh number obtained for a horizontal layer of fluid with corresponding hydrodynamical boundary conditions. For intermediate values of Da a smooth transition of the curves between these limits is observed.

Considering the Brinkman model, the onset of convection in a fluid-saturated permeable layer has been investigated

recently by Rudraiah et al. (1980). Using a single-term Galerkin expansion, the critical Rayleigh number was obtained for various boundary conditions in terms of the Darcy number. In particular, for the case of a cavity with all rigid boundaries heated from the bottom with a constant heat flux, it was found that

$$Ra_c = 720 + 17.14\ Da^{-1} \tag{3.65}$$

such that $Ra_c = 720$ when $Da \to \infty$ and $R_c = 17.14$ when $Da \to 0$. Although the above equation predicts the viscous situation correctly, it obviously gives the wrong result in the case of a Darcy medium. On the basis of this result it was concluded by Nield (1983) that it is not always justifiable to use the Brinkman equation within the bulk of a porous medium whose porosity is not close to unity. However, Eq. (3.65) does not predict correctly the critical Darcy-Rayleigh number for a Darcy medium due to the inaccurate approximation used by Rudraiah et al. (1980) to solve the Brinkman equation, rather than on some limitation of the equation itself. In fact, the exact solution of this problem is given by Eq. (3.42), which yields the correct result $R_c = 12$ as $Da \to 0$. The case of a Brinkman layer with lower boundary rigid and upper boundary free has also been considered by Rudraiah et al. (1980), for which it was found that

$$Ra_c = 320 + 15.238\ Da^{-1} \tag{3.66}$$

while, for a layer with both boundaries free,

$$Ra_c = 120 + 12.143\ Da^{-1} \tag{3.67}$$

Here also, the above results predict the exact critical Rayleigh number for the viscous case but show discrepancies with the Darcy's law solution.

Attention will now be directed to a vertical cavity ($\varphi = 90^\circ$), this situation being of practical interest. Fig. 3.10 and 3.11 show respectively, the stream function at the center of the cavity, Ψ_c, and the Nusselt number, Nu, as a function of R for different Da obtained from the analysis together with the corresponding results calculated from the numerical procedure described in the previous section. The curve for Da =0 represents the limiting case of a Darcy medium while that for Da=1 corresponds, approximately, to a viscous fluid. The effect of an increase in the Darcy number appears to be very similar at all Rayleigh numbers. As the permeability of the porous medium, and hence Da, is increased the boundary frictional resistance (Brinkman) becomes gradually more important, adding to the bulk frictional drag induced by the solid matrix and thus reducing the convective motion (see Fig. 3.10). As a result, relatively less heat is removed from the thermally active walls and the Nusselt number decreases with Da. From Fig. 3.11 it is also evident that,

when the Rayleigh number is high, the Nusselt number increases at a faster rate with a decrease in Da. The analytical solution of the boundary layer regime obtained by Vasseur and Robillard (1987) using an Oseen approach is shown on these graph by dotted lines. Good agreement between both theories is observed when the Rayleigh number is high enough. It can also be observed from Figs. 3.10 and 3.11 that much larger Rayleigh number are required at high Darcy numbers for the boundary layer flow regime to start. In both Figs. 3.10 and 3.11 the numerical results are seen to be in good agreement with the analytical solution.

Consideration will be given next to the effect of angle of inclination, typical results being presented in Figs. 3.12 to 3.15.

Figures 3.12(a)-(c) show the velocity profiles at mid-height of the enclosure for R=100 and various values of Da at $\varphi=30^\circ$, 90° and 120° respectively. At a fixed inclination angle a significant change in the velocity field with an increase in the Darcy number is observed to occur. The smaller the Darcy number, the closer it follows the Darcy medium profile (Da=0) which is shown as a dotted line in the graphs. With Darcy's model the no-slip boundary condition is not satisfied and the velocity is maximum at the wall. In

Brinkman's model, the velocity is zero at the wall, increases to a peak value and then drops back to zero in the core region of the enclosure. As the value of Da increases, not only does the position of the peak velocity shift away from the wall but its magnitude is considerably reduced. It is noted in Figs. 3.12(a)-(c) that, for some values of Da, the velocity in the core of the cavity can be greater than the Darcy velocities. In fact for a given x it is seen that in the core, v goes through a maximum as Da is reduced. A similar trend has been reported recently by Lauriat and Prasad (1983) and was found to be related to the relative magnitudes of the diffusion and the buoyancy terms. Thus, for a given R, when Da is small enough the viscous forces have no effect in the core. The diffusion term is confined between the walls and the velocity peaks as well as the velocity profiles in the core follow Darcy's law. At higher Darcy numbers, the viscous and buoyancy terms are of the same magnitude and the vorticity diffuses through the entire cavity. The velocity in the core may then be greater than the Darcy profile, as depicted by the curves for $Da=10^{-3}$ and 10^{-2} in Fig. 3.12(a). With Da increased further, viscous effects become more important, the buoyancy induced convection within the cavity is reduced, and the velocity profiles approach those in a fluid cavity. Thus the curves for $Da=10^{-1}$ and $Da=1$ in Fig. 3.12(a) are below the Darcy profile. The effect of

the orientation angle on the velocity profile, at a fixed Darcy number, is illustrated in Figs. 3.12(a)-(c). The curves illustrate the fact that, in general, the convection becomes less and less vigorous as the orientation angle of the cavity is increased. The effect of Da and φ on temperature profiles at y=0 is illustrated in Figs. 3.13(a)-(c). All the curves have a constant slope on the wall (x=-1/2) since constant heat flux is prescribed on it. When Da is small, the convective motion is high since the only resistance to the flow within the porous medium results solely from the presence of the solid matrix. Since the same quantity of heat is extracted from the wall, the wall temperature drops to a minimum value when Da=0. However, as Da is increased the effect of the viscous term becomes more important, the convection motion reduces, less heat is removed from the wall and its temperature increases significantly.

Figure 3.14 shows the variation of Ψ_c, the stream function at the center of the layer, with angle of inclination φ, for various values of Da at a fixed R=500. Figure 3.14 shows the corresponding variation of Nu. Since the transformation $\varphi \to -\varphi$, $\Psi \to -\Psi$, $T \to T$, $y \to -y$, $x \to -x$ does not alter the governing equations, nor the boundary conditions (3.10)-(3.13), the flow is symmetric in opposite quadrant. Therefore only results in quadrant 1 and 4 are presented. The

continuous lines in the first quadrant represent natural flow (for $\varphi > 0$) while the dashed lines in the third quadrant represent the anti-natural flow (for $\varphi<0$). Thus the antinatural flow for $\varphi>0$, in the second quadrant would be the mirror image of the antinatural flow for $\varphi<0$ in the fourth quadrant. When Da=1, there is only one steady state for each inclination φ. However, for Da$\geq$0.35 three values of Ψ_c and Nu are possible for inclination around zero. The range of inclination for multiple steady states is a function of both the Darcy number and the Rayleigh number. Verification of the results of analysis by numerical computation is also indicated on Figs. 3.14 and 3.15.

Figure 3.16 shows the variation of the angle at which the maximum heat transfer rate across the cavity occurs, φ_n, with Rayleigh number for various values of the Darcy number. For small R, i.e. the pseudo-conduction regime, the temperature field is conduction dominated. The largest buoyancy force and circulation take place when the cavity is vertical, i.e. when the temperature gradient is horizontal. Thus all the curves in Fig. 3.16 tend towards $\varphi_n=90^\circ$ when R is small enough. Naturally, as the Darcy number is increased the effect of the viscous term is enhanced and the pseudo-conduction regime is maintained up to relatively higher values of R. For intermediate R, i.e. in the asymptotic regime, the variation of the

angle φ_n with R is complex. For all the Darcy numbers considered, when R increases φ_n first decreases down to a value of approximately 33.5° and then starts to increase again. The smaller the Darcy number, the smaller the Rayleigh number required to reach the minimum value of φ_n. Finally, when R is large enough, i.e. in the boundary layer regime, all the curves tend again towards φ=90°, i.e. the maximum heat transfer occurs when the cavity is vertical. a similar trend has been reported in the past by several authors while studying numerically the natural convection of a fluid (Da>> 1) in an inclined cavity with two opposing isothermal wall (see for instance Catton, (1978)).

3.6 SUMMARY

In the present Chapter, the problem of laminar convection within a thin (A>>1) inclined rectangular cavity, filled with a fluid saturated porous layer, has been solved by both numerical and analytical methods. In the formulation of the problem use has been made of the viscous shear stress term due to Brinkman in order to satisfy both the no-slip and impermeable conditions on the bounding rigid surfaces. A constant heat flux is applied for heating and cooling the two opposing walls of the layer while the other two walls are insulated. It is demonstrated that for this heating process,

the flow is quasi-parallel almost everywhere, except in regions adjacent to the end walls, provided that the aspect ratio of the cavity is large enough. Of course, for fixed values of Da and φ, the analytical solution becomes more accurate when either A or R is increased. It can also be expected that in boundary layer regime ($R\to\infty$), the analytical solution can be applied to cavities with an aspect ratio $A=O(1)$. the present analytical solution is found to reduce to the regular Darcy porous medium and viscous flow solutions in the limit of low ($Da<<1$) and high ($Da >>1$) porosities, respectively.

Detailed results for the flow field, temperature distribution, and heat transfer rates have been obtained. From these results, the following remarks are in order.

1. Horizontal cavity:

Two types of thermal boundary conditions are considered. In the first case the cavity is heated from the bottom by a constant heat flux, while in the second the heat flux is applied on the side walls. Results are obtained for (1) a cavity with all rigid boundaries, (2) a cavity with a free upper surface, and (3) a cavity with both horizontal boundaries free.

The results demonstrate the dependence of the Nusselt number on the Darcy-Rayleigh and Darcy numbers. As $Da \to 0$, the flow field is similar to that given by an analysis using Darcy's law, except in a thin region next to a boundary. The viscous effects are largely confined to this region, where the horizontal velocity increases from a zero value at the wall to a peak value. Results obtained from Darcy's law are valid when Da is approximately smaller than 10^{-6}. An increase in Da results in a decrease of the peak velocity and an increase of the thickness of the viscous region. The overall heat transfer reduces significantly with an increase of the permeability (Da) of the porous medium, the reduction being larger at higher Darcy-Rayleigh numbers. When Da is high enough, that is, when the Darcy resistance due to the solid matrix becomes negligible with respect to that resulting from the boundary effects, the present solution approaches that for a viscous fluid. This situation is approximately reached when $Da \approx 1$ for $R=10^2$ and $Da \approx 0.3$ for $R=500$.

For a given set of R and Da, the presence of a free surface was found to increase the heat transfer rate through the cavity significantly, especially when the permeability of the medium is large. For instance, when $R=100$ and $Da=0.01$, the percentage increase in the heat transfer rate, with respect to a cavity with all rigid boundaries, is approxi-

mately 22% for a cavity with a free upper surface and 52% for a cavity with two free surfaces.

The critical Darcy-Rayleigh number for the onset of motion has been obtained explicitly in terms of the Darcy number for each of the hydrodynamical boundary conditions considered in this study. It is shown that the results of viscous fluid ($Da \to \infty$) and the Darcy medium ($Da \to 0$) emerge from the present solution as special cases. The basic reason for this agreement is that a layer heated from the bottom by a constant heat flux becomes unstable at zero wavenumber for which the present analysis is exact.

2. Inclined cavity:

The orientation of the cavity has, for given values of Rayleigh and Darcy numbers, a large effect on the heat transfer rate. For a given value of Da, the maximum heat transfer rate across the cavity occurs at an angle $\varphi_N \to 90^0$ (boundary layer regime). For intermediate values of R (asymptotic regime) the value of φ_N reaches a minimum value of approximately 33.5^0 independently of the Darcy number.

At a given Rayleigh number and for small enough inclinations around bottom heating multiple steady states exist

provided that the Darcy number is sufficiently small. The range of tilt angles for multiple steady states is function of both R and Da.

CHAPTER 4

A POROUS LAYER WITH MULTIPLE PARTITIONS

4.1 LITERATURE REVIEW

Available studies of natural convection in a partitioned cavity are concerned mostly with vertical air- filled enclosures, with the vertical walls held at different temperatures. Duxbury (1979) experimentally investigated vertical rectangular enclosures, divided by heat conducting partitions, for Rayleigh numbers approaching 10^6. The effect of thermal radiation on the configuration considered by Duxbury has been studied numerically and experimentally by Nakamura et al. (1984). Nishimura et al. (1985, 1987) have proposed a boundary layer solution for this system and confirmed its validity by experiments. It was found that the heat transfer rate is independent of the position of the partition if the boundary layer thickness is less than the half-width of each cell constructed by the partition.

Also, the effect of partition position on the heat transfer rate has been investigated numerically by Tony and Gerner (1986). It was concluded that a centrally located partition produces the maximum reduction in heat transfer. Anderson and

Bejan (1981) measured the overall heat transfer through single or double partitions. The net heat transfer was shown to vary inversely with $(1+N)^{0.61}$, where N is the number of vertical partitions inserted in the middle of the enclosure. Numerical results for the case of a vertical cavity with five partitions have been reported by Jones (1980). It was found that the effect of dividing the enclosure into six cells reduces the heat transfer by, approximately, a factor of 6. The effect of inclination angle on the present problem has been considered by Acharya and Tsang (1985). For an enclosure with an aspect ratio of 2 the maximum average Nusselt number is obtained when the system is tilted at an angle of approximately 60^0 with respect to the horizontal plane. A few studies have also been devoted to the case of horizontal enclosures, with multiple partitions, heated from below. The Rayleigh-Bénard stability limit for the multi-layer situation was predicted by Lienhard (1987). The same problem was also considered by Kamiuto (1985,1986) who concluded that equal spacings of the partitions yield the minimum heat transfer rate through the system. Finally, it was demonstrated experimentally by Mishimura et al. (1989) that natural convection in each cell of the multi-layer system is identical to the ordinary Bénard problem, i.e. thermal coupling by conduction through thin partitions with a high conductivity is minute.

The objective of the present chapter is to study analytically and numerically the behavior of natural convection heat transfer in a rectangular, tilted, porous layer with multiple partitions. A constant heat flux is applied for heating and cooling the two opposing walls of the enclosure while the other two walls are insulated. An approximate solution, valid for long shallow systems, is developed. The results of the analysis are verified through numerical calculations.

4.2 STATEMENT OF THE PROBLEM

Consider the natural convective motion of a fluid filling a homogeneous, isotropic, porous medium confined by an impermeable rectangular enclosure divided by N unequally spaced diathermal partitions. The enclosure, shown in Fig. 4.1, is of height H′, width L′ and is tilted at an angle φ with respect to the horizontal plane. The two end walls of the enclosure are insulated while a uniform heat flux q′ is applied along both side walls. The present fully partitioned enclosure may be viewed as N+1 non-partitioned cavities sharing in common N thermally active surfaces. The thermal conditions along those partitions are not known a priori.

Assuming the validity of Darcy's law and the Boussinesq approximation and neglecting inertial effects, the equations

describing, in each of the N+1 non-partitioned cavities, conservation of momentum and energy in the porous medium are, respectively

$$\nabla^2 \Psi_i = -R\left[\frac{\partial T_i}{\partial x} \sin\varphi + \frac{\partial T_i}{\partial y} \cos\varphi\right] \tag{4.1}$$

$$\nabla^2 T_i = \frac{\partial \Psi_i}{\partial y} \frac{\partial T_i}{\partial x} - \frac{\partial \Psi_i}{\partial x} \frac{\partial T_i}{\partial y} \tag{4.2}$$

$$u_i = \frac{\partial \Psi_i}{\partial y}, \qquad v_i = -\frac{\partial \Psi_i}{\partial x} \tag{4.3}$$

where $R=g\beta KL'^2 q'/\alpha\nu k$ is a Darcy-Rayleigh number based on the constant heat flux q', the permeability K of the medium and the overall width L' of the enclosure. In the above equation i (=1, to N+1) refers to a given non-partitioned cavity.

Equations. (4.1) to (4.3) have been reduced to dimensionless form by introducing the following scales

$$(x,y) = (x',y')/L' \qquad \Psi_i = \Psi_i'/\alpha$$
$$T_i = (T'_i - T'_0)/(q'L'/k) \tag{4.4}$$

where the symbols are defined in the nomenclature and primes demote dimensional variables.

The hydrodynamical boundary conditions are zero normal

velocities on all walls, i.e

$$\Psi_i = \frac{\partial \Psi_i}{\partial n} = 0 \qquad \text{on all walls} \qquad (4.5a)$$

where the direction of n is normal to a given wall.

The thermal boundary conditions are

$$x = \eta_k \quad \left[\begin{array}{ll} \left.\frac{\partial T}{\partial x}\right|_{\eta_k} = 1 \; ; & k = 0 \text{ and } N+1 \qquad (4.5b) \\ T_{\eta_k^+} = T_{\eta_k^-} \; ; & k = 1, N \qquad (4.5c) \\ \left.\frac{\partial T}{\partial x}\right|_{\eta^+{}_k} = \left.\frac{\partial T}{\partial x}\right|_{\eta^-{}_k} & \end{array} \right.$$

and

$$y = \pm A/2 \; ; \qquad \frac{\partial T_i}{\partial y} = 0 \qquad (4.5d)$$

where A=H'/L' is the enclosure aspect ratio and η_k (k= 0,N+1) is the position, in the x-direction, of the N partitions and the two side walls of the enclosure. The subscripts + and - indicate the right and the left side of a partition respectively.

Equations. (4.5c) express the continuity of temperature and heat flux at the surfaces of each of the N partitions while Eqs (4.5b) and (4.5d) result from the thermal boundary conditions applied on the enclosure.

Equations. (4.1) to (4.3) together with boundary conditions (4.5), complete the formulation of the problem. The controlling parameters are R, A, φ and η_k (k=1 to N) the position of the N partitions.

4.3 NUMERICAL METHOD

To obtain numerical solution of the complete governing Eqs. (4.1) and (4.2), finite-differences were used. The solutions consist of the stream function and temperature fields in the x and y directions as well as the Nusselt number.

Numerical results have been obtained for the case of an enclosure with a single off-center partition. As mentioned before the thermal conditions along the partition are not known a priori. The solution methodology involves obtaining consecutive solutions for each cell of the enclosure. The calculation process is initiated by solving the left cell with an assumed heat flux distribution along the partition. The resulting temperature at each grid point along the partition is used as the thermal boundary condition for the right cell. Thus, the solution for the right cell can be obtained which provides an updated heat flux distribution along the partition. The calculation is repeated until converged solu-

tions have been obtained in both cavities. Typically 7~10 consecutive calculations are required for complete convergence for which consecutive changes in both the heat flux and the temperature along the partition are less than 1%. This procedure becomes complex as the number of partition increases and for this reason only an enclosure with a single partition has been considered.

4.4 APPROXIMATE ANALYTICAL SOLUTION

In this section an approximate solution to the present problem is presented for the case of a long shallow cavity ($A = H'/L' >> 1$). In this limit, as discussed in Chapter 2 the flow and temperature fields in each of the N+1 cells must be respectively of the following form:

$$\Psi_i(x,y) = \Psi_i(x) \tag{4.6}$$

and

$$T_i(x,y) = Cy + \theta_i(x) \tag{4.7}$$

where C is the temperature gradient along the y direction. The fact that C is the same in each cell follows from Eq. (4.5c).

Substituting Eqs. (4.6) and (4.7) into Eqs. (4.1)-(4.2), the governing equations can be reduced to the following ordi-

nary differential equations

$$\frac{d^3\theta_i}{dx^3} - \alpha^2 \frac{d\theta_i}{dx} = \alpha^2 C \cot\varphi \tag{4.8}$$

and

$$\frac{d^2\theta_i}{dx^2} = -C \frac{d\Psi_i}{dx} \tag{4.9}$$

where $\alpha^2 = RC \sin\varphi$.

Integrating Eqs. (4.8) and (4.9) and making use of Eq. (4.7) and the boundary conditions, Eqs. (4.5), one obtains respectively for each of the i= 1, N+1 cavities

$$\Psi_i = \frac{B}{C}\left[1 - \frac{\cosh\alpha(x - P_i)}{\cosh(\alpha M_i)}\right] \tag{4.10}$$

and

$$T_i = Cy + \frac{B}{\alpha}\left[\frac{\sinh\alpha(x - P_i)}{\cosh(\alpha M_i)} + \tanh(\alpha M_i) + 2\Sigma_1\right] - C\cot\varphi(x - \eta_{i-1}) \tag{4.11}$$

where

$$\Sigma_1 = \begin{cases} 0 & , \quad i = 1 \\ \sum_{k=1}^{i-1} \tanh \alpha M_k & , \quad i \geq 2 \end{cases} \tag{4.12}$$

$$P_i = \frac{(\eta_i + \eta_{i-1})}{2} \quad ; \quad M_i \ (\text{or } M_k) = \frac{\eta_i - \eta_{i-1}}{2}$$

$$B = (1 + C \cot\varphi)$$

In the above equations the constant temperature gradient C depends upon R, φ, η_k (k=1, N) and the thermal boundary conditions imposed on the end region of the enclosure (adiabatic walls). Following the procedure described in Chapter2 (see Eq. (2.14)) it may be shown that the value of C is given by

$$C = - \sum_{i=1}^{N+1} \int_{\eta_{i-1}}^{\eta_i} \left[\frac{d\Psi_i}{dx} T_i \right]_y dx \qquad (4.13)$$

In the above equations the integrations are a sum of the convective heat fluxes in the N+1 cavities. This is derived from the condition of uniform heat flux at the boundaries.

Substituting Eqs. (4.10) and (4.11) into Eq. (4.13) and integrating yields:

$$C = \frac{B^2 \sin\varphi}{2\alpha C} \sum_{i=1}^{N+1} \frac{\sinh(2\alpha M_i) - 2\alpha M_i}{\cosh^2(\alpha M_i)}$$

$$+ \frac{2B}{\alpha} \cos\varphi \sum_{i=1}^{N+1} \tanh(\alpha M_i) - \alpha M_i \qquad (4.14)$$

The value of the axial temperature gradient C may be evaluated numerically from the above equation, for a given

Rayleigh number R, inclination angle φ and position of the N partitions η_k, using a Newton-Raphson scheme.

Since the temperature of each thermally active wall varies linearly in y, the heat transfer rate can be expressed in terms of a Nusselt number at the y=0 section, defined as:

$$Nu = \left[\frac{q'}{\Delta T'} \right] \frac{L'}{k} = \frac{1}{\Delta T} \tag{4.15}$$

where the dimensionless temperature differences $\Delta T = T(1,0) - T(0,0)$. This definition of Nu results from the fact that in the present problem, contrarily to the case of isothermal walls, the effect of convection is not to increase the heat flux across the boundaries but to decrease instead the temperature induced within the enclosure during this heating process.

Substitution of Eq. (4.11) into Eq. (4.15) yields:

$$Nu = \frac{1}{\frac{2B}{\alpha} \left[\sum_{i=1}^{N+1} \tanh(\alpha M_i) \right] - C \cot\varphi \, (1 - \eta_N)} \tag{4.16}$$

In the particular case of a cavity divided by N partitions equally spaced we have $\eta_k = k/N$, $\eta_{k-1} = (k-1)/N$ and Eq. (4.16) reduces to

$$Nu = \frac{1}{\frac{2B}{\alpha}(N+1)\tanh(1/2N) - C\cot\varphi/N} \tag{4.17}$$

where, according to Eq. 4.14, the value of C is given by

$$C = \frac{R}{\alpha^3}(N+1)\,B\left[\frac{B\sin\varphi}{2\cosh^2(\alpha/2N)}(\sinh(\alpha/N) - \alpha/N) - C\cos\varphi\,(\alpha/N - 2\tanh(\alpha/2N))\right] \tag{2.18}$$

4.4.1 The horizontal cavity heated from the bottom

It is of interest to examine the particular case of an horizontal layer heated from the bottom. For this situation $\varphi=0$ and $\alpha\to 0$ and it may be shown that the flow and temperature fields, in each of the i=1, N+1 cells, are given by

$$\Psi_i = \frac{-RC}{2}\left[x^2 - 2P_i\,x + \eta_i\eta_{i-1}\right] \tag{4.19}$$

$$T_i = Cy + \frac{RC^2}{2}\left[\frac{x^3}{3} - P_i\,x^2 + \eta_i\eta_{i-1}\,x - \eta_i\eta^2_{i-1}/2 + \Sigma_2/2\right] + x \tag{4.20}$$

$$C = \pm\frac{1}{2R}\sqrt{5\left[R\sum_{k=1}^{N+1}2M^3_k - 3\right]\Big/\sum_{k=1}^{N+1}M^5_k} \tag{4.21}$$

$$Nu = \frac{1}{1 - \frac{RC^2}{12}\left[\eta^3{}_N + (1 - \eta_N)^3 - 6\,\Sigma_3\right]} \tag{4.22}$$

where

$$\Sigma_2 = \begin{cases} 0 & , \quad i \leq 2 \\ \sum_{k=2}^{i-1} (\eta_k \ \eta_{k-1} \ M_k) & , \quad i \geq 3 \end{cases} \tag{4.23}$$

and

$$\Sigma_3 = \begin{cases} 0 & , \quad N = 1 \\ \sum_{k=2}^{N} (\eta_k \ \eta_{k-1} \ M_k) & , \quad N \geq 2 \end{cases} \tag{4.24}$$

From Eq. (4.21) it is seen that when $R \leq 3/(2\ \Sigma_{k=1}^{N+1} M^3{}_k)$, C=0 is the only value of C and there is no convection possible (Nu=1). For $R > 3/(2\ \Sigma_{k=1}^{N+1} M^3{}_k)$ two symmetric counter-rotating convection cells bifurcate from the rest state and the resulting velocity and temperature distribution are given by Eqs. (4.19) and (4.20) respectively. The present analysis can also predict the critical Rayleigh number R_c for the onset of motion since, as demonstrated by Nield (1968), this happens at zero-wave number (parallel flow) for a layer heated from bottom by a constant heat flux. Substituting $R=R_c$ and C=0 into Eq. (4.21), it is found that

$$R_c = \frac{3}{2 \sum_{k=1}^{N+1} M^3{}_k} \tag{4.25}$$

such that when N=0 we get R_c=12 which is the known result for a Darcy medium between two rigid boundaries (Nield, 1968).

For a layer divided by N partitions equally spaced, Eq. (4.25) reduces to

$$R_c = 12\ (N + 1)^2 \tag{4.26}$$

The above result indicates that, in the case of thin partitions with a high conductivity, natural convection in each cell constructed by the partitions is identical to the ordinary Bénard problem.

4.4.2 The vertical cavity heated from the side

The case of a vertical cavity heated from the side is of practical interest. For this situation $\varphi=90^0$, α^2=RC and Eqs. (2.10), (2.11), (2.14) and (2.16) reduce to

$$\Psi_i = \frac{R}{\alpha^2} \left[1 - \frac{\cosh\alpha(x - P_i)}{\cosh(\alpha M_i)} \right] \tag{4.27}$$

$$T_i = Cy + \frac{1}{\alpha}\left[\frac{\sinh\alpha(x - P_i)}{\cosh(\alpha M_i)} + \tanh(\alpha M_i) + 2\Sigma_1\right] \tag{4.28}$$

$$\alpha^5 = \frac{R^2}{2}\sum_{i+1}^{N+1}\frac{\sinh(2\alpha M_i) - 2\alpha M_i}{\cosh^2(\alpha M_i)} \tag{4.29}$$

$$Nu = \frac{1}{\frac{2}{\alpha}\sum_{i=1}^{N+1}\tanh(\alpha M_i)} \tag{4.30}$$

For a cavity divided by N partitions equally spaced Eqs. (4.29) and (4.30) reduce to

$$\alpha^5 = \frac{(N+1)}{2} R^2 \frac{\sinh(\alpha/(N+1)) - \alpha/(N+1)}{\cosh^2(\alpha/2(N+1))} \tag{4.31}$$

and

$$Nu = \frac{\alpha}{2(N+1)} \coth[\ \alpha/2(N+1)\ ] \tag{4.32}$$

The boundary layer regime may be deduced from the above results. For this situation $R\to\infty$ and Eq. (4.31) yields that $\alpha\to(N+1)^{1/5}\ R^{2/5}$ such that $C\to(N+1)^{2/5}\ R^{-1/5}$. The resulting Nusselt number is given, according to Eq. (2.32), by:

$$Nu = \frac{1}{2} R^{2/5}\ (N+1)^{-4/5} \tag{4.33}$$

The above result is consistent with the face that (1+N) represents the total number of boundary layer pairs (thermal resistances) encountered by the end-to-end heat flow.

4.5 TWO POROUS LAYERS SEPARATED BY A THERMAL BARRIER

In this section we suppose that we have a system consisting of a thermal barrier which is sandwiched between two porous layers. A constant heat flux is applied for heating and cooling the two opposing walls of the inclined system. The porous medium occupies the region $0 \leq x \leq \eta_1$ and $\eta_2 \leq x \leq 1$ and the thermal barrier occupies the region $\eta_2 \leq x \leq \eta_3$. In general the thermal conductivity k_b of the thermal barrier differs form the thermal conductivity k of the two porous layers.

The governing Eqs. (4.8) and (4.9) and boundary conditions, Eqs. (4.5), can be applied to the present problem. However, at the interfaces between the porous layers and the thermal barrier, the continuity of the heat fluxes requires that:

$$\left.\frac{\partial T_1}{\partial x}\right|_{x=\eta_1} = K^* \left.\frac{\partial T_2}{\partial x}\right|_{x=\eta_1} \tag{4.34a}$$

and

$$K^* \frac{\partial T_2}{\partial x}\bigg|_{x=\eta_2} = \frac{\partial T_3}{\partial x}\bigg|_{x=\eta_2} \tag{4.34b}$$

where $K^* = k_b/k$ is the solid to porous conductivity ratio.

Proceeding as in the preceeding section it may be shown that the velocity and temperature distributions, in the two porous layers, are given respectively by:

$$\Psi_1 = \frac{B}{C}\left[1 - \frac{\cosh\alpha(x-\eta_1/2)}{\cosh(\alpha\eta_1/2)}\right] \tag{4.35}$$

$$T_1 = Cy + \frac{B}{\alpha}\left[\frac{\sinh\alpha(x-\eta_1/2)}{\cosh(\alpha\eta_1/2)} + \tanh(\alpha\eta_1/2)\right] - xC\cot\varphi \tag{4.36}$$

and

$$\Psi_3 = \frac{B}{C}\left[1 - \frac{\cosh\alpha[x-(1+\eta_2)/2]}{\cosh\alpha[(1-\eta_2)/2]}\right] \tag{4.37}$$

$$T_3 = Cy + \frac{B}{\alpha}\left[\frac{\sinh\alpha[x-(\eta_2+1)/2]}{\cosh\alpha(1-\eta_2)/2} + 2\tanh(\alpha\eta_1/2)\right.$$

$$\left. + \tanh[(1-\eta_2)/2]\right] + \left(\frac{1}{K^*} + C\cot\varphi\right)(\eta_2 - \eta_1) - xC\cot\varphi \tag{4.38}$$

The temperature distribution within the thermal barrier is obtained by solving the Laplace equation $\nabla^2 T_2 = 0$, with appropriate boundary conditions, as:

$$T_2 = Cy + \frac{x}{K^*} + \frac{2B}{\alpha}\tanh(\alpha\eta_1/2) - \eta_1\left(\frac{1}{K^*} + C\cot\varphi\right) \qquad (4.39)$$

and the value of c is

$$C = P\left[\frac{(\sinh(\alpha\eta_1) - \alpha\eta_1)}{\cosh^2(\alpha\eta_1/2)} + \frac{\sinh\alpha(1-\eta_2) - \alpha(1-\eta_2)}{\cosh^2\alpha(1-\eta_2)/2}\right]$$

$$- Q\left[\alpha(1+\eta_1-\eta_2) - 2\tanh(\alpha\eta_1/2) - 2\tanh[\alpha(1-\eta_2)/2]\right]$$

(4.40)

Where

$$P = RB^2 \sin\varphi/2\alpha^3 D$$

$$Q = RBC \cos\varphi/\alpha^3 D$$

$$D = [1 + (\eta_2-\eta_1)(K^* - 1)]$$

From Eqs. (4.15) and (4.38) the Nusselt number is given by

$$Nu = \frac{1}{\frac{2B}{\alpha}\tanh\frac{\alpha\eta_1}{2} + \tanh\frac{1-\eta_2}{2} + \frac{1}{K^*}(\eta_2-\eta_1) - C\cot\varphi\,(1+\eta_1-\eta_2)}$$

(4.41)

In the special case of a horizontal system heated from the bottom we have $\varphi\to 0^0$ and $\alpha\to 0$, such that Eq. (4.40) reduces to

$$C = \pm \frac{1}{R} \sqrt{10(Rb - 12c)/a} \tag{4.42}$$

where

$$a = \eta_1{}^5 + (1-\eta_2)^5$$

$$b = \eta_1{}^3 + (1-\eta_2)^3 \tag{4.43}$$

$$c = 1 + (\eta_2 - \eta_1)(K^* - 1)$$

From the above equation it follows that the critical Rayleigh number R_c, for the onset of motion, is given by

$$R_c = \frac{12[1 + (\eta_2 - \eta_1)(K^* - 1)]}{\eta_1{}^3 + (1-\eta_2)^3} \tag{4.44}$$

while Eq. (4.41) Yields

$$Nu = \frac{1}{1 - \frac{RC^2}{12} b + \frac{(1-K^*)}{K^*} (\eta_2 - \eta_1)} \tag{4.45}$$

The problem of a porous layer, of extension η, borded by a solid layer, of extension $(1-\eta)$, may be deduced from the above results by letting $\eta_1 = \eta$ and $\eta_2 = 1$.

For a vertical system heated from the side it may be shown that, in the boundary layer regime $(R \to \infty)$ and

$\alpha \rightarrow R^{2/5}[1+(1-\eta)(K^*-1)]^{-1/5}$ such that the Nusselt number is given by:

$$Nu = \frac{1}{\frac{2}{\alpha}\tanh(\alpha\eta/2) + \frac{(1-\eta)}{K^*}} \tag{4.46}$$

For a horizontal system heated from the bottom the marginal stability is given by:

$$R_c = \frac{12\ [\eta + (1-\eta)K^*]}{\eta^3} \tag{4.47}$$

The critical Rayleigh number thus varies with the thermal conductivity of the solid. When $K^*=0$, it is the same as for a single layer, i.e $R_c=720/\eta^2$. However, with increasing K^*, R_c increases linearly. This is due to the distribution of thermal resistance in each layer.

4.6 ANALYTICAL AND NUMERICAL RESULTS

Numerical solution of the complete governing Eqs. (4.1) and (4.2) under the boundary condition (4.5) were obtained for a wide range of Rayleigh numbers and for various values of ψ. All results were obtained for a system with an overall aspect ratio of 3 and a single off-center partition. some typical results are presented in Figs. 4.2a - 4.2f. Figure

4.2a, with R=50, $\varphi=90^0$ and $\eta=0.5$ represents the isotherms and streamlines of a pseudo conduction regime. At higher Rayleigh numbers, the evolution of the flow structure can be observed from Figs 4.2b - 4.2c corresponding to R = 300 and 500. Effects of the position of the partition can be seen by comparing Figs 4.2c and 4.2d where $\eta=0.5$ and 0.2 respectively. Finally, effects of the inclination φ are illustrated in Figs 4.2c, 4.2e and 4.2f with R=500, $\eta=0.5$ and $\varphi=90^0$, 60^0 and 0^0 respectively. An examination of the streamlines in the above figures clearly shows that, except in regions close to the upper and lower boundaries, the flow can be considered as parallel. Consequently, the velocity and temperature profiles are invariant in the y-direction.

The heat transfer results for a vertical porous layer divided by a single partition is presented in Fig. 4.3 as a function of R for different positions η of the partition. The case with $\eta=0$ corresponds to a non partitioned enclosure while that with $\eta=0.5$ to an enclosure containing a central partition. Due to the symmetry of the problem with respect to $\eta=0.5$, results are only presented for $0\leq\eta\leq0.5$. In the intermediate regime, $10\leq R\leq100$, the presence of a partition is seen to decrease Nu and the greatest reduction in heat transfer is obtained for a centrally located partition. A similar trend has been reported numerically in the past by

Tong and Gerner (1986), for a partitioned air-filled enclosure with vertical isothermal walls at different temperatures. In the boundary layer regime, it has been shown recently (Anderson and Bejan (1981), Vasseur et al., 1987) that the Nusselt number, in a non partitioned porous layer (n=0), is given by $Nu= R^{2/5}/2$. According to Eqs. (4.29)-(4.30), the heat transfer through a partitioned layer tends asymptotically towards $Nu=R^{2/5}/(2)^{9/5}$ as $R\rightarrow\infty$ and this, independently of the position η of the partition. As illustrated in Fig. 4.3, the Rayleigh number necessary to reach this asymptotic limit increases considerably as the value of η is made smaller. Recently, a boundary layer model has been proposed by Nishimura et al. (1987) to study heat transfer in air-filled enclosures with an off-center partition. It was also found by these authors that, in the boundary layer regime, the heat transfer rate is independent of the position of the partition if the boundary layer thickness is less than the half-width of each cell constructed by the partition. In the present problem the dimensionless boundary layer thickness is given by $\delta=\alpha^{-1}=(2R^2)^{-1/5}$. Thus the minimum width η_{min} of a cell satisfying the boundary layer approximation is given by $\eta_{min}=2\delta=(4R^{-1})^{2/5}$.

The effects of N equally spaced partitions on the heat transfer through a vertical layer are presented in Fig. 4.4.

On increasing the number of partitions N the Nusselt number decreases drastically but, the introduction of the partitions, does not produce a proportional reduction in heat transfer. In the boundary layer regime the heat transfer is given by Eq. (4.33) as $Nu=R^{2/5}(N+1)^{-4/5}/2$. The Rayleigh number necessary to reach this regime had to be increased considerably as the number of partitions is increased. From Eq. (4.33) it is noted that a number of partitions between 1-5 has the effect of reducing the heat transfer rate by 42-76%.

The effects of η, N and R on heat transfer through a horizontal system heated from bottom are illustrated in Figs. 4.5 and 4.6. Figure 4.5 shows Nu versus the position η, of a single partition, for various values of R. According to Eq. (4.25) the critical Rayleigh number for the onset of motion in a system with a single partition is given by: $R_c=12/[\eta^3+(1-\eta)^3]$. Thus, as depicted by Fig. 4.5, convection is possible for all the values of η only when $R\geq 48$. For Rayleigh numbers up to approximately 100 the greatest reduction in heat transfer is obtained when the partition is located at the center of the layer ($\eta=0.5$). However, as the Rayleigh number is increased further the position of the partition, for a minimum heat transfer, is shift towards lower (or, by symmetry higher) values of η. Thus, when $R\rightarrow\infty$, the greatest

reduction in heat transfer is obtained for $\eta \approx 0.27$ (0.73) while no reduction in heat transfer is observed for a centrally located partition (Nu=6 for η=0, 0.5 and 1). This surprising result is a consequence of the particular thermal boundary conditions considered here. As discussed by Vasseur et al. (1987) the Nusselt number, for a layer of porous medium heated from the bottom by a constant heat flux, tends asymptotically towards $Nu \to 6$ as $R \to \infty$. Thus, for a system with N equally spaced partitions, the same asymptotic value of Nu will be reached provided that R is made large enough. Naturally, in the absence of a stability analysis, the existence of a unicellar flow at large R is questionable. However, it must be mentioned that such flows have been observed numerically, in a single layer of porous medium, up to a Rayleigh number of approximately 800 (Vasseur et al. (1987)). For higher values of R the flow patterns were found to be slightly oscillating.

The case of an horizontal porous layer with N equally spaced partitions is depicted in Fig. 4.6. The Nusselt number decreases drastically on increasing the number of partitions N but the introduction of the partition does not produce, similarly to the vertical case, a proportional reduction in heat transfer. For each value of N there is a critical Rayleigh number $R_c = 12\ (N+1)^2$, Eq. 4.26, below which the fluid

is at rest and heat transfer occurs only by pure conduction (Nu=1). As already discussed, when R is made large enough all the curves tend asymptotically towards Nu=6.

Figure 4.7 shows Nu as a function of the inclination angle φ, for $R=10^3$, in the case of a porous layer with N equally spaced partitions. As the angle of inclination φ approaches 180^0 all the curves tend towards unity, indicating that the heat transfer is mainly due to conduction. This is expected since $\varphi=180^0$ corresponds to the case of a system heated from the top which causes no convection as the density gradient is stable. For a given number of partitions N it is seen that the Nusselt number starts first to increase with decreasing φ, passes through a peak and then begins to decease. The peak in Nusselt number occurs at about 65^0 for N =0 but is at about 35^0 for N=3. Therefore, the peak in Nusselt number takes place at a lower inclination angle when the number of partitions is increased.

Tables 4.1 to 4.3 present a verification by numerical computation of the results of analysis for the Nusselt number as a function of Rayleigh number and inclination angle. As can be seen from these tables the Nusselt numbers predicted by the analytical solution compare satisfactorily (within a few percent) with the results of the numerical solution.

The streamline and isotherm contour plots at a Rayleigh number of $8x10^2$ are presented in Figs. 4.8a-4.8c for a system consisting in a vertical porous layer of extension η, borded by a solid slab of extension $(1-\eta)$. Effects of the porous layer thickness η are illustrated in Figs. 4.8a and 4.8b for $K^*=1$, where $K^*=k_b/k$ is the solid to porous conductivity ratio. Effects of increasing the conductivity ratio can be seen by comparing Figs 4.8b and 4.8c corresponding to $K^*=1$ and 5 respectively.

The heat transfer through this system, as predicted by Eqs. (4.40) and (4.41) (with $\varphi=90^0$, $\eta_1=\eta$ and $\eta_2=1$), is presented in Fig. 4.9 as a function of η and K^* for R=800. The limit $\eta\rightarrow1$ corresponds to a single layer of porous medium for which Nu=7.25 while $\eta\rightarrow0$ corresponds to a solid slab for which $Nu=K^*$. Figure 4.9 indicates that, for $K^* \leq 1$, the Nusselt number increases monotonically with η since the natural convection heat transfer is enhanced as the thickness of the porous layer is made larger. However, for $K^* >1$ i.e. when the conductivity of the solid is higher than that of the porous medium; the Nusselt number is seen to reach a minimum value at a position η which depend upon K^*. This follows from the fact that, for $\eta=0$, the heat transfer by pure conduction through the solid slab is given by $Nu= K^* (>1)$. As the value of η increases slightly the natural convection within

the porous layer is weak and heat transfer through this medium is also approximately by conduction. However, since the conductivity of the porous layer is lower than that of the solid slab the heat transfer starts first to decrease. As the value of η is further increased the natural circulation and the resulting heat transfer within the porous layer are both enhanced and the Nusselt number begins to increase up to a maximum value at η=1. Verification of the results of analysis by numerical computation is also indicated on the figure.

4.7 SUMMARY

The solution of the natural convection heat transfer in a partitioned, inclined, porous layer with uniform wall heat flux is discussed in this Chapter. The problem of a single layer is obtained as a limiting case, and this compare well with the known results. The problem is solved for the case of constant-flux boundary conditions. Results obtained for this special case should be useful for estimating heat transfer in a system with more general boundaries conditions. The following conclusions can be made:

1. In the case of a vertical porous layer divided by N equally spaced partitions, the Nusselt number, in the bound-

ary layer regime, varies inversely with $(1+N)^{4/5}$. For a porous layer divided by a single partition, the greatest reduction in heat transfer, in the intermediate regime, is reached when the partition is centrally located. However, in the boundary layer regime, the heat transfer is independent of the position of the partition provided that the boundary layer thickness is less than the half-width of each cell constructed by the partitions.

2. The critical Rayleigh number for the onset of motion in a bottom horizontal porous layer divided by N diathermal partitions has been obtained. Each cell constructed by the partitions behaves identically like the ordinary Bénard problem, i.e. thermal coupling by conduction through partitions is nil. When the system consists of a solid slab and a porous layer, the conductivity of the solid has an important effect on the critical Rayleigh number , which increases linearly with the conductivity ratio of the solid and the porous medium.

3. The orientation of the partitioned porous layer has, for a given Rayleigh number, a large effect on the heat transfer rate. The maximum heat transfer occurs when the system is heated from the bottom, i.e. for $0 \leq \varphi \leq 90^0$. For a given Rayleigh number, as the number of equally spaced partitions

increases the angle at which maximum energy transfer takes place shifts towards lower values of φ.

4. The present theory is limited by the assumption of two-dimensional, unicellular, steady laminar flows and nothing can be inferred about the possible development of three-dimensional flows within the range of inclination angles considered in this study. Such flows are expected to occur when the system is slightly inclined with respect to the horizontal plane. On the other hand, it is possible with the present theory to predict the critical Rayleigh number for the onset of convection in a system at zero tilt angle. This is due to the fact that a layer, heated from the bottom by a constant heat flux, becomes unstable at zero wave numbers for which the present analysis is exact.

CHAPTER 5

THERMAL INSTABILITY AND NATURAL CONVECTION IN A FLUID LAYER OVER A POROUS SUBSTRATE

5.1 LITERATURE REVIEW

The thermal stability of superposed porous and fluid layers has been studied in the past by Nield (1977,1983) , using linear stability analysis, for various boundary conditions at the upper and lower surfaces of the system. In particular, an exact solution was reported for the case of a porous layer sandwiched between two fluid layers with rigid top and bottom boundaries when a constant heat flux is applied at the bottom. The same physical situation was also considered by Pillatsis et al. (1987) for the case of free, fixed-temperature boundaries. Somerton and Catton (1982) studied the stability of fluid-saturated porous medium with internal heat generation under a fluid layer with a fixed temperature difference between two rigid boundaries. Experimental data relevant to the critical Rayleigh number in a composite layer have been reported by Sun (1973).

Recently the natural convection in a rectangular enclosure horizontally divided into fluid and porous regions has been studied numerically by Nishimura et al. (1986) . The

numerical calculation was found to satisfactorily predict experimental data obtained for a rectangular enclosure filled with silicone oil and glass beads. Poulikakos (1986) used a general flow model to describe the convection inside the porous bed of a horizontal composite layer. This flow model accounts for friction caused by macroscopic shear as well as for the inertia effects. Extensive numerical results were obtained for the heat and fluid flow phenomena at Rayleigh numbers considerably higher than critical.

The purpose of the present chapter is to consider buoyancy-driven convection in a cavity consisting of a fluid layer over a saturated porous layer. The system is heated from the bottom by a constant heat flux and it is assumed that the cavity is shallow. Under these conditions, approximate analytical solutions for unicellular convection in the central region of the cavity can be obtained using a parallel flow assumption. Results are presented for critical Rayleigh numbers as well as the effect of Rayleigh number, Darcy number and other parameters on the convective heat transfer.

5.2 FORMULATION OF THE PROBLEM

The composite system investigated in the present study is shown schematically in Fig. 5.1. A horizontal fluid layer of

thickness h'_f extends over a porous substrate of thickness h'_p. The overall thickness of the composite layer is denoted by L'. The fluid is assumed to have constant properties, excluding density in a buoyant term, which is assumed to vary linearly with temperature; i.e., the Boussinesq approximation is utilized. The fluid-saturated porous medium is considered homogeneous and isotropic with the fluid and the porous matrix being in local thermal equilibrium. The interface between the fluid and porous layers remains horizontal. The vertical walls of the enclosure are insulated while the lower and upper walls are heated and cooled respectively by a uniform heat flux q'.

The fluid layer occupies the region $0 \leq x < \eta$ where $\eta = h'_f/L'$, while the porous medium is in $\eta \leq x \leq 1$. The governing equations for each region will be discussed separately.

5.2.1 Porous layer

In the present analysis, Brinkman's extension has been incorporated to the Darcy formulation governing flow in a porous medium. This, together with the equations of mass and energy conservation in the porous region are

$$\frac{\partial u'_p}{\partial x'} + \frac{\partial v'_p}{\partial y'} = 0 \tag{5.1}$$

$$u'_p = \frac{K}{\mu_f}\left[-\frac{\partial p'_p}{\partial x'} + \mu_p \nabla^2 u'_p - \rho g\beta(T'_p - T'_r)\right] \tag{5.2}$$

$$v'_p = \frac{K}{\mu_f}\left[-\frac{\partial p'_p}{\partial y'} + \mu_p \nabla^2 v'_p\right] \tag{5.3}$$

$$u'_p\frac{\partial T'_p}{\partial x'} + v'_p\frac{\partial T'_p}{\partial y'} = \frac{k_p}{\rho c_p}\nabla^2 T'_p \tag{5.4}$$

where the symbols are defined in the nomenclature and primes denote dimensional variables. It should be noted that μ_p and μ_f are generally different from one another. Using the dimensionless variables

$$(x,y) = (x',y')/L'$$

$$(u^*,v^*) = (u'_p,v'_p)L'/\alpha_f$$

$$T^* = (T'_p - T'_r)/\Delta T' \tag{5.5}$$

$$\Delta T' = q'L'/k_f$$

$$\Psi^* = \Psi'_p/\alpha_f$$

we transform Eqs. (5.1) to (5.4) to the following dimensionless form in terms of the stream function

$$\nabla^2\Psi^* = \frac{Da}{G}\nabla^4\Psi^* - R\frac{\partial T^*}{\partial y} \tag{5.6}$$

$$u^* \frac{\partial T^*}{\partial x} + v^* \frac{\partial T^*}{\partial y} = \gamma \nabla^2 T^* \tag{5.7}$$

$$u^* = \frac{\partial \Psi^*}{\partial y} \quad , \quad v^* = \frac{\partial \Psi^*}{\partial x} \tag{5.8}$$

where $Da=K/L'^2$ is the Darcy number, $R=gK\beta q'L'^2/\alpha_f k_f \nu_f$ is a Darcy-Rayleigh number based on the permeability K of the porous medium and constant heat flux q', $G=\mu_f/\mu_p$ the ratio of the viscosity of the fluid and that of the porous medium and $\gamma=k_p/k_f$ the ratio of the effective thermal conductivity of the porous medium and the thermal conductivity of the fluid.

5.2.2 Fluid layer

Using the scales defined in Eq. (5.5) the dimensionless governing equations for the fluid layer are

$$u \frac{\partial \omega}{\partial x} + v \frac{\partial \omega}{\partial x} = Pr\ \nabla^2 \omega + Ra\ Pr \frac{\partial T}{\partial y} \tag{5.9}$$

$$u \frac{\partial T}{\partial x} + v \frac{\partial T}{\partial y} = \nabla^2 T \tag{5.10}$$

$$\omega = - \nabla^2 \Psi \tag{5.11}$$

$$u = \frac{\partial \Psi}{\partial y} \quad , \quad v = - \frac{\partial \Psi}{\partial x} \tag{5.12}$$

where $Pr=\nu_f/\alpha_f$ is the Prandtl number and $Ra=g\beta L'^4 q'/\alpha_f k_f \nu_f$ is a Rayleigh number. It is noted that Ra, R and Da, in Eqs. (5.6) and (5.9), are related by

$$R = Ra\ Da \tag{5.13}$$

5.2.3 Boundary conditions

The non-dimensional boundary conditions at the four walls of the enclosure are

$$x = 0, \quad \Psi = \frac{\partial \Psi}{\partial x} = 0, \quad \frac{\partial T}{\partial x} = 1 \tag{5.14a}$$

$$x = 1, \quad \Psi^* = \frac{\partial \Psi^*}{\partial x} = 0, \quad \frac{\partial T^*}{\partial x} = \frac{1}{\gamma} \tag{5.14b}$$

$$y = \pm \frac{A}{2}, \quad \Psi = \Psi^* = \frac{\partial \Psi}{\partial y} = \frac{\partial \Psi^*}{\partial y} = 0, \quad \frac{\partial T}{\partial y} = \frac{\partial T^*}{\partial y} = 0 \tag{5.14c}$$

where $A = H'/L'$ is the cavity aspect ratio.

At the interface ($x=\eta$) six continuity conditions can be specified in the following form, coupling the fluid region to the porous region

$$u^* = u \tag{5.15a}$$

$$v^* = v \tag{5.15b}$$

$$\frac{\partial v^*}{\partial x} = G \frac{\partial v}{\partial x} \tag{5.15c}$$

$$\frac{\partial^2 v^*}{\partial x^2} - v^* \frac{G}{Da} = G \frac{\partial^2 v}{\partial x^2} \tag{5.15d}$$

$$T^* = T = 0 \tag{5.15e}$$

$$\frac{\partial T^*}{\partial x} = \frac{1}{\gamma} \frac{\partial T}{\partial x} \tag{5.15f}$$

The above equations express the fact that the velocity,, shear stress, temperature and heat flux at the interface are all continuous. The continuity of the pressure at the interface, in general, imposes a condition on both components of the velocity field (see Nishimura et al. (1986)). However, in the present analysis, only a condition on the horizontal velocity, Eq. (5.15d), will be required. It is to be noted that velocity and shear stress matching at the interface is possible only if Brinkman's extension is considered for the porous medium. It is also because of this that the physically real no slip condition on the solid walls of the system is possible to satisfy.

Equations (5.6) to (5.12) together with boundary conditions (5.14) and (5.15), complete the formulation of the problem. The controlling parameters are A, Pr, G, γ, Da and

$Ra = R/Da$.

5.2.4 Approximate solution

An approximate solution can be sought for a long shallow cavity ($A=H'/L'\to\infty$). In this limit, as discussed in previous chapters, the flow velocity in the central portion of the cavity can be assumed to be parallel and in the y-direction. Thus,

$$u^* = u = 0; \quad v^* = v^*(x) \text{ and } v = v(x) \tag{5.16}$$

in the core region of the system.

As the fluid moves with a constant velocity in the central part of the cavity, the uniform heat flux q' at the walls increases its temperature linearly. There is, however, an unknown transverse variation of the temperature in the x-direction. One way of taking this into account is to write

$$T^* = Cy + \theta^*(x); \qquad T = Cy + \theta(x)$$

where C is the y-temperature gradient. The fact that C is the same in the two layers follows from Eq. (5.15e).

Substituting Eqs. (5.16) and (5.17) into Eqs. (5.6) to (5.12), the governing equations for the porous region can be

reduced to the ordinary differential equations

$$\frac{d^3 v^*}{dx^3} - \alpha^2 \frac{dv^*}{dx} = - RC\alpha^2 \tag{5.18}$$

and

$$\frac{d^2 \theta^*}{dx^2} = v^* C \tag{5.19}$$

where α^2=G/Da. For the fluid region we have

$$\frac{d^3 v}{dx^3} = -RC \tag{5.20}$$

and

$$\frac{d^2 \theta}{dx^2} = vC \tag{5.21}$$

The constant C depends upon Ra, R, Da, G and γ and the thermal boundary conditions imposed on the end regions of the cavity. Following the procedure described in Chapter 2 the value of C can be evaluated from the following equation:

$$\int_0^{\eta} v\theta\, dx + \gamma \int_{\eta}^{1} v^* \theta^* dx = C[\eta + \gamma(1-\eta)] \tag{5.22}$$

at any y. The integrals are a sum of the convective heat fluxes in the fluid and in porous medium respectively. This is derived from the condition of uniform heat flux at the boundaries.

The heat transfer rate can be expressed in terms of a Nusselt number at the y=0 section, defined as

$$Nu = \frac{1}{\Delta T} \tag{5.23a}$$

where the temperature difference ΔT across the section is given by

$$\Delta T = T^*(1/2,0) - T(-1/2,0) \tag{5.23b}$$

5.3 ALL BOUNDARIES RIGID

The hydrodynamical boundary conditions over the whole perimeter of the enclosure are the no-slip conditions. The solutions to Eqs. (5.18) and (5.19) satisfying boundary conditions (5.14a) and (5.15e) are

$$v^* = E(e^{\alpha x} - e^{\alpha}) + F(e^{-\alpha x} - e^{-\alpha}) + RC(x - 1) \tag{5.24}$$

and

$$\theta^* = \frac{C}{\gamma}\left[\frac{E}{\alpha^2}\left[e^{\alpha x} - e^{\alpha\eta} - \alpha(x-\eta)e^{\alpha}\left[\frac{\alpha}{2}(x+\eta) + (1-\alpha)\right]\right]\right.$$

$$+ \frac{F}{\alpha^2}\left[e^{-\alpha x} - e^{-\alpha\eta} - \alpha(x-\eta)e^{-\alpha}\left[\frac{\alpha}{2}(x+\eta) - (1+\alpha)\right]\right]$$

$$\left. + \frac{RC}{6}(x-\eta)\left[(x+\eta)(x-3) + \eta^2 + 3\right]\right] + \frac{x-\eta}{\gamma} \tag{5.25}$$

while the solutions to Eqs. (5.20) and (5.21) satisfying boundary conditions (5.15c) are

$$v = - RaC\frac{x^3}{6} + Ax^2 + Bx + D \tag{5.26}$$

and

$$\theta = C\left[-\frac{RaC}{120}(x^5 - \eta^5) + \frac{A}{12}(x^4 - \eta^4) + \frac{B}{6}(x^3 - \eta^3) + \frac{D}{2}(x^2 - \eta^2)\right] + (x - \eta) \tag{5.27}$$

In order to satisfy the no-slip condition, Eq. (5.14a), D=0 in the above equations. However, the following derivations will be written in terms of this constant since, the case of a system with an upper free surface will be considered for which the value of D is not zero.

From the matching conditions at the porous medium-fluid interface, Eqs. (5.15b) to (5.15d), it follows that

$$2AG\eta + BG - \alpha(Ee^{\alpha\eta} - Fe^{-\alpha\eta}) = \frac{RaCG\eta^2}{2} + RC \tag{5.28}$$

$$2AG - \alpha^2(Ee^{\alpha} + Fe^{-\alpha}) = RaCG\eta - RC\alpha^2(\eta - 1) \tag{5.29}$$

$$A\eta^2 + B\eta + D - E(e^{\alpha\eta} - e^{\alpha}) - F(e^{-\alpha\eta} - e^{-\alpha})$$

$$= \frac{RaC\eta^3}{6} + RC(\eta - 1) \qquad (5.30)$$

while the conservation of mass requires that

$$A\eta^3 + B\frac{\eta^2}{2} + D\eta - \frac{E}{\alpha}\left[e^{\alpha\eta} - e^{\alpha}\,[1 + \alpha(\eta - 1)]\right]$$

$$+ \frac{F}{\alpha}\left[e^{-\alpha\eta} - e^{-\alpha}[1 - \alpha(\eta - 1)]\right] = \frac{RaC\eta^4}{24} + \frac{RC}{2}(\eta - 1)^2 \qquad (5.31)$$

Since D=0 in the present situation the four constants A, B, E and F can be obtained explicitly (or numerically from Eqs. (5.28) to (5.31) but are not presented here because the resulting expressions are lengthy.

The next task is to determine C, the unknown constant temperature gradient in the y-direction in the core region. Substituting equations (5.24) to (5.27) into equations (5.22) and integrating yields, after some straightforward but laborious algebra, an expression of the form

$$K_1 C^3 - (K_2 - K_3)C = 0 \qquad (5.32)$$

The constants, K_1, K_2 and K_3, in Eq. (5.32), depend upon

$Ra = R/Da$, Da, η, G and γ.

Equation (5.32) yields the three following solutions

$$C = 0 \quad \text{or} \quad C = \pm\sqrt{(K_2 - K_3)/K_1} \tag{5.33}$$

where K_1 is always positive.

From Eq. (5.33) it is seen that when $K_2 > K_3$ two symmetric counterrotating convection cells bifurcate from the rest state. For this situation Eq. (5.32) can be solved numerically, using for instance a Newton-Raphson scheme, to obtain C as a function of the parameters of the problem. The temperature and velocity distributions as well as the Nusselt number can then be evaluated from Eqs. (5.24) to (5.31) and (5.23) respectively. When $K_2 > K_3$, C=0 is the only real value of C and there is no convection. The marginal state, which determines the critical Rayleigh number, Ra_c, is when $K_2 = K_3$. Eq. (5.32) then yields

$$\frac{Ra_c}{120}\eta^5 + \frac{R_c}{6}(\eta - 1)^3 - \frac{A'}{12}\eta^4 - \frac{B'}{6}\eta^3 - \frac{D'}{2}\eta^2$$

$$+ E'\left[\frac{e^{\alpha\eta}}{\alpha^2} + e^{\alpha}\left[\frac{\alpha - \eta\alpha - 1}{\alpha^2} - \frac{(\eta - 1)^2}{2}\right]\right]$$

$$+ F'\left[\frac{e^{-\alpha\eta}}{\alpha^2} - e^{-\alpha}\left[\frac{\alpha - \eta\alpha + 1}{\alpha^2} + \frac{(\eta - 1)^2}{2}\right]\right] = \eta + \gamma(1-\eta) \tag{5.34}$$

where A′, B′, D′, E′ and F′ are the coefficients A, B, D, E and F in Eqs. (5.28) to (5.31) divided by C. It is possible to predict directly, from a parallel flow analysis, the critical Rayleigh number for the onset of motion, because when heating is by a constant heat flux, the convection occurs at zero-wave number (Nield (1968,1977,1983)) for which the present solution is exact. Naturally the present method cannot be applied in the case of a layer heated isothermally from the bottom.

We can check the above formula against known results for some special cases.

(i) Let $\eta = 1$, $\gamma = 1$; or $\gamma = 1$, $G = 1$, $Da \to \infty$, η. We get

$$Ra_c = 720 \tag{5.35}$$

which is the known result for a viscous layer between two rigid boundaries (Sparrow et al. (1964)).

(ii) If we let $\eta = 0$, $G = \gamma = 1$, we have

$$R_c = \frac{1}{Da + \frac{1}{12} - \sqrt{Da}\,\coth(1/\sqrt{Da})/2} \tag{5.35}$$

the result for a Brinkman medium between two rigid boundaries (Vasseur et al. (1988)).

(iii) If, however, $\eta = 0$, $G = \gamma = 1$, $Da \to 0$, we find that

$$R_c = 12 \tag{5.37}$$

which is the result for a Darcy medium between two rigid boundaries (Nield (1968)).

The solution for the particular case of two immiscible layer of fluids in a shallow cavity, can be deduced from the present analysis by taking the limit of Eqs. (5.24) to (5.32) for $Da \to \infty$. The same result can be obtained more simply by solving the governing equations when the cavity is filled with two different, viscous, immiscible fluids. It is found that the critical Rayleigh number, for the onset of motion, is given by

$$Ra_c = \frac{\eta + \gamma(1 - \eta)}{x} \tag{5.38}$$

where

$$x = \frac{G}{12}\left[A(\eta^4 - 6\eta^2 + 8\eta - 3) + 2F(\eta^3 - 3\eta^2 + 3\eta - 1) - \frac{1}{10}(\eta^5 - 10\eta^2 + 15\eta - 6)\right] - \frac{\eta^3}{12}\left(A\eta + 2F - \frac{\eta^2}{10}\right)$$

$$A = \frac{3}{M}(N - FQ/2)$$

$$F = \frac{RM - 3NP}{M[\eta + G(1-\eta)] - 3PQ/2}$$

$$N = \frac{1}{24}[\eta^4 - G(\eta^4 - 4\eta + 3)]$$

$$M = \eta^3 - G(\eta^3 - 3\eta + 2)$$

$$P = \eta^2 - G(\eta^2 - 1)$$

$$Q = \eta^2 - G(1 - \eta)^2$$

$$R = \frac{1}{6}\left[\eta^3 - G(\eta^3 - 1)\right]$$

The critical Rayleigh number $Ra_c = 720$ (Sparrow et al.(1964)) for a single layer of fluid between two rigid boundaries can be recovered from Eq. (5.38) by setting $\gamma = 1$, $\eta = 1$ or $\gamma = 1$, $G = 1$ (η)

The present analysis can also predict the behavior of a system consisting of a liquid layer over a solid layer. letting G=0 (i.e., $\mu_p \to \infty$) into Eq. (5.38) it is found that the marginal stability condition is given by

$$Ra_c = \frac{720\ [\eta + \gamma(1 - \eta)]}{\eta^5} \tag{5.39}$$

However, substituting G=1 into Eq. (5.38) yields the critical Rayleigh number for a system consisting of two liquid layers with equal viscosity but different conductivities which is

$$Ra_c = 720[\eta + \gamma(1-\eta)] \tag{5.40}$$

From Eqs. (5.39) and (5.40) it is seen that the critical Rayleigh increases linearly with increasing γ.

5.4 UPPER SURFACE FREE

In this section it is assumed that the upper boundary of liquid layer is open to the ambient air. Thermocapillary forces acting at the free surface are taken into account but, for simplicity in the analysis, we consider that the free surface remains horizontal everywhere. For this case, the dimensionless Eqs. (5.6) to (5.12) and boundary conditions (5.14) and (5.15) would still apply, with the exception that the no-slip condition $\partial\Psi/\partial x=0$ on the upper surface x= 0(see condition (5.14a)) should be replaced by the condition $\partial^2\Psi/\partial x^2=-Ma\partial T/\partial y$. Thus, making use of Eq. (5.17), we now have

$$x = 0, \quad \Psi = 0, \quad \frac{\partial^2 \Psi}{\partial x^2} = -Mac, \quad \frac{\partial T}{\partial X} = 1 \tag{5.40}$$

Where Ma is the Marangoni number, defined as

$$Ma = \frac{SL}{\alpha_f \mu_f} \frac{q'L}{k_f} \tag{5.41}$$

in which S is the surface tension gradient with respect to the temperature, i.e., $S=-\partial\sigma/\partial T$.

For this situation the core solution for the system may still be given by Eqs. (5.24) to (5.27) but with

$$B = MaC \tag{5.42}$$

from boundary condition, Eq. (5.40).

The four unknown constants A, D, E and F may be evaluated from Eqs. (5.28) to (5.31) and an expression for the constant temperature gradient C for the present case can be derived in the form of Eq. (5.32). The marginal state, which determines the critical Rayleigh number, is still given by expression (5.34) which can be checked against known results for some special cases

(i) let $\eta = 1$, $\gamma = 1$ or $\gamma = 1$, $G = 1$, $Da \to \infty$, η, we get

$$\frac{Ra_c}{320} + \frac{Ma_c}{48} = 1 \tag{5.43}$$

which agrees with the prediction of Nield (1964) . Thus when the Marangoni effect is negligible ($Ma_c=0$) , we find that the critical value for the onset of buoyancy-driven instability is

$$Ra_c = 320 \tag{5.44}$$

which was obtained by Sparrow et al (1964) . Also under microgravitational condition ($Ra_c=0$) the onset of motion in a surface tension driven fluid layer occurs at

$$Ma_c = 48 \tag{5.45}$$

(ii) Letting $\eta = 0$, $Ma_c = 0$, $G = \gamma = 1$, we get

$$R_c = \left[\frac{1}{12} + \frac{\cosh^2\frac{\sqrt{Da}}{2}\left(\sqrt{Da}-2\tanh\frac{\sqrt{Da}}{2}\right)}{2Da\left(\sinh\sqrt{Da}-\sqrt{Da}\cosh\sqrt{Da}\right)}\left[2+\left(\sqrt{Da}-4/\sqrt{Da}\right)\tanh\left(\sqrt{Da}/2\right)\right]\right]^{-1} \tag{5.46}$$

as obtained by Vasseur et al. (1988) for a Brinkman layer with an upper surface free.

The marginal stability for a system of two immiscible layer of fluids is obtained by taking the limit of Eqs. (5.24) to (5.32) for Da→∞. It is found that

$$\frac{Ra_c}{120} GP + \frac{Ma_c}{6} GQ = \eta + \gamma(1 - \eta) \tag{5.47}$$

$$P = 9\eta^5 (1 - 1/G) - 15\eta + 6 + \frac{15}{8} T\left[\eta^4 (1 - G) + G\right]$$

$$Q = -2\eta^3 (1 - 1/G) + 3\eta - 1 - \frac{3}{8} T\left[\eta^2 (1 - G) + G\right]$$

$$T = \frac{-5\eta^4 (1 - 1/G) + 8\eta - 3}{\eta^3 - G(\eta - 1)(\eta^2 + \eta + 1)}$$

By setting $\gamma = 1$, $\eta = 1$ or $\gamma = 1$, $G = 1$ (η) in the above result, Eqs. (5.43) to (5.45) can be recovered. On the other hand, letting G=0 (i.e., $\mu_p \to \infty$) into Eq. (5.47) it is found that the marginal stability in a liquid layer over a solid layer is given by

$$\frac{Ra_c \ \eta^5}{320} + \frac{Ma_c \ \eta^3}{48} = \eta + \gamma(1 - \eta) \tag{5.48}$$

Letting G=1 in Eq. (5.47) yields the marginal stability for two liquid layers with equal viscosity and different con-

ductivities as

$$\frac{Ra_c}{320} + \frac{Ma_c}{48} = \eta + \gamma(1-\eta) \tag{5.49}$$

5.5 CRITICAL RAYLEIGH AND MARANGONI NUMBER RESULTS

We have obtained analytical solutions for the heat and fluid flow in a shallow horizontal composite system, consisting of a fluid layer over a porous substrate, heated from below by uniform heat flux. The hydrodynamic boundary conditions include both rigid and free upper surfaces with a rigid lower bounding surface. As a by-product we have also obtained threshold values, i.e., the critical Rayleigh and Marangoni numbers, marking the onset of motion in the system. In this section the onset of buoyancy-thermocapillary instability will be first discussed.

5.5.1 Composite system with a rigid upper surface

The marginal stability of the composite system considered in this study is given, in general, by Eq. (5.34). For the case of a system with a rigid upper surface $Ma_c=0$ and Ra_c depend upon η, G, γ, Da and $Ra_c=R_c/Da$. The effects of each of these parameters will be considered separately. Fig. 5.2 show

the variation of Ra_c with Da and η, for $G=\gamma=1$, as predicted by Eq. (5.34). The bounding case of the porous (Brinkman) bed problem, Eq. (5.36), results when $\eta=0$ and the bounding case of the fluid layer , Eq. (5.35), results when $\eta=1$. Both limits are seen to be favorably reproduced by the method used in this work. The presence of a porous bed ($\eta<1$) leads to a more stable situation since, for a given Da, a larger Ra_c is required to destabilize the system. For a given value of η, as Da increases, the porous bed becomes more permeable, it is easier for the fluid to move, and a smaller Ra_c is required to cause motion. It is also observed in Fig. 5.2 that as Da is made large enough, all the curves tend towards the bounding case of the fluid layer ($Ra_c=720$). This behavior is expected since it is well known that, in the absence if inertia effects, the Brinkman equation reduces to the Navier-Stokes equation as $Da\rightarrow\infty$.

Table 5.1 illustrates the effect if $G=\mu_f/\mu_p$ on the marginal stability of a liquid-porous bed system for $\gamma=1$, $\eta=0.5$ and various values of Da. The case G=0 (i.e., $\mu_p\rightarrow\infty$) corresponds to a single layer of fluid, of extension η, bounded by rigid walls. The values obtained in this study are in good agreement with the critical Rayleigh number predicted by Sparrow et al. (1964) i.e., $Ra_c=720/\eta^5$, where η^5 is an

effect of geometry and temperature difference on the layer. The case G=1 and Da→∞ also corresponds to a single fluid layer, of unit extension, for which Ra_c=720. We calculated Ra_c for G=1, γ=1 and Da=1, 10 and 10^2, and obtained Ra_c =728.6, 720.9 and 720.1 respectively. It is seen from Table 5.1 that, for a given value of Da, decreasing the parameter G enhances the stability of the system. Although various models, such as Lundgren's (1972), have been postulated in the past in order to predict G it does not yet appear possible to accurately estimate μ_f/μ_p for any given porous medium. Nevertheless, Lundgren's predictions for porous media composed of stationary spheres of uniform size, indicate that G can possess values greater than as well as less than unity. Thus, in the case of foametal, the value of G can range from 0.0625 to 100 (Neale et al. (1974)).

The effect of G on Ra_c for a system consisting of two superposed layers of immiscible fluids (Da→∞), equation (5.38), is illustrated in Fig. 5.3 for γ=1 and various values of η. Results are presented only for G≤1 because of the principle of symmetry (Ra_c for given values of η and G is equal to Ra_c for (1-η) and 1/G). The case G=1 (η) corresponds to a single layer of fluid (of viscosity μ_f) for which Ra_c=720. the case η=0 also corresponds to a single layer of fluid (of viscosity μ_p) for which Ra_c=720/G.

The variation or the critical Rayleigh number with the conductivity ratio $\gamma=k_p/k_f$ may be expressed as

$$Ra^*_c = Ra_c \; [\eta + \gamma(1-\eta)] \tag{5.50}$$

where Ra_c is the critical Rayleigh number of the fluid-porous system in the absence of conductivity ratio effect (i.e., when $\gamma=1$). When G=1, the value of Ra_c is given in Fig. 5.2 as a function of Da and η. It is seen, from Eqs. (5.35), (5.36) and (5.50) that $Ra^*_c=720$ for a single layer of fluid ($\eta=1$) and $Ra^*_c=\gamma/\{Da[(Da+1/12)-Da^{1/2}/2\coth(Da^{1/2}/2)]\}$ for a single layer of Brinkman medium ($\eta=0$). When $\gamma\to0$ (i.e. $k_p\to0$) the porous layer behaves as an insulator and $Ra^*_c=Ra_c\eta$, where η is an effect of temperature difference. When $\gamma\to\infty$ (i.e., $k_p\to\infty$) the porous bed behaves like a perfect conductor and $Ra^*_c=Ra_c\gamma(1-\eta)$. Equation (5.50) indicates that increasing γ leads to a more stable situation and that the effect of γ is more pronounced as the porous layer becomes thicker relative to the fluid layer ($\eta\to0$).

5.5.2 Composite system with a free upper surface

For the case of a system with a free upper surface, with surface-tension effects allowed for, the Marangoni number is not zero and all the parameters appearing in Eq. (5.34) have

to be considered. Table 5.2 illustrates the effects of η and Da on the marginal stability of a fluid-porous bed system when $G=\gamma=1$. The threshold values for Bénard-Marangoni convection may be expressed as

$$\frac{Ma_c}{A} + \frac{Ra_c}{B} = 1 \tag{5.51}$$

where the coefficients A and B depend upon Da, the Darcy number of the porous bed, and η, the dimensionless position of the interface between the fluid layer and the porous bed. For a given value of η, the case $Da \to \infty$ corresponds to a single layer of fluid, for which $A \to 48$ and $B \to 320$ in agreement with the values predicted by Sparrow et al. (1964). The stability of the system can be enhanced either by decreasing Da, for a fixed value of η, or by decreasing η, for a fixed value of Da. This follows from the fact that, by decreasing the permeability (Da) of the porous medium or increasing the relative presence of the porous medium (η), it is more difficult for the fluid to move and greater Ra_c and Ma_c are required to cause motion.

Threshold values for the onset of motion of Bénard-Marangoni convection for a two fluid layer system are predicted by Eq. (5.47). When the thermal conductivity of the fluid layers is the same ($\gamma=1$) Eq. (5.47) reduces to Eq.

(5.51) where A and B depend now upon η and G. Samples of results, for this situation, are listed in Table 5.3.

5.6 FLOW AND HEAT TRANSFER RESULTS

The steady state natural convection heat transfer, occurring in the present system, when the Rayleigh and Marangoni numbers are well above the critical values, is now discussed. For this situation the resulting velocity and temperature fields in the core region of the cavity are described by Eqs. (5.24) to (5.32) while the Nusselt number is given by Eq. (5.21).

In Figs. 5.4(a) and 5.4(b) the analytically predicted horizontal velocity distributions and temperature profiles, at the vertical center line of a system with all rigid boundaries, are presented for $Ra=10^4$, $\eta=0.5$, $G=\gamma=1$ and various values of Da. Since the Brinkman equation has been used to model the porous layer, the no-slip boundary condition can be imposed on the bottom boundary of the cavity and the velocity at the upper and lower surfaces is zero. A significant change with the velocity and temperature fields with an increase in Da is demonstrated in Figs. 5.4. If the permeability of the porous medium is high, for example for a Darcy number equal

to 1, the fluid flow penetrates easily into the porous medium and the resulting velocity profile approaches that for a viscous fluid layer. In this case, the convective heat transfer is important, just as the temperature profile in Fig. 5.4(b) suggests. The flow structure is made up a layer of cold fluid under a layer of hot fluid, near the horizontal center line of the cavity, these two layers being sandwiched between two layers of cold and hot fluid located respectively near the upper and the lower horizontal boundaries. Decreasing permeability (i.e., Da) quickly reduces the intensity of the fluid motion inside the system. The major part of the flow becomes confined in the pure fluid space and the resulting heat transfer becomes gradually quasi-conductive. Thus, when $Da=5x10^{-4}$, the temperature profile is very close to that of pure conduction, shown as a dotted line in Fig. 5.4(b). The flow structure now simply consists of a layer of hot fluid in the lower part of the system, under a layer of cold fluid in the upper part.

Predicted horizontal velocity distributions and temperature profiles, at the vertical center line of a system with a free upper surface, are presented in Figs. 5.5(a) and 5.5(b) respectively. The governing parameters are $Ra=10^4$, $\eta=0.5$, $G=\gamma=1$, $Da=5x10^{-3}$ and various values of Ma. It is evident from Figs. 5.4(a) and 5.5(a) that, for the same values

of the governing parameters, the magnitude of the core velocity is higher in the case of a free upper surface than that in the case of a rigid upper surface. This is due to the fact that the condition of zero shear at the free surface allows larger horizontal velocities within the cavity. When surface tension forces augment buoyancy forces (Ma>0) increased velocities occur throughout the system, as depicted in Fig. 5.4(a). The increased core velocity for the free surface system (Ma$\geq$0) leads to an enhancement of the longitudinal convective transport of heat. Accordingly, more hot fluid is carried in the upper part of the cavity and cold fluid in the lower part and the resulting vertical temperature stratification is reduced (compare Figs. 5.4(b) and 5.5(b)). As result, it is expected that the Nusselt number, for a system with a free surface, must be larger than that for a system with a rigid upper surface.

For the purpose of presenting the heat transfer results, a system with γ=G=1 and Da=10^3 is considered. The variation of Nu with η and Da is illustrated in Figs. 5.6(a) and 5.6(b) for a system with a rigid upper surface and a free upper surface (Ma=0) respectively. For a given η there is a critical Rayleigh number Ra_c, Eq. (5.34), below which convection is not possible (pure conduction state). Thus for each of the η considered in Figs. 5.6, the Nusselt number approaches the

pure conduction solution (v=0, Nu=1), as Ra tends toward the value of the corresponding critical Rayleigh number. When Ra is higher than Ra_c the Nusselt number is seen to first increase, as usual, with Ra. But it is clear, from Fig. 5.6, that Nu tends asymptotically toward a constant value which depends upon η (when γ, G and η are fixed). This phenomena has already been discussed in the past for the case of a horizontal porous layer heated from the bottom by a constant heat flux (Vasseur et al. (1988)).

5.7 SUMMARY

Thermal instability and natural convection heat transfer for a porous bed under a fluid in a shallow cavity heated from the bottom by a constant heat flux are studied analytically. Navier-Stokes equation and Brinkman's equations are used for the fluid motion in the fluid region and for that in the porous region, respectively. The equations are solved using a parallel flow assumption. The major conclusions of this study are as follows.

1. Critical Rayleigh numbers for a system with a rigid upper surface depend upon η, G, γ and Da. The limiting cases of single layer of porous medium (η=1) and of a pure fluid (η =0)have been obtained and these compare well with known

results. The presence of a porous bed ($\eta<1$) leads to a more stable situation. Large Da results in a less stable situation due to the increased freedom for fluid motion in the porous layer allowed by the increase in permeability. Also increasing γ or decreasing G results in a more stable system.

2. The upper boundary condition, for a cavity with a free upper surface, has a pronounced influence on the critical Rayleigh and Marangoni numbers for marginal stability of the system. A free upper boundary will result in much smaller critical values. As a by-product results have also been obtained for a single layer of fluid. For this situation, when buoyancy and surface tension gradients are operative, the critical states are given by Eq. (5.43) which is the result obtained by several authors, using a linear stability analysis.

3. Analytical expression for the heat and fluid flow phenomena at Rayleigh and Marangoni numbers considerably higher than critical have been obtained. The effect of several dimensionless groups on the flow pattern at these high Rayleigh numbers is documented. The present analysis shows that the presence of a free surface can significantly increase the heat transfer rate through the cavity.

CHAPTER 6

A SHALLOW CAVITY FILLED WITH TWO IMMISCIBLE FLUIDS

6.1 LITERATURE REVIEW

In a recent paper Villers and Platten (1988) presented some interesting experimental results concerning the mechanism of natural convection in a system containing two immiscible superposed liquid layers of different density. The system studied consisted of a combination of water and heptanol in a shallow rectangular cavity with differentially heated end walls. The horizontal velocity profiles in each layer were measured, as a function of elevation, using laser Doppler Anemometry. The resulting velocity profiles revealed the existence of three convective cells; not only was there one buoyancy induced cell in each layer but also a third intermediate convective cell in the water layer. The position (i.e., in which layer) and the relative size of the third cell were speculated to depend on various parameters like expansion coefficient, viscosity, thickness of each fluid layer and, more likely, on the interfacial tension (the so-called Marangoni or thermocapillary convection). Many interesting questions were raised by these authors who pointed out the need for a theoretical investigation on this fundamental problem in fluid dynamics.

Investigations concerning heat and fluid flow phenomena caused by natural convection in systems containing multiple fluid layers are scarce. Numerical simulations of steady state free convection heat transfer results for a closed, square container filled with a liquid and a gas were published by Oosthuizen and Paul (1983). The transport phenomena in horizontal annuli formed by two circular cylinders and filled with two immiscible fluids was studied numerically by Projahn and Beer (1987). Streamlines and temperature distributions were obtained over a wide range of Rayleigh numbers, and it was found that the thermocapillary convection improves heat transfer. However, no studies of the problem addressed in this Chapter seem to be available in the literature despite its importance for many technical applications.

6.2 FORMULATION OF THE PROBLEM

The problem under consideration is that of two-dimensional, laminar convection in two immiscible fluids of different densities in a stable configuration enclosed within a shallow rectangular cavity. A schematic representation of the geometric arrangement is depicted in Fig. 6.1 with the heavier fluid at the bottom. Each layer is of height h_i' The thermal conditions which are also shown are heating and cooling by a constant heat flux q' through the horizontal walls

(i.e., bottom heating), or through the vertical walls (i.e., side wall heating). Thus, for bottom heating a=1, b=0, while for sidewall heating a=0, b=1. All fluid properties are taken to be constant except the density of the fluids, for which the validity of the Oberbeck-Boussinesq approximation is assumed.

The dimensionless Navier-Stokes and energy equations governing the problem are

$$J(\Psi_i, \nabla^2 \Psi_i) = \begin{bmatrix} 1 \\ \alpha^* \end{bmatrix} Pr_i \left[\nabla^4 \Psi_i - \begin{bmatrix} 1 \\ \alpha^{*2} k^* \end{bmatrix} Ra_i \frac{\partial T_i}{\partial x} \right] \tag{6.1}$$

$$J(\Psi_i, T_i) = \begin{bmatrix} 1 \\ \alpha^* \end{bmatrix} \nabla^2 T_i \tag{6.2}$$

$$u_i = \frac{\partial \Psi_i}{\partial y}, \qquad v_i = -\frac{\partial \Psi_i}{\partial x} \tag{6.3}$$

where

$$J(f,g) = \frac{\partial f}{\partial x}\frac{\partial g}{\partial y} - \frac{\partial f}{\partial y}\frac{\partial g}{\partial x}.$$

$Ra_i = g\beta_i q' H'^4 / \nu_i \alpha_i k_i$ and $Pr_i = \nu_i / \alpha_i$ are the Rayleigh and Prandtl numbers respectively in each fluid layer i (i=1,2). The upper number within [ ] refers to i=1, and the lower number to i=2.

Dimensionless variables were used to obtain Eqs. (6.1) to (6.3). The scaling factors are H′ for the spatial coordinates, α_1/H' for the velocity, $q'H'/k_1$ for the characteristic temperature difference and α_1 for the stream function. The physical property rations of the two layers are defined as

$$\gamma^* = \gamma_2/\gamma_1 \tag{6.4}$$

where γ^* stands for $\alpha^*, \beta^*, \mu^*, \rho^*$ and k^* respectively. It is noted that the thermophysical properties of the heavier fluid (i=1) are chosen for reference to obtain consistent dimensionless equations for both fluid regions.

The non-dimensional boundary conditions at the four walls of the enclosure are

$$\Psi_1 = \frac{d\Psi_1}{dy} = 0; \qquad \frac{\partial T_1}{\partial y} = -a \qquad \text{at } y=0 \tag{6.5a}$$

$$\Psi_2 = \frac{d\Psi_2}{dy} = 0; \qquad k^* \frac{\partial T_2}{\partial y} = -a \qquad \text{at } y=1 \tag{6.5b}$$

$$\Psi_i = \frac{d\Psi_i}{dx} = 0; \quad \frac{\partial T_1}{\partial x} = -b, \; k^* \frac{\partial T_2}{\partial x} = -b \qquad \text{at } x=\pm A/2 \tag{6.5c}$$

where A=L′/H′ is the cavity aspect ratio.

At the interface between the two fluid layers $y=\eta$ (where $\eta=h_1'/H'$) the continuity of temperature, heat flux, velocity, pressure and shear stress require that

$$T_1 = T_2 \; ; \qquad \frac{\partial T_1}{\partial y} = k^* \frac{\partial T_2}{\partial y} \tag{6.6a}$$

$$\Psi_1 = \Psi_2 \; ; \qquad \frac{\partial \Psi_1}{\partial y} = \frac{\partial \Psi_2}{\partial y} \tag{6.6b}$$

$$\frac{\partial \Psi_1}{\partial x} = \frac{\partial \Psi_2}{\partial x} = 0 \tag{6.6c}$$

$$\frac{\partial^2 \Psi_1}{\partial y^2} = \mu^* \frac{\partial^2 \Psi_2}{\partial y^2} - Ma \frac{\partial T}{\partial x} \tag{6.6d}$$

where $Ma=Sq'H'^2/\alpha_1 \mu_1 k_1$ is the Marangoni number and $S= -\partial\sigma/\partial T$ is the surface tension gradient with respect to the temperature. In the present mathematical model the surface between the two fluids is assumed to be flat and to remain unchanged under flow conditions (an assumption which seems reasonable for the relatively low velocities occurring in natural convection processes).

Equations (6.1) and (6.2) together with the boundary conditions, Eqs. (6.5)-(6.6), complete the problem definition. The solution to this problem is dependent on the following

parameters: A, η, α^*, k^*, μ^*, Ma, Ra_i and Pr_i (i=1,2). It can be noted that $Ra_2 = Ra_1 \rho^* \beta^* / (\alpha^* \mu^* k^*)$.

6.3 APPROXIMATE SOLUTION

The present problem can also be significantly simptifical by the approximation of parallel flow for which

$$\Psi_i = \Psi_i(y) \quad \text{and} \quad T_i = C_i x + \theta_i(y) \tag{6.7a,b}$$

where the C_i's are constants representing the unknown temperature gradients in the x direction in the two fluid layers.

In order to satisfy the continuity of temperature at the interface ($y=\eta$), it follows that

$$C_1 = C_2 = C \tag{6.8}$$

Substituting Eqs. (6.7) and (6.8) into Eqs. (6.1)-(6.2) the governing equations can be simplified to

$$\frac{d^4 \Psi_i}{dy^4} = \left[\frac{1}{\alpha^* k^*}\right] Ra_i \; C \tag{6.9}$$

and

$$\frac{d^2 \theta_i}{dy^2} = \left[\frac{1}{\alpha^*}\right] \frac{d^2 \Psi_i}{dy^2} \; C \tag{6.10}$$

Solutions to Eq. (6.9) with boundary conditions (6.6) are

$$\Psi_1 = \frac{Ra_1 C}{24} y^2 (y-\eta) \; [(y+\eta) + \ddot{A}_1] \tag{6.11}$$

$$\Psi_2 = \frac{Ra_1 C}{24} y^{*2} (y^* - \eta^*) \left[\frac{K}{\mu} (y^* + \eta^*) + \ddot{A}_2 \right] \tag{6.12}$$

where $y^* = (1-y)$, $\eta^* = (1-\eta)$, and

$$\ddot{A}_1 = \frac{1}{\eta H} [K\eta^{*3} - \eta^2 \; (4\mu^* \eta + 5\eta^*) - \eta^* G]$$

$$\ddot{A}_2 = \frac{1}{\eta^* H} \left[\eta^3 - \frac{K}{\mu^*} \eta^{*2} \; (4\eta^* + 5\mu^* \eta) + \eta G \right] \tag{6.13}$$

$$G = 12Ma/Ra_1, \quad H = 2(\eta^* + \mu^* \eta), \quad K = \rho^* \beta^*$$

Solutions to Eq. (6.10) with boundary conditions (6.6) are

$$\theta_1 = \frac{Ra_1 C^2}{24} \left[\left[\frac{(y^5 - \eta^5)}{5} - \eta^2 \frac{(y^3 - \eta^3)}{3} \right] \right.$$

$$\left. + \ddot{A}_1 \left[\frac{(y^4 - \eta^4)}{4} - \eta \frac{(y^3 - \eta^3)}{3} \right] \right] - a(y-\eta) \tag{6.14}$$

and

$$\theta_2 = -\frac{Ra_1 C^2}{24}\left[\frac{K}{\mu^*}\left[\frac{(y^{*5}-\eta^{*5})}{5} - \eta^{*2}\frac{(y^{*3}-\eta^{*3})}{3}\right]\right.$$

$$\left. + \ddot{A}_2\left[\frac{(y^{*4}-\eta^{*4})}{4} - \eta^*\frac{(y^{*3}-\eta^{*3})}{3}\right]\right] - \frac{a}{k^*}(y-\eta) \qquad (6.15)$$

It is noted that, due to the normalization, the dimensionless temperatures are zero at the interface $y=\eta$.

An integral condition on the average heat flux can be imposed at any x section,

$$\int_0^\eta u_1\theta_1\, dy + \frac{k^*}{\alpha^*}\int_\eta^1 u_2\theta_2\, dy = C(\eta + k^*\eta^*) - b \qquad (6.16)$$

Substituting all the quantities in the above equations, the integrals were solved by using symbolic algebra. The resulting expression yields a transcendental equation for the constant C, which was solved numerically by a secant method to obtain C as a function of the parameters of the problem. Typical values of C are presented in Tables 6.1 to 6.4 (for convenience the absolute values of C is given). With the thermal boundary conditions considered in this study, C is negative for sidewall heating but can be indifferently positive or negative in the case of bottom heating.

The heat transfer rate for the bottom heated cavity can be expressed in terms of a Nusselt number at the x=0 section, defined as

$$Nu = \frac{q'H'}{\Delta T' k_1} = \frac{1}{\Delta T} \tag{6.17}$$

where the temperature difference $\Delta T = T(0,0) - T(0,1)$. The Nusselt number for sidewall heating is very much dependent on the flow pattern in the end regions and thus cannot be suitably predicted here with the parallel flow approximation.

6.4 RESULTS AND DISCUSSION

As observed experimentally by Villers and Platten (1988), the pattern of convection of the present system is characterized by two cells in each of the fluid layers as well as the possible appearance of an additional secondary cell in one of the fluid layers. A secondary cell will appear in the bottom layer if $\Psi_1 = 0$ at a position y_1 such that $0 < y_1 < \eta$. Similarly a secondary cell will occur in the upper layer if $\Psi_2 = 0$ at a position which satisfies $\eta < y_2 < 1$. From Eqs. (6.11) to (6.13) the values of y_1 and y_2 are given respectively by:

$$y_1 = [\eta^2 (2\mu^* \eta + 3\eta^*) - K\eta^{*3} + \eta^* G]/\eta H \tag{6.18}$$

and

$$y_2 = 1 - [K\eta^2(2\eta^* + 3\mu^*\eta) - \mu^*\eta(\eta^2 + G)]/k\eta^* H \qquad (6.19)$$

Form Eq. (6.18) it follows that two cells will be observed in the bottom layer when the conditions

$$z < 0 \text{ and } z > -2\eta^2(1 + \mu^*\eta/\eta^*) \qquad (6.20a,b)$$

are satisfied, where $z=\eta^2-K\eta^{*2}+G$. This flow pattern is illustrated schematically in Fig. 6.2(b) and will be referred as regime II in the following discussion. As the value of y_1 decreases from η to zero the size of the secondary circulation is enhanced due to the boundary surface effect, while the primary circulation, weakened gradually due to the buoyancy effect, disappears when

$$z \leq -2\eta^2(1 + \mu^*\eta/\eta^*) \qquad (6.21)$$

Under this condition , the resulting flow pattern consists of a clockwise, buoyancy induced, primary circulation in the upper layer driving a secondary counterclockwise circulation in the bottom layer, regime I in Fig. 6.2(a). On the other hand, for

$$z > 0 \text{ and } z < 2K\eta^{*2}(1 + \eta^*/\mu^*\eta) \qquad (6.22a,b)$$

the secondary circulation will appear in the upper layer, regime III in Fig. 6.2(c). Naturally, as the value of y_2 increases from η to unity secondary circulation in the upper

layer is strengthened progressively; the primary circulation is weakened and disappears when

$$z \geq 2K\eta^{*2}(1 + \eta^*/\mu^*\eta) \tag{6.23}$$

as illustrated in Fig. 6.2(d), regime IV. For this situation the secondary circulation in the upper layer is driven by the primary buoyancy induced flow in the lower layer.

It should also be mentioned that, since conditions (6.20a) and (6.22a) cannot be satisfied at the same time, it is impossible for a secondary circulation to appear simultaneously in the two fluid layers. From the above equation it is seen that the parameters responsible for the appearance of the secondary cell are G, K, μ^* and η. However, the flow structure is independent of the particular thermal conditions applied on the system, i.e. sidewall heating or bottom heating.

The limiting case of a single layer of fluid with an upper rigid surface can be recovered by setting $\eta=0$ or $\eta=1$ in the present solution. For this situation, a clockwise gravity induced circulation results as illustrated by regime V in Fig. 6.2(e). The case of a single layer of fluid, with an upper free boundary, can also be predicted by the present analysis by letting $\mu^*\to 0$ and $\eta\to 1$. For this situation, fluid

motion occurs due to the combined influences of buoyancy and surface tension and two cell will be observed if $0<y_1<\eta$, i.e. when the condition

$$-3 < G < -1 \tag{6.24}$$

is satisfied.

The above equation requires that G be negative in order to observe two cells in the fluid layer. This will be the case only when the two driving forces, buoyancy and surface tension, counteract each other. This happens in certain situations like in the case of water below 4°C or for some particular liquid metal alloys. However, in general, surface tension effects augment buoyancy, i.e. induce fluid motion in the same direction, resulting in a positive value of G.

The zones of occurrence of the various flow structures described in Fig. 6.2 are presented in Fig. 6.3. Figs. 6.3(a) and 6.3(b) are for a system with two fluid layers of equal viscosity ($\mu^*=1$), and the effect of the viscosity ratio μ^* of the two fluid layers is illustrated in Fig. 6.3(c). In Fig 6.3(a) G (i.e. Ma) is zero, resulting in a K-η diagram, while in Fig. 6.3(b) K=1, resulting in a G - η diagram. All diagrams are divided into four zones by three lines corresponding to $y_1=0$, $y_1=y_2=\eta$ and $y_2=1$ respectively. The line

η=0 and η=1 correspond to regime V. As mentioned earlier, the flow structures predicted by the present analysis is independent of the thermal conditions applied on the system (i.e. sidewall or bottom heated by a constant heat flux) as long as the flow inside the system remains approximately parallel for a shallow cavity. These results are also valid for the case of a system with differentially heated isothermal vertical end walls since, as demonstrated by Cormack et al. (1974a), a parallel flow solution is also possible for this situation. However, they cannot be applied to the case of a system heated isothermally from the bottom since it is well known that the resulting flow pattern, contrary to the case of a system heated from the bottom by a constant heat flux, is not parallel, corresponding rather to multicellular Benard cells.

Figures 6.4(a) to 6.4(c) show the effects of the parameters K, G and μ^* on the variation of horizontal velocity with depth for η=0.5, i.e. when both fluid layers have the same thickness. In all the graphs $u^*=10u/(Ra_1 C/24)$ such that the resulting velocity profiles are valid for both heating modes considered in this chapter. The flow structures of Figs. 6.2 are also identified on Figs. 6.4 for easier interpretation of the graphs. Referring to the velocity profiles in Figs. 6.4(a) and 6.4(b), it is observed that a secondary

circulation is present in the top layer when the fluid flows from the hot to the cold vertical wall along the interface surface, and in the bottom layer when it flows in the opposite direction. The case where the velocity vanishes at the interface between the two fluid layers(K=1 in Fig. 6.4(a) and G=0 in Fig. 6.4(b)) corresponds to a transition, from regime II to regime III, where the secondary cell is located exactly at the interface and has a zero thickness. From Fig. 6.4(b)it is seen that when the interfacial tension plays a major role (G=0.4), the velocity profile is characterized by a change of sign in the slope near the interface. This result is in agreement with the experimentally obtained velocity profiles reported by Villers and Platten (1988). However, interfacial surface tension is not the only factor responsible for the appearance of secondary flows since the parameters K and μ^* play an equivalent role, as demonstrated by Figs. 6.3(a) and 6.3(c). Finally, the effect of the viscosity ratio μ^* is illustrated in Fig. 6.4(c) for G=0 and K =1. As expected, when $\mu^*=1$ the velocity profiles are the same, but in opposite directions, in the two fluid layers of equal thickness. Also, the velocity magnitude in the upper layer is enhanced (or reduced) when the viscosity ratio is smaller (or greater) than unity.

The effects of the parameters K, G and μ^* on the variation of vertical temperature distributions, $\theta^*=1000/(Ra_1 C^2/24)$, are presented in Figs. 6.5(a) to 6.5(c) for a system of two fluid layers of equal thickness (η=0.5), heated from the side (a=0, b=1). All the temperature profiles become normal to the ceiling and the floor of the layer system, because these boundaries are adiabatic. Also, due to the normalization, $\theta^*=0$ at the interface between the two fluid layers. The temperature distributions in Figs. 6.5(a) and 6.5(b) vary in accordance with the configuration of the flow regime corresponding to the particular values of K and G considered.

Since we are dealing with a multicellular system, the maximum stream function Ψ_m, within each fluid layer, can be used to identify the sense and magnitude of the various possible circulations. The coordinates are chosen such that clockwise (or counterclockwise) movement will be associated with positive (or negative) Ψ_m. Figure 6.6 shows Ψ_m as a function of G, with fixed values of Ra_1 and η, for the case of a system heated from the bottom. For this situation there is a critical Rayleigh number Ra_{1c}, below which no motion is possible. Following the procedure described by Vasseur (1988) it can be shown that, for the present problem, the critical Rayleigh number is given by

$$Ra_{1c} = \frac{720\ (\eta + \eta^* k^*)\ H\ \alpha^* \mu^*}{H(\alpha^* \mu^*\ \eta^5 + K\eta^{*5}) + 5/2\mu^* \eta\eta^* (\alpha^* \eta^2 - \eta^{*2})(\eta^2 - K\eta^{*2} + G)} \tag{6.25}$$

Figure 6.7 shows the marginal stability curve as a function of parameter G for various values of η, when $\mu^*=1$ and K =1. When $\eta=0$ or 1, $Ra_{1c}=720$, in agreement with single layer results obtained by Sparrow et al (1964) using a linear stability analysis. When $\eta=0.5$, $Ra_{1c}=16x720$, independent of the value of G. For all other values of η the critical Rayleigh number is a strong function of G as depicted in Fig. 6.7.

The values of Ψ_m in Figs. 6.6(a)-(c) correspond to a system with K=1, $\mu^*=1$, $Ra_1=4x10^4$ and $\eta=0.5$, 0.45 and 0.55 respectively. Figure 6.7 indicates that, for η = 0.5, the critical Rayleigh number for the onset of motion is $Ra_{1c}=1.152x10^4$ independent of the parameter G. Thus, in Fig. 6.6(a) there is always motion within the system, for all the values of G considered, since Ra_1 is well above the critical values. When G=0, i.e. in the absence of Marangoni effect, the flow is driven solely by the buoyancy effect and one cell of equal size and strength develops in each of the two fluid layers. Due to the symmetry of the system the circulation within the two fluid layers can be indifferently clockwise (C

negative) or counterclockwise (C positive). For convenience, only the clockwise circulation is shown in Figs. 6.6(a)-6(c). For G>0 a boundary surface tension gradient is induced at the interface between the two fluid layers which give rise to the formation of a secondary counterclockwise circulation in the upper layer (regime III). As G increases further, the secondary circulation grows up and progressively displaces the original clockwise cell, in the upper layer, which disappears completely at G=1. For G>1, regime IV prevails and the flow, consisting of a clockwise circulation in the bottom layer, and a counterclockwise circulation in the top layer, is driven progressively more and more by the Marangoni effect. The strength of the circulation in each fluid layer tends asymptotically towards the value $|\Psi_m|=2.38$. Finally, it is observed in Fig. 6.6(a) that the flow pattern is perfectly symmetrical with respect to the sign of the parameter G.

The results obtained for the same conditions, but when η =0.45, are presented in Fig. 6.6(b). It is first observed that the symmetry with respect to G is now destroyed. Also it is seen that when G>1.74 rest state, with parallel straight line isotherms, prevails inside the system. This follows from the fact that, according to Fig. 6.7, $Ra_1 = 4\times10^4$ is above the critical Rayleigh number. Onset of motion

at G=1.74 ($Ra_{1c}=4x10^4$) can be observed in Fig. 6.6(b) at which the rest state $\Psi_m=0$ becomes unstable and two convective states bifurcate from it. As already mentioned, for convenience and due to the symmetry of the two possible flow circulations a single convective state is represented in Fig. 6.6(b) with a clockwise circulation in the bottom layer (dashed line)and a counterclockwise circulation in the top layer (continuous line). This flow pattern, corresponding to regime IV, prevails down to G=1.44 below which an intermediate cell appears in the upper layer (regime III). As the value of G decreases further the size of the intermediate cell gradually extends inside the top layer while that of the counterclockwise circulation progressively disappears. Thus, when G =0.1 the flow in the upper layer consists of a single clockwise circulation. This situation corresponds to the case G=0 in Fig. 6.6(a) except that the size and strength of the cells in the two layers are now not equal due to the fact that the two fluid layers do not have the same thickness. For G<0.1, a counterclockwise secondary cell appears in the bottom layer (regime II), this circulation progressively displacing the original clockwise circulation which disappears when G=-0.64. For G<-0.64 flow regime I, with a clockwise circulation in the upper layer and a counterclockwise circulation in the bottom layer prevails. However, as the value of G decreases further towards $G\to\infty$ the magnitude of Ψ_m does not

approach asymptotically a given value, as for the case with η =0.5 but rather continues to increase continuously. The results obtained for η=0.55 are presented in Fig. 6.6(c). The sequence of events are observed to the same but are reversed with respect to the values of G, Fig. 6.6(c) being the mirror image of Fig. 6.6(d).

For the purpose of presenting the heat transfer results, a system, heated from the bottom, with μ^*=1 is considered. The variation of Nu with G and η is illustrated in Fig. 6.8(a) for Ra_1=4x10^4 and K=1, i.e. for the conditions considered in Fig. 6.6. When η=0.5 the curve is symmetrical with respect to G, and Nu is maximum at G=0 i.e. when the convection is driven solely by the buoyancy effect. As the value of G increases (or decreases) toward infinity the Marangoni effect becomes more and more predominant. The flow is then driven by the surface tension at the interface between the two fluid layers and the Nusselt number tends to unity although, as indicated by Fig. 6.6(a), $|\Psi_m|$ tends toward a fixed value, namely 2.38. For this situation it is seen from Table 6.3 that the axial temperature gradient C becomes very small, i.e. the convective terms in the energy equation are negligible such that now the energy and the momentum equation are decoupled. The results obtained for η= 0.45 and 0.55 are similar, the two curves are the mirror

image of each other, but the symmetry with respect to G is now destroyed due to the different thickness of the two fluid layers.

The effects of K and Ra on Nu for a system with G=1, μ^* =1.0 and η=0.5 are illustrated in Fig. 6.8(b). As the value of K is increased the curves for Nu are seen to first increase up to a peak value and then decrease monotonously down to a value of Nu=1.14 for all the Rayleigh numbers considered. The peak in the maximum Nu occurs at K=1 when Ra is large but shifts towards larger values of K as the Rayleigh number is decreased. From Fig. 6.8(b) it is also seen that, although in general Nu increases with Ra_1, it is clear that the Nusselt number tends asymptotically toward a constant value. This phenomenon has already been observed in the past for the case of a single fluid layer (Vasseur (1987)) and is related to the particular heating mode considered in this study.

The effect of G on the Nusselt number Nu for the case of a single layer of fluid heated from below with a free upper surface is depicted in Fig. 6.9. When G>0, i.e. when the surface tension forces augment buoyancy forces the heat transfer is almost constant for the range of G considered. However, when G<0, i.e. when surface tension counteracts

buoyancy the Nusselt number decreases rapidly reaching the value Nu=1 at G=-1.79. This behavior can be explained from Eq. (6.25) which predicts that when $G \geq -1.79$ the critical Rayleigh number Ra_{1c}, for the onset of motion in the system, is equal or above 4×10^4. It is recalled that, for the case a single layer of fluid with a free upper surface, a two cell structure will be observed for $-3<G<-1$ as predicted by Eq. (6.24). This result is independent of the heating mode (side or bottom) of the system.

6.5 SUMMARY

The problem of natural convection in two immiscible fluids heated from the side or from below by uniform heat flux has been studied analytically. The solution is based on the parallel flow approximation which is expected to be valid when the aspect ratio of the system is greater than approximately two. The present work has attempted to clarify the variety of flow patterns which might occur and the conditions under which they do. Four different convection patterns are possible as a result of the complex interaction between buoyant and interfacial surface tension forces. Limiting cases of a single layer can also be obtained from the analysis. Despite its simplicity the model developed in this Chapter is qualitatively in good agreement with experimental results.

Also, the critical Rayleigh number for the onset of motion has been predicted explicitly, in the case of a system heated from the bottom, as a function of the relative importance of the different physical properties of the two layers.

CHAPTER 7

CONCLUSIONS

The problem concerning natural convective heat transfer in a shallow rectangular cavity (A>>1) with uniform heating and cooling through opposite walls has been investigated both theoretically and numerically. The theoretical phase of the investigation was primarly concerned with the development of analytical solutions based mainly on the parallel flow approximation introduced by Cormack et al. (1974a) to study the problem of a horizontal fluid enclosure with differentially heated end walls. A number of separate problems have been considered and they are summarized below along with the important results:

1. CONVECTIVE HEAT TRANSFER IN AN INCLINED SHALLOW POROUS CAVITY

The analysis is based on the Brinkman equation which is applicable to porous media with high permeability and can account for the no-slip conditions at a solid surface. The results demonstrate the dependence of the Nusselt number on R and Da. As Da→0, the flow field is similar to that given by an analysis using Darcy's law, except in a thin region next

to a boundary. The viscous effects are largely confined to this region, where the axial velocity increases from a zero value at the wall to a peak value. Results obtained from Darcy's law are valid when Da is approximately smaller than 10^{-6}. The overall heat transfer reduces significantly with an increases of the permeability (Da) of the porous medium, the reduction being larger at higher R. When Da is high enough, that is, when the Darcy resistance due to the solid matrix becomes negligible with respect to that resulting from the boundary effects, the present solution approaches that for a viscous fluid .

The orientation of the cavity has, for given values of R and Da, a large effect on the heat transfer rate. For a given value of Da, the maximum heat transfer rate across the cavity occurs at an angle $\varphi_N \rightarrow 90^0$ when R is relatively large (boundary layer regime). For intermediate values of R (asymptotic regime) the value of φ_N reaches a minimum value of approximately 33.5^0 independently of Da. At a given R and for small enough inclinations φ around bottom heating multiple steady states exist provided that the Darcy number is sufficiently small. The range of tilt angles for multiple steady states is function of both R and Da.

In the special case of a horizontal porous layer ($\varphi=0$) heated from the bottom results have been obtained for (1) a cavity with all rigid boundaries, (2) a cavity with a free upper surface, and (3) a cavity with both horizontal boundaries free. The critical Darcy-Rayleigh number for the onset of motion has been obtained explicitly in terms of the Darcy number for each of these three hydrodynamical boundary conditions. It is shown that the results of viscous fluid ($Da\to\infty$) and the Darcy medium ($Da\to 0$) emerge from the present solution as special cases. The basic reason for this agreement is that a layer heated from the bottom by a constant heat flux becomes unstable at zero wavenumber for which the parallel flow approximation is exact.

2. AN INCLINED POROUS LAYER DIVIDED BY MULTIPLE PARTITIONS

The effects of multiple heat conducting partitions on natural convection within a rectangular, tilted, porous layer is considered. An approximate solution is obtained by assuming the validity of Darcy's law and neglecting inertial effects. It is found that:

i) In the case of a vertical porous layer divided by N equally spaced partitions, the Nusselt number, in the boundary layer regime, varies inversely with $(1+N)^{4/5}$. For a

porous layer divided by a single partition, the greatest reduction in heat transfer, in the intermediate regime, is reached when the partition is centrally located. However, in the boundary layer regime, the heat transfer is independent of the position of the partition provided that the boundary layer thickness is less than the half-width of each cell constructed by the partitions.

ii) The critical Rayleigh number for the onset of motion in a horizontal porous layer divided by N diathermal partitions has been obtained. Each cell constructed by the partitions behaves identically like the ordinary Bénard problem, i.e. thermal coupling by conduction through partitions is nil. When the system consists of a solid slab and a porous layer, the conductivity of the solid has an important effect on the critical Rayleigh number, which increases linearly with the conductivity ratio of the solid and the porous medium.

3. THERMAL STABILITY OF SUPERPOSED POROUS AND FLUID LAYERS

The buoyancy driven convection in a system consisting of a fluid over a saturated porous layer heated from below is studied. Use is made of the Brinkman model for the porous medium in order to ensure the matching of the velocities and

shear stresses at the interface between the two medium. It is found that:

i) The critical Rayleigh numbers for a system with a rigid upper surface depend upon η, G, γ and Da. The presence of a porous bed ($\eta<1$) leads to a more stable situation. Large Da results in a less stable situation due to the increased freedom for fluid motion in the porous layer allowed by the increase in permeability. Also increasing γ or decreasing G results in a more stable system.

ii) The upper boundary condition, for a cavity with a free upper surface, has a pronounced influence on the critical Rayleigh and Marangoni numbers for marginal stability of the system. A free upper boundary will result in much smaller critical values.

iii) Analytical expression for the heat and fluid flow phenomena at Rayleigh and Marangoni numbers considerably higher than critical have been obtained. The effect of several dimensionless groups on the flow pattern at these high Rayleigh numbers is documented.

4. CONVECTION IN TWO IMMISCIBLE SUPERPOSED LIQUID LAYERS

The problem of natural convection in two immiscible fluids heated from the side or from below by an uniform heat flux is considered. The present work has attempted to clarify the variety of flow patterns which might occur and the conditions under which they do. Four different convection patterns are possible as a result of the complex interaction between buoyant and interfacial surface tension forces. Despite its simplicity the model is qualitatively in good agreement with the experimental results obtained by Villers and Platten (1988), Also, the critical Rayleigh number for the onset of motion is predicted explicitly, in the case of a system heated from the bottom, as a function of the relative importance of the different physical properties of the two layers.

REFERENCES

Acharya, S. and Tsang, C.H., 1985, "Natural Convection in a Fully Partitioned Inclined Enclosure", Num. Heat Transfer, Vol. 8, pp. 407-428.

Anderson, R. and Bejan, A., 1981, "Heat Transfer Through Single and Double Vertical Walls in Natural Convection: Theory and Experiment", Int. J. Heat Mass Transfer, Vol. 24, pp. 1611-1620.

Beavers, G.S. and Joseph, D.D., 1967, "Boundary Condition at a Naturally Permeable Wall", J. Fluid Mechanics, Vol. 30, pp. 197-207.

Bejan, A., 1984, "Convection Heat Transfer" Wiley, New York.

Bejan, A. and Tien, C.L., 1978a, "Laminar Natural Convection Heat Transfer in a Horizontal Cavity with Different End Temperatures", J. Heat Transfer, Vol. 100, pp. 641-647.

Bejan, A. and Tien, C.L., 1978b, "Natural Convection in a Horizontal Porous Medium Subjected to an End-to-End Temperature Difference", J. Heat Transfer, Vol. 100, pp. 191-198.

Bejan, A., 1979, "On the Boundary Layer Regime in a Vertical Enclosure Filled with a Porous Medium", Lett. Heat Mass Transfer, Vol. 6, pp. 93-102.

Bejan, A., 1981, "Lateral Intrusion of Natural Convection into a Horizontal Porous Structure", J. Heat Transfer, Vol.103, p. 237-241.

Bejan, A., 1983, "The Boundary Layer Regime in a Porous Layer with Uniform Heat Flux from the Side", Int. J. Heat Mass Transfer, Vol. 26, pp. 1339-1346.

Blythe, P.A., Simpkins, P.G., and Daniels, P.F., 1983, "Thermal Convection in a Cavity Filled with a Porous Medium: a Classification of Limiting Behavior", Int. J. Heat Mass Transfer, Vol. 26, pp. 701-708.

Bories , S.A. and Combarnous, M.A., 1973, "Natural Convection in a Sloping Porous Layer", J. Fluid Mechanics, Vol. 57, pp. 63-79.

Brinkman, H.C., 1948, "A Calculation of the Viscous Force Exerted by a Flowing Fluid on a Dense Swarm of Particles", Appl. Scient. Res., Vol. 81, pp. 27-34.

Burns, P.J., Chow, L.C., and Tien, C.L., 1976, "Convection in a Vertical Slot Filled with Porous Insulation", Int. J. Heat Mass Transfer, Vol. 20, pp. 919-926.

Caltagirone, J.P., 1981, " Convection in a Porous Medium. Convective Transport and Instability Phenomena", G. Braun (editor), pp. 199-232.

Caltagirone, J.P. and Bories, S., 1985, "Solutions and Stability Criteria of Natural Convective Flow in an Inclined Porous Layer", J. Fluid Mechanics, Vol. 155, pp. 267-287.

Catton, I., 1978, "Natural Convection in Enclosures", Proceedings 6th International Heat Transfer Conference, Toronto, Vol. 6, pp. 13-43.

Chan, B.K.C, Ivey, C.M., and Barry, J.M.,1970, "Natural Convection in Enclosed Porous Media with Rectangular Boundaries", J. Heat Transfer, Vol. 92, pp. 21-27.

Cheng, P. 1978, "Heat Transfer in Geothermal Systems", Adv. Heat Transfer. Vol. 14, pp. 1-105.

Combarnous, M. A. and Bories, S. A., 1975, "Hydrothermal Convection in Saturated Porous Media", Adv. Hydroscience Vol. 10, pp. 231-245.

Cormack, D.E., Leal L.G., and Imberger, J., 1974a, "Natural Convection in a Shallow Cavity with Differentially Heated End Walls: Part 1, Asymptotic Theory", J. Fluid Mechanics, Vol. 65, pp 209-230.

Cormack, D.E., Leal, L.G., and Seinfeld, J., 1974b, "Natural Convection in a Shallow Cavity with Differentially Heated End Walls: Part 2, Numerical Solutions", J. Fluid Mechanics, Vol. 65, pp. 231-240.

Daniels, P.G., 1983, "A Numerical Solution of the Vertical Boundary-Layer Equation in a Horizontally Heated Porous Cavity", J. Engng. Math., Vol. 17, pp. 285-300.

Denloye, A.O.O., and Botterill, J.S.M., 1977, "Heat transfer in Flowing Packed Beds", Chem. Engng. Sci., Vol.32, pp. 461.

Duxbury, D., 1979, "An Interferometric Study of Natural Convection in Enclosed Plane Air Layers with Complete and Partial Central Vertical Divisions", Ph.D. Thesis, University of Salford.

Ehrhard, P. and Muller, U., 1990, "Dynamic Behaviour of Natural Convection in a Single-Phase Loop", J. Fluid Mechanics, Vol. 217, pp. 487-518.

Weber, J.E., 1974, "Convection in a Porous Medium with Horizontal and Vertical Temperature Gradients", Int. J. Heat Mass Transfer, Vol. 17, pp. 241-248.

Gill, A.E., 1966, "The Boundary-Layer Regime for Convection in a Rectangular Cavity", J. Fluid Mechanics, Vol. 26, pp. 515-536.

Georgiadis, J., and Catton, I., 1985, "Free Convection Motion in an Infinite Vertical Porous Slot: the Non-Darcian Regime", ASME Paper No. 85-HT-58.

Haber, S., and Mauri, R., 1983, "Boundary Condition for Darcy's flow through Porous Media", Int. J. Multiphase Flow, Vol. 9, pp. 561-576.

Heat, J.E., 1972, "Stability of Thin Non-Regime Hadkey Circulations", J. Atmos. Sci., Vol. 29, pp. 687-697.

Hickox, C.E., and Gartling, D.K., 1981, "A Numerical Study of Natural Convection in Horizontal Porous Layer Subjected to an End-to-End Temperature Difference", J. Heat Transfer, Vol. 103, pp. 797-802.

Hinch, E.J., 1977, "An Averaged Equation Approach to Particle Interactions in a Fluid Suspension", J. Fluid Mechanics, Vol. 83, pp. 695-720.

Holst, P.H. and Aziz, K., 1972, "Transient Natural Convection in Confined Porous Media", Int. J. Heat Mass Transfer, Vol. 15, pp. 73-90.

Hong, J.T., Tien, C.L., and Kaviany, M., 1985, "Non-Darcian Effects On Vertical-Plate Natural Convection in Porous Media with High Porosities", Int. J. Heat and Mass Transfer, Vol. 28, pp. 2149-2157.

Horton, F.T., and Rogers, C.W., 1945, "Convection Currents in a Porous Medium", J. Appl. Physics, Vol. 16, pp. 367-370.

Howells, I.D., 1974, "Drag due to the Motion of a Newtonian Fluid through a Sparse Random Array of Small Fixed Rigid Objects", J. Fluid Mechanics, Vol. 64, pp. 449-475.

Hurle, D.T.J., Jakeman, E., and Pike, E.R. 1967, "On the Solution of the Benard Problem with Boundaries of Finite Conductivity", Proc. Roy. Soc. Lond., Vol. A296, pp. 469-475.

Imberger, J., 1974 , "Natural Convection in a Shallow Cavity with Differentially Heated End Walls. Part 3. Experimental Results", J. Fluid Mechanics, Vol., 65, PP. 247-260.

Jones, I.P., 1980, "Numerical Predictions from the IOTA2 Code for Natural Convection in Vertical Cavities", ASME Paper No 82-HT-70.

Kamiuto, K., 1985, "Design Consideration for Unevacuated Horizontal Multi-Layer Insulation Systems", Applied Energy, Vol. 20, pp. 241-252.

Kamiuto, K., 1986, "Further Design Consideration for Unevacuated Horizontal Multi-Layer Insulation Systems", Applied Energy, Vol. 23, pp. 297-305.

Katto, Y., and Masuoka, T., 1967, "Criterion for the Onset of Convective Flow in a Fluid in a Porous Medium" Int. J. Heat Mass Transfer, Vol. 10, pp. 297-309.

Kimura, S., and Bejan, A., 1984, "The Boundary Layer Natural Convection Regime in a Rectangular Cavity with Uniform Heat Flux from The Side", ASME J. Heat Transfer, Vol. 106, pp. 98-103.

Koplik, J., Levine, H and Zee, A., 1983, "Viscosity Rennormalization in the Brinkman Equation", Phys. Fluids, Vol. 26, pp. 2864-2870.

Lapwood, E.R., 1948, "Convection of a Fluid in a Porous Medium", Proc. Camb. Philos. Soc., Vol. 44,pp. 508-521.

Lauriat, G., and Prasad, V., 1987, "Natural Convection in a Vertical Porous Cavity: A Numerical Study for Brinkman-Extended Darcy Formulation", J. Heat Transfer, Vol. 109, pp. 681-696.

Lienhard, J.H., 1987, "An Improved Approach to Conductive Boundary Conditions for the Rayleigh-Benard Instability", J. Heat Transfer, Vol. 109, pp. 378-387.

Lundgren, T.S., 1972, "Slow Flow Through Stationary Random Beds and Suspensions of Spheres", J. Fluid Mechanics, Vol. 51, pp. 273-299.

Moya, S.L., Ramos, E., and Sen, M., 1987, "Numerical Study of Natural Convection in a Tilted Rectangular Porous Material", Int. J. Heat Mass Transfer, Vol. 30, pp. 741-756.

Muskat, M., 1946, "The Flow of Homogeneous Fluid through Porous Media", Edward, Michigan.

Nandakumar, k., and Masliyah, J.H., 1982, "Laminar Flow Past a permeable Sphere", Can.J. Chem. Engng. Vol.60, pp. 202.

Nakamura, H., Asako, Y. and Hirata, T., 1984, "Natural Convection and Thermal Radiation in Enclosures with Partition Plate", Trans. Jap. Soc. of Mech. Eng. Series B, Vol. 50, pp. 2647-2654.

Neale G., and Nader, W., 1974, "Practical Significance of Brinkman's Extension of Darcy's Law: Coupled Parallel Flows within a Channel and a Bounding Porous Medium", Canadian J. Chem. Eng., Vol. 52, pp. 75-478.

Nield, D.A., 1968, "Onset of Thermohaline Convection in a Porous Medium", Water Resources Research, Vol. 4, pp. 535-560.

Nield, D. A., 1977, "Onset of Convection in a Fluid layer Overlying a layer of Porous Layer."J. Fluid Mechanics, Vol. 81, pp. 513-522.

Nield, D.A., 1983, "The Boundary Correction for the Rayleigh-Darcy Problem: Limitations of the Brinkman Equation", J. Fluid Mechanics, Vol. 128, pp. 37-46.

Nield, D.A., 1964, "Surface Tension and Buoyancy Effects in Cellular Convection", J. Fluid Mechanics, Vol. 19, pp. 341-352.

Nishimura, T., Shiraishi, M., and Kawamura, Y., 1985, "Analysis of Natural Convection Heat Transfer in Enclosures Divided by a Vertical Partition Plate", Proceedings International Symposium Heat Transfer, Beijing, Paper no. 85-ISHT-I-6.

Nishimura, T., Takumi, T., Shiraishi, M., Kawamura Y., and Ozoe, H., 1986, "Numerical Analysis of Natural Convection in a Rectangular Enclosure Horizonally Divided into Fluid and Porous Regions." ASME J. Heat Transfer, Vol. 29, pp. 889-898.

Nishimura, T., Shiraishi, M., and Kawamura, Y., 1987, "Natural Convection in Horizontal Enclosures with Multiple Partitions", Int. J. Heat Mass Transfer, Vol. 32, pp. 1641-1647.

Oosthuizen, P.H. and J.T. Paul, 1983, "Heat Transfer through a Closed Square Container Filled with a Liquid and a Gas", ASME Paper 83-WA/HT-101, ASME Winter Annual Meeting.

Ostrach, S., Loka, R.R., and Kumar, A., 1980, "Natural Convection in Enclosures", H.T.D., Vol. 8, P. 1.

Peaceman, D.W., and Rachford, H. A., 1955, "The Numerical Solution of Parabolic and Elliptic Difference Equations", Journal Society Applied Mathematics, Vol. 1, pp. 28-43.

Pillatsis, G., Taslim M.E., and Narusawa, U., 1987, "Thermal Instability of a Fluid-Saturated Porous Medium Bounded by Thin Fluid Layers", ASME J. Heat Transfer, Vol. 109, pp. 677-682.

Poulikakos, D. and Bejan, A., 1984, "Natural Convection in a Porous Layer Heat and Cooled Along One Vertical Side", Int. J. Heat Mass Transfer, Vol. 27, pp. 1879-1891.

Poulikakos, D., 1986, "Buoyancy-Driven Convection in a Horizontal Fluid Layer Extending over a Porous Substrate." Phys. Fluids, Vol. 29, pp. 3949-3957.

Prasad, V., Kulacki, F.A., 1984a, "Natural Convection in a Rectangular Porous Cavity with Constant Heat Flux on One Vertical Wall", ASME J. Heat Transfer, Vol. 106, pp. 152-157.

Prasad, V., Kulacki, F.A., 1984b, "Convective Heat Transfer in a Rectangular Porous Cavity-Effect of Aspect Ratio on Flow Structure and Heat Transfer", ASME J. Heat Transfer, Vol. 106, pp. 158-165.

Projahn, U. and H. Beer, 1987, "Thermogravitational and Thermocapillary Convection Heat Transfer in Concentric and Eccentric Horizontal, Cylindrical Annuli Filled with Two Immiscible Fluids", Int. J. Heat Mass Transfer, Vol. 30, pp. 93-107.

Rudraiah, N., Veerappa, B., and Rao, B., 1980, "Effects of Nonuniform Thermal Gradient and Adiabatic Boundaries on Convection in Porous Media", J. Heat Transfer, Vol.102, pp. 254-260.

Rudraiah, N., and Masuoka, T., 1982, "Asymptotic Analysis of Natural Convection through Horizontal Porous Layer", Int. J. Eng. Sci., Vol. 47, pp. 63-79.

Saffman, P.G., "On the Boundary Condition at the free surface of a Porous Medium", Stud. Appl. Math., Vol.2, pp. 93.

Sen, A.K., 1987, "Natural Convection in a Shallow Porous Cavity - The Brinkman Model", Int J. Heat Mass Transfer, Vol. 30, pp. 855-868.

Sen, M., Vasseur, P. and L. Robillard, 1987, "Multiple Steady States for Unicellular Natural Convection in an Inclined Porous Layer", Int. J. Heat Mass Transfer, Vol. 30, pp. 2097-2113.

Sen, M., 1988, "Parallel Flow Convection in a Tilted Two-Dimensional Porous Layer Heated From All Sides", Phys. Fluids, Vol. 31, pp. 3480-3487.

Somerton C.W., and Catton, I., 1982, "On the Thermal Instability of Superposed Porous and Fluid Layers", ASME J. Heat Transfer, Vol. 104, pp. 160-165.

Shiralkar, G.S., Haajizadeh, M. and Tien, C.L., 1983, "Numerical Study of High Rayleigh Numbers in a Vertical Porous Enclosure", Num. Heat Transfer, Vol. 6, pp. 223-234.

Slattery, J.C., 1968, "Multiphase Viscoelastic Flow through Porous Media", A. I. Ch. E., Vol. 14, pp. 50.

Sparrow E.M., Goldstein R.J., and Jonsson, V.K., 1964, "Thermal Instability in a Horizontal Fluid Layer: Effect if Boundary Conditions and Nonlinear Temperature Profile", J. Fluid Mechanics, Vol. 18, pp. 513-528.

Sun, W.J., 1973, "Convective instability in Superposed porous and Free Layers", Ph.D. Dissertation, University of Minnespolis, 1973.

Tam, C.K.W.,1969 "The Drag on a Cloud of Spherical Particles in a Low Reynolds Number Flow", J. Fluid Mechanics, Vol. 38, pp. 537-546.

Tong, T.W., and Subramanian, E., 1985, "A Boundary-Layer Analysis for Natural Convection in Vertical Porous Enclosures-Use of The Brinkman-extended Darcy model", Int. J. Heat Mass Transfer, Vol. 28, pp. 563-571.

Tong, T.W., and Gerner, F.M., 1986, "Natural Convection in Partitioned Air-Filled Rectangular Enclosures", Int. Comm. Heat Mass Transfer, Vol. 13, pp. 99-108.

Vafai, K., and Tien, C.L., 1981, "Boundary and Inertia Effect of Flow and Heat Transfer in Porous Media", Int. J. Heat Mass Transfer, Vol. 24, pp. 195-210.

Vasseur, P., and Robillard, L., 1987, "The Brinkman Model for Boundary Layer Regime in a Rectangular Cavity with Uniform Heat Flux from the Side", Int J. Heat Mass Transfer, Vol. 30, pp. 717-727.

Vasseur P., L. Robillard and M. Sen, 1987, "Unicellular Convective Motion in an Inclined Fluid Layer with Uniform Heat Flux. Bifurcation Phenomena in Thermal Processes and Convection", ASME Winter Annual Meeting, (Ed.) H. Bau, HTD-Vol. 94, pp. 23-30.

Vasseur, P., Satish, M.G., and Robillard, L., 1987, "Natural Convection in a Thin, Inclined, Porous Layer Exposed to a Constant Heat Flux", Int. J. Heat Mass Transfer, Vol. 30, pp. 537-549.

Vasseur, P., Wang, C.H., and Sen, M, 1988, "The Brinkman Model for Natural Convection in a Shallow Porous Cavity with Uniform Heat Flux", ASME Proceedings of the 1988 National Heat Transfer, (Ed.) H.R. Jacobs, Vol. 1, pp. 581-586.

Vasseur, P., Wang, C.H., and Sen, M., 1989a, "Thermal Instability and Natural Convection in a Fluid Layer Over a Porous Substrate", Warme-und Stoffubertragung, Vol. 24, pp. 337-347.

Vasseur, P., Wang, C.H., and Sen, M., 1989b, "The Brinkman Model for Natural Convection in a Shallow Porous Cavity with Uniform Heat Flux", Num. Heat Transfer, Part A, Vol. 15, pp. 221-242.

Villers, D., and J.K. Platten, 1988, "Thermal Convection in Superposed Immiscible Liquid Layers", Appl. Scien. Res., Vol. 45, pp. 145-152.

Vlasuk, M.P., 1972, "Convection Heat Transfer in a Porous Layer", 4th All-Union Heat Mass Transfer Conference, Minsk.

Walch, J.P. and Dulieu, B., 1979, "Convection Naturelle dans une Boîte Rectangulaire Légèrement Inclinée Contenant un Milieu Poreux", Int. J. Heat Mass Transfer, Vol. 22, pp. 1607-1612.

Walker, K.L., and Homsy, G.M., 1978, "Convection in a Porous Cavity", J. Fluid Mechanics, Vol. 87, pp. 449-474.

Weber, J.E., 1975, "The Boundary Layer Regime for Convection in a Vertical Porous Layer", Int. J. Heat Mass Transfer, Vol. 18, pp. 569-573.

Whitaker, S., 1969, "Advances in the Theory of Fluid Motion in Porous Media", Ind. Engng Chem. Vol. 61, pp. 110-121.

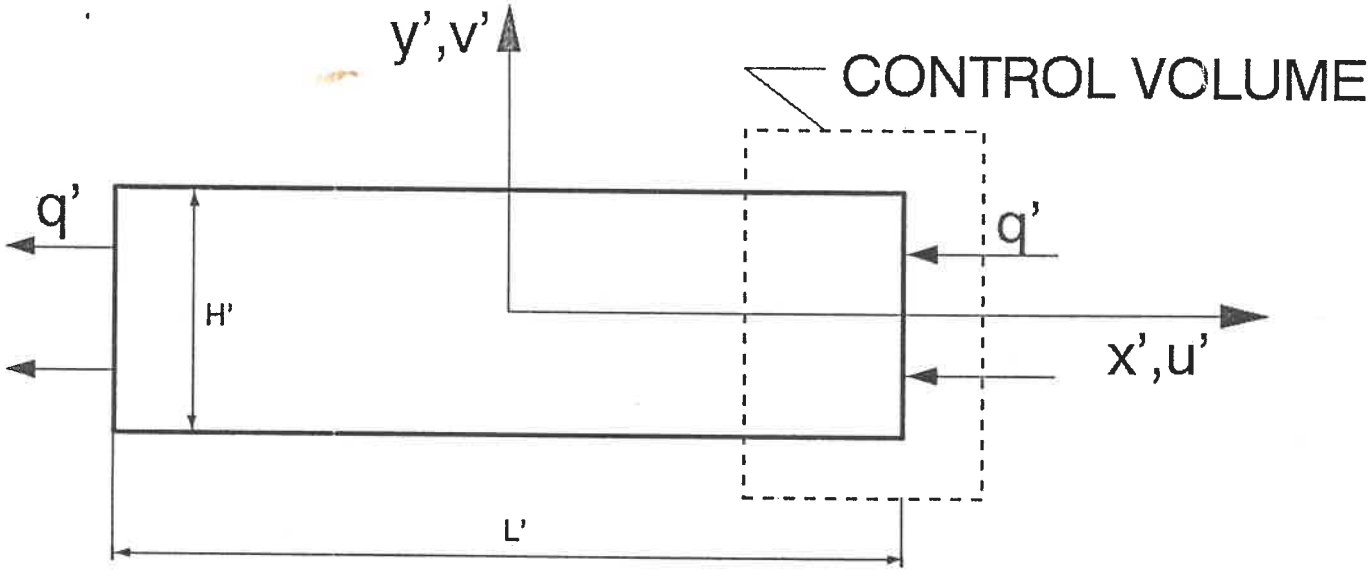

2.1: Schematic diagram of the two-dimensional porous layer

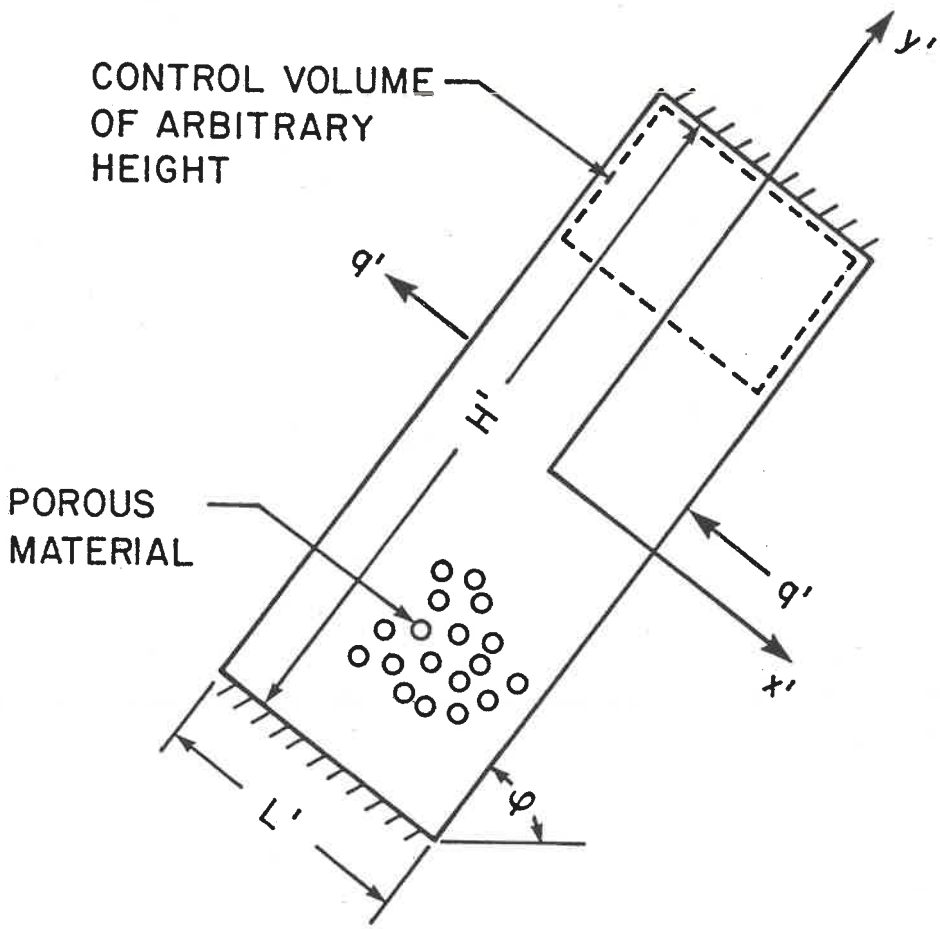

3.1: Flow configuration considered.

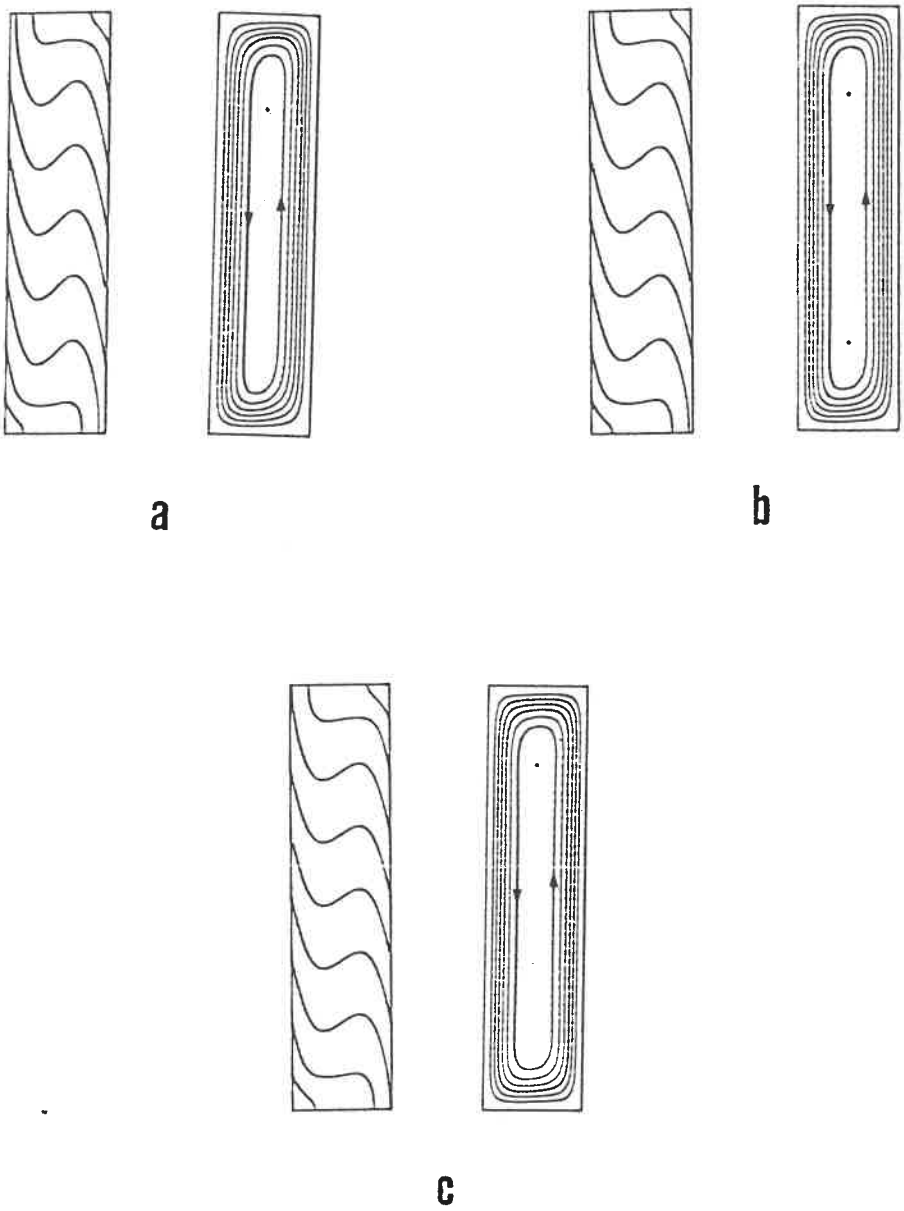

3.2: Isotherms and streamlines for

R=400, Da=10^{-2}, (a) $\varphi=20^0$, (b) $\varphi=35^0$, (c) $\varphi=50^0$
R=250, $\varphi=90^0$, (d) Da=10^{-4}, (e) Da=10^{-2}, (f) Da=1
Da=10^{-3}, $\varphi=80^0$, (g) R=50, (h) R=250, (i) R=500

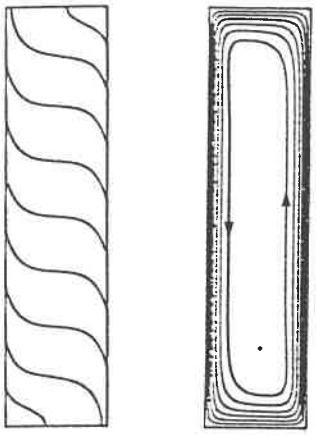

d

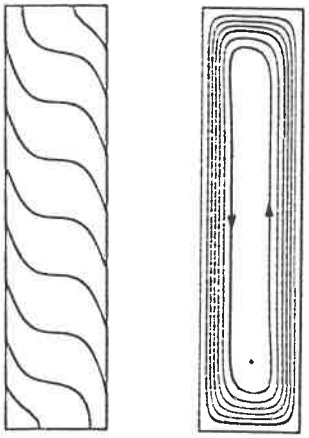

e

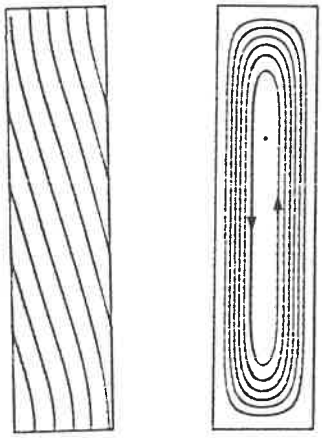

f

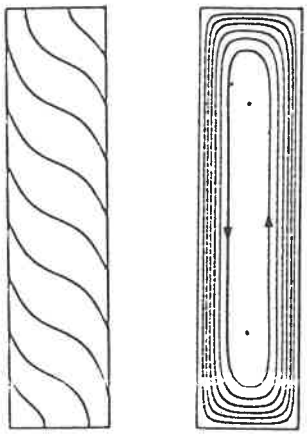

g

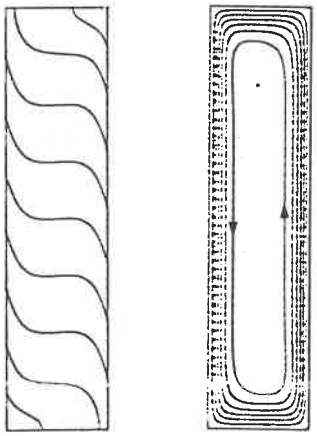

h

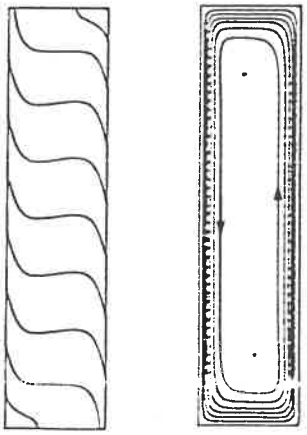

i

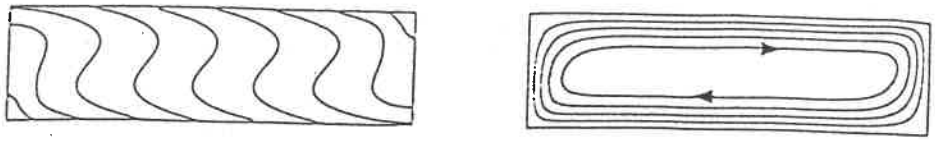

a) $R = 250$, $Da = 10^{-4}$, $\Psi_{max} = 5.957$, $T_{max} = 0.576$, $T_{min} = -0.576$, $Nu = 4.400$

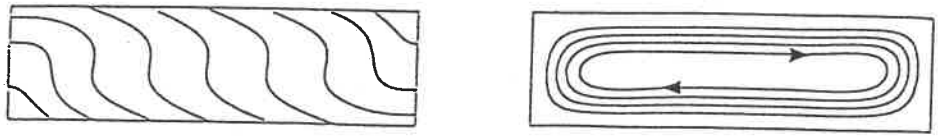

b) $R = 250$, $Da = 5 \times 10^{-2}$, $\Psi_{max} = 3.117$, $T_{max} = 0.991$, $T_{min} = -0.991$, $Nu = 2.324$

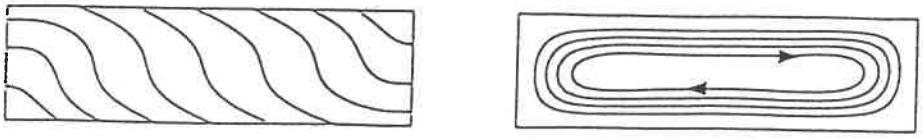

c) $R = 250$, $Da = 10^{-1}$, $\Psi_{max} = 2.200$, $T_{max} = 1.131$, $T_{min} = -1.131$, $Nu = 1.872$

3.3: Numerical solutions for the flow and temperature field.

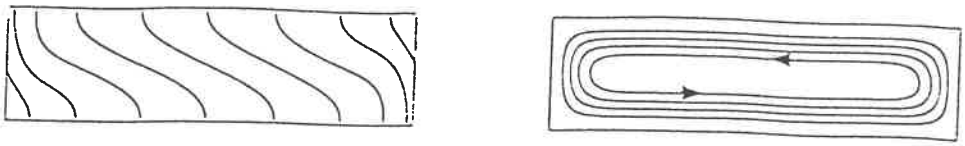

d) $R = 250$, $Da = 5 \times 10^{-2}$, $\Psi_{max} = 2.443$, $T_{max} = 0.233$, $T_{min} = -0.233$, $\Delta T = 0.377$

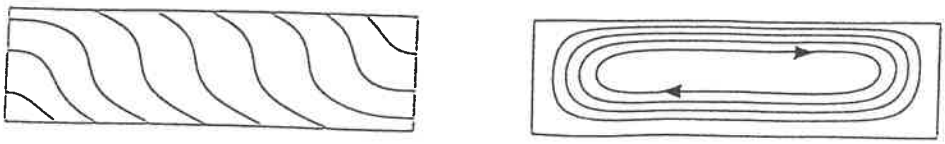

e) $R = 100$, $Da = 5 \times 10^{-2}$, $\Psi_{max} = 2.282$, $T_{max} = 1.119$, $T_{min} = -1.150$, $Nu = 2.148$

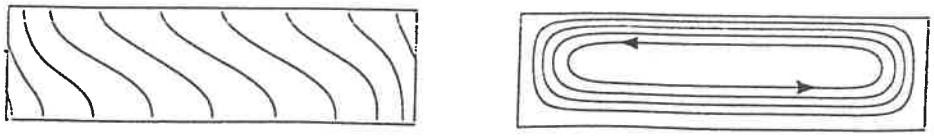

f) $R = 100$, $Da = 5 \times 10^{-2}$, $\Psi_{max} = 1.974$, $T_{max} = 0.266$, $T_{min} = -0.258$, $\Delta T = 0.415$

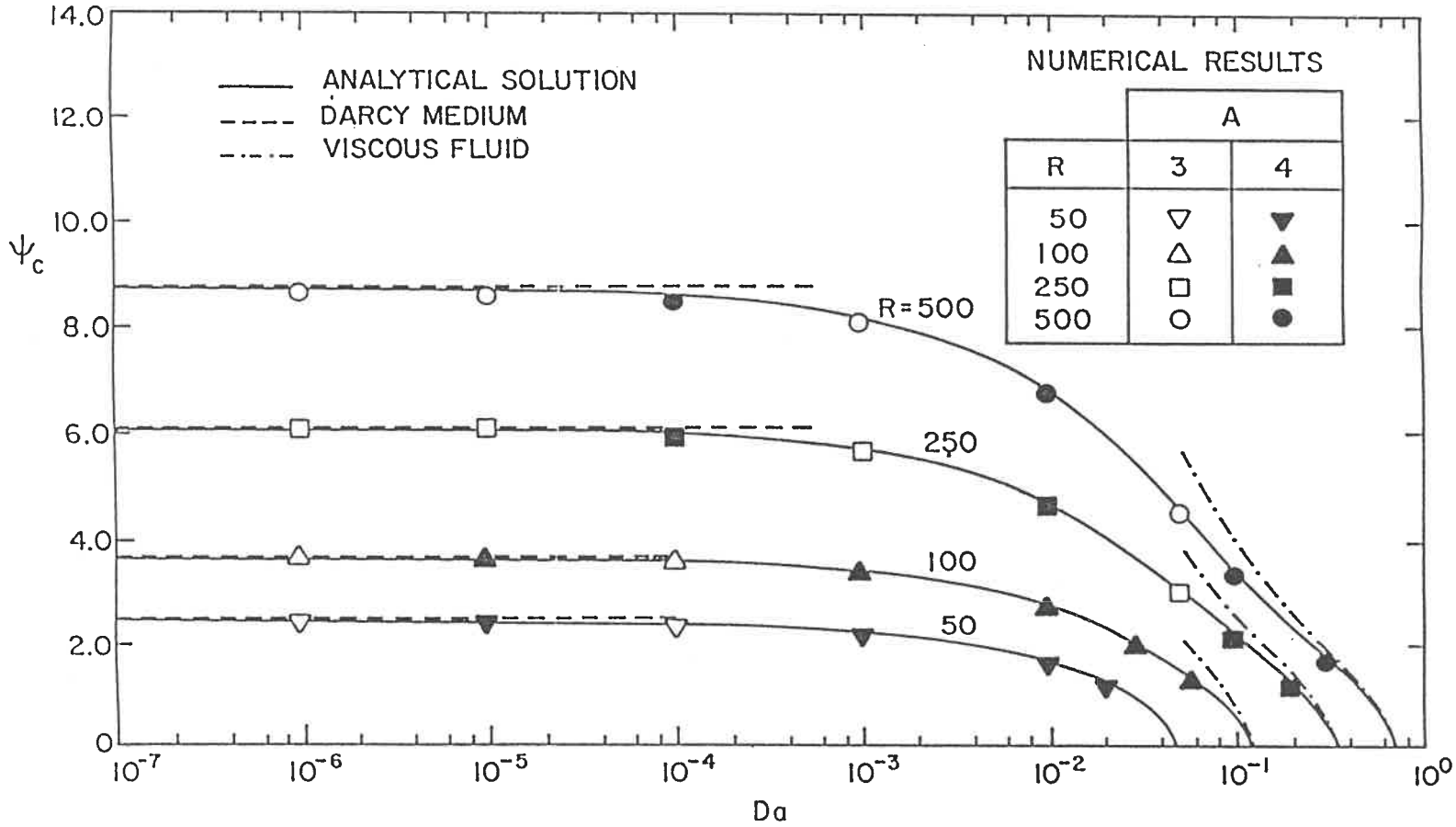

3.4(a): Stream function at center of layer Ψ_c as a function of Darcy number Da and Darcy-Rayleigh number R for bottom heating.

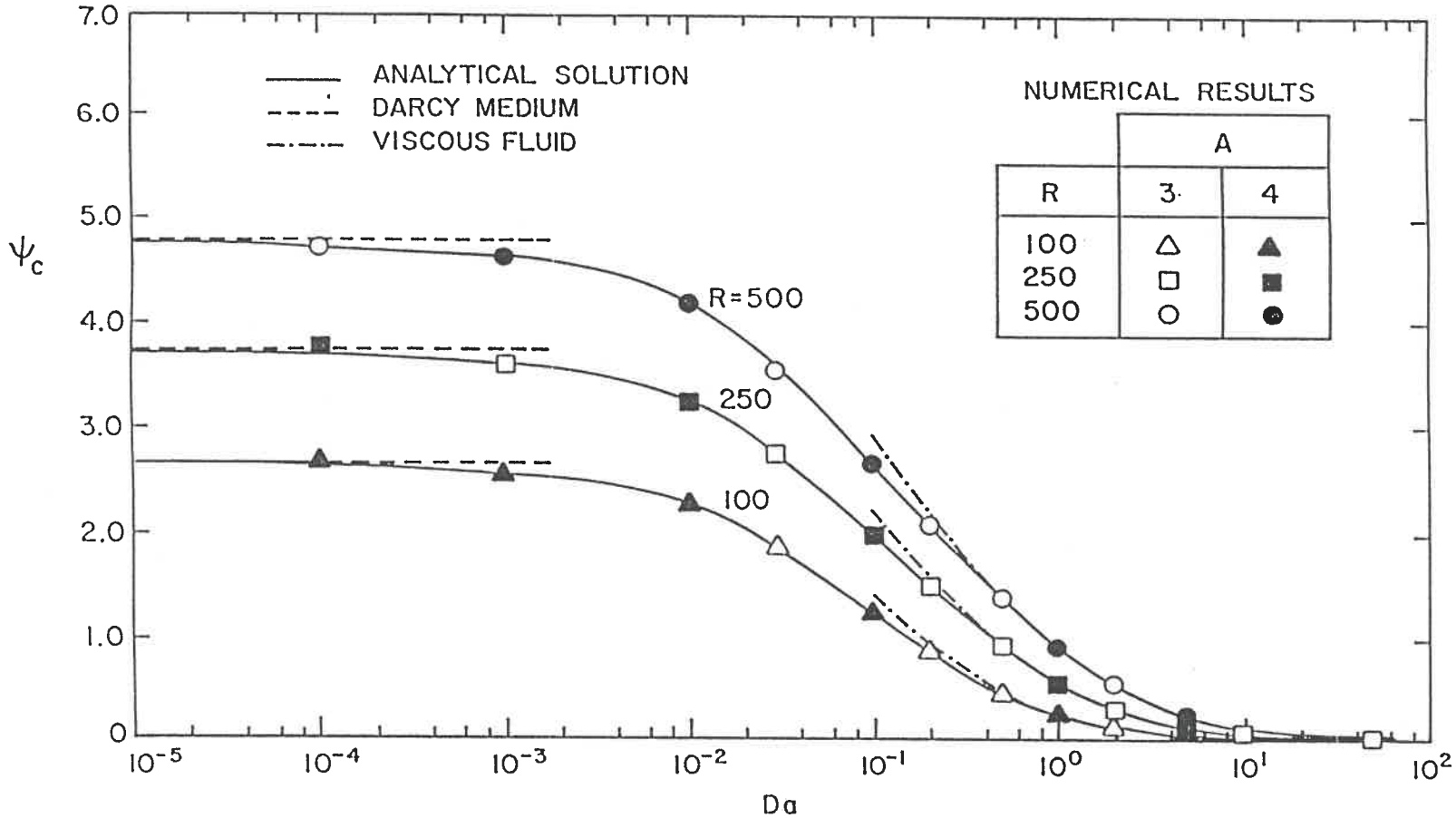

3.4(b): Stream function at center of layer Ψ_c as a function of Darcy numbser Da and Darcy-Rayleigh number R for side wall heating.

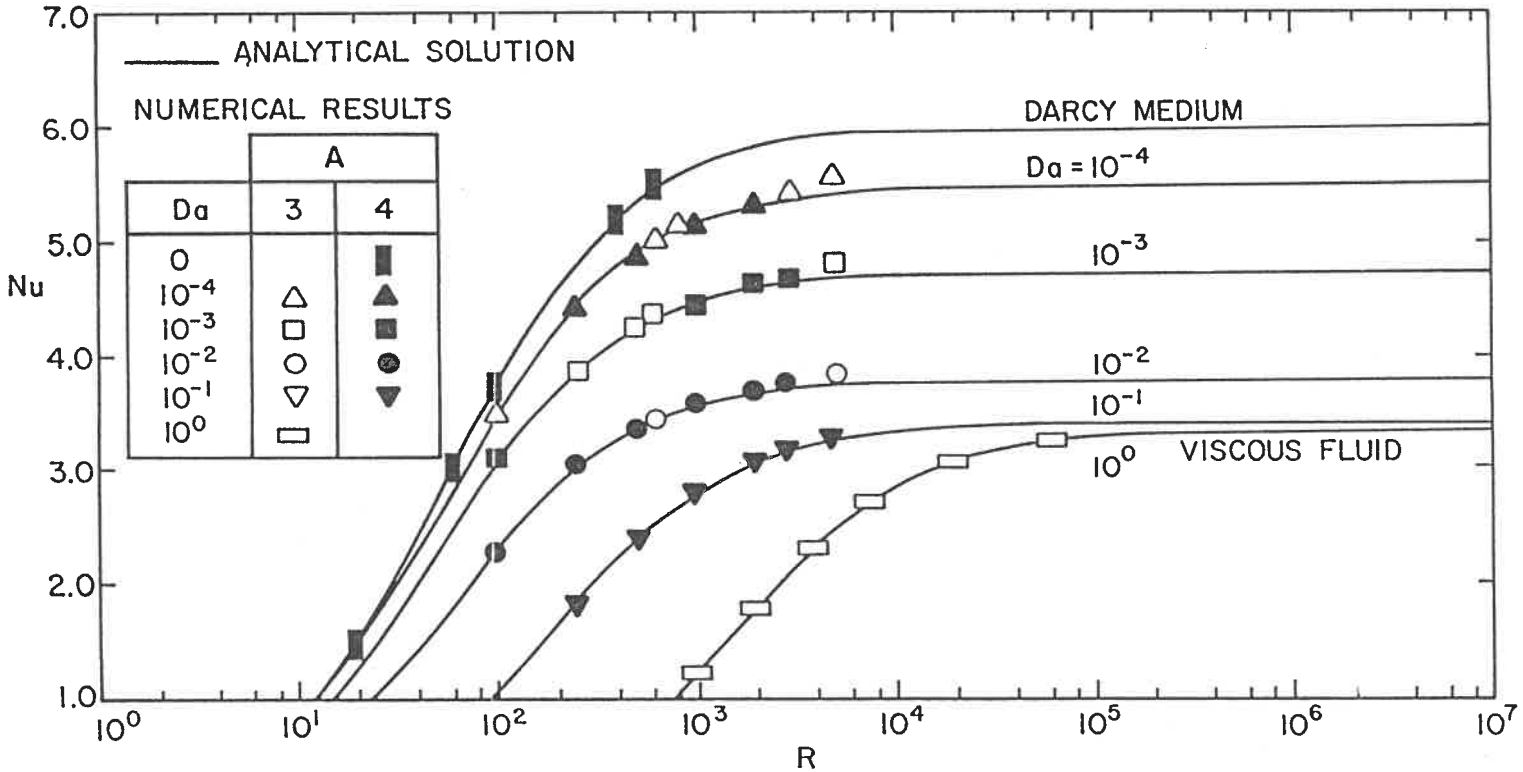

3.5: Nusselt number Nu as a function of Darcy-Rayleigh number R for selected values of Darcy number Da for bottom heating.

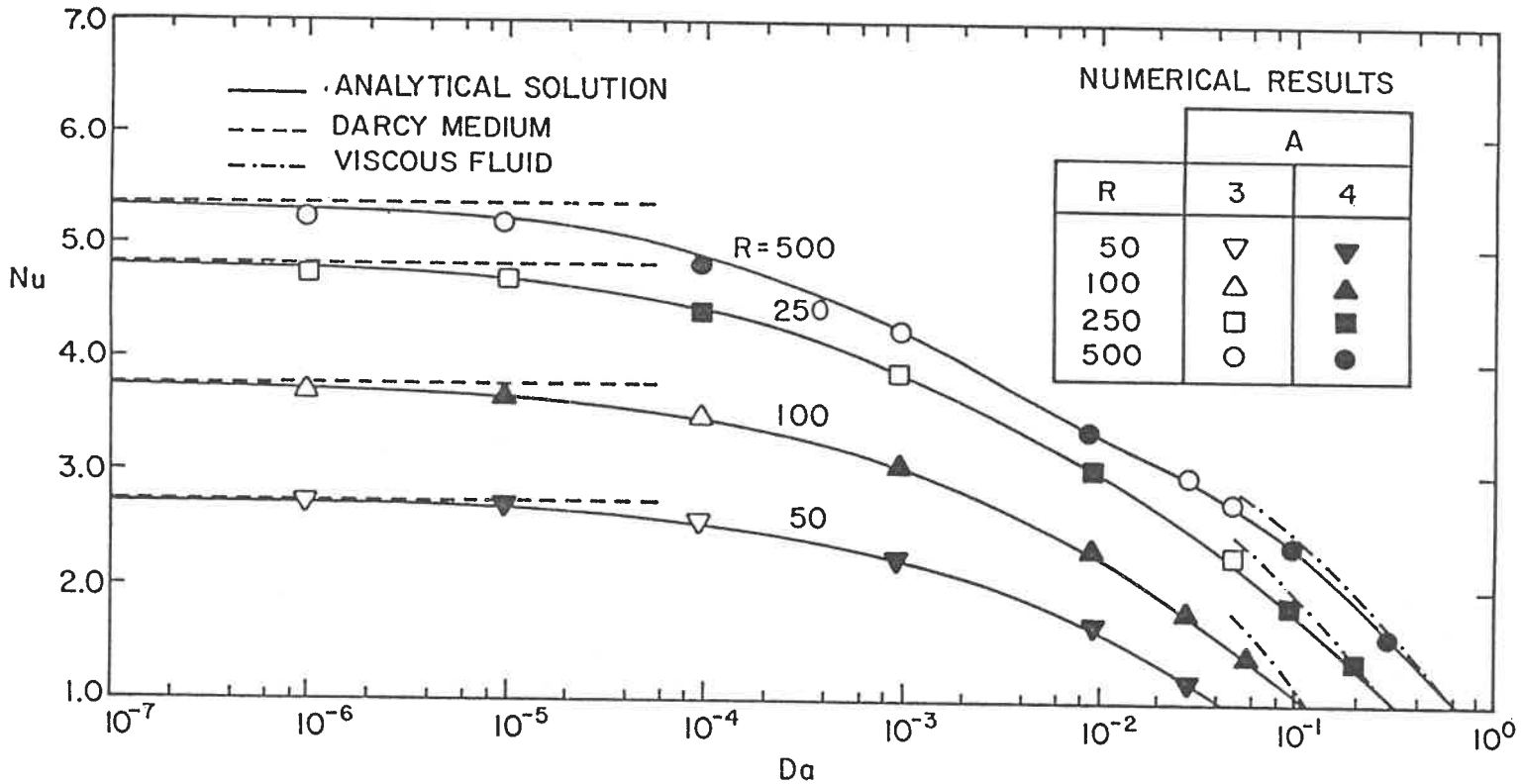

3.6: Nusselt numbesr Nu as a function of Darcy number Da for selected values of Darcy-Rayleigh number R for bottom heating.

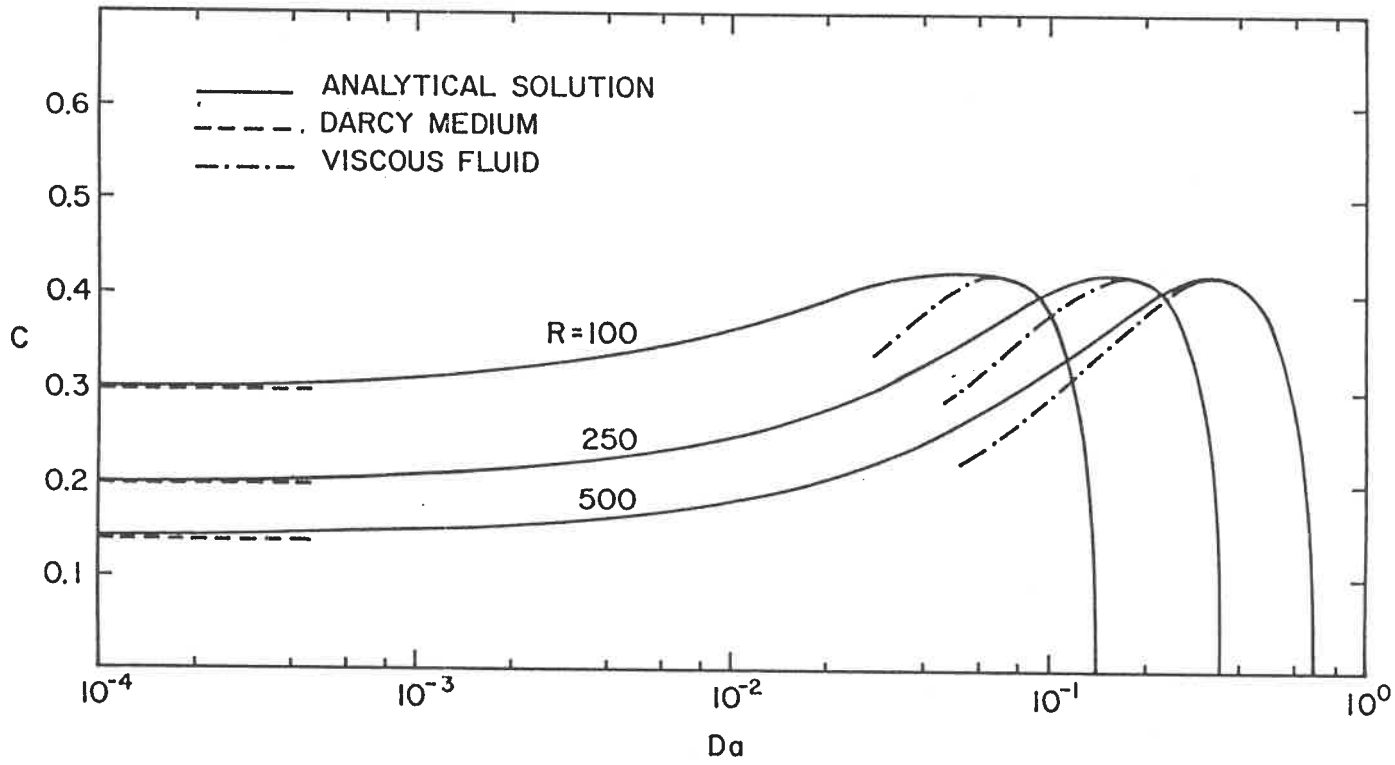

3.7: Temperature difference ΔT as a function of Darcy number Da for selected values of Darcy-Rayleigh number R for side wall heating

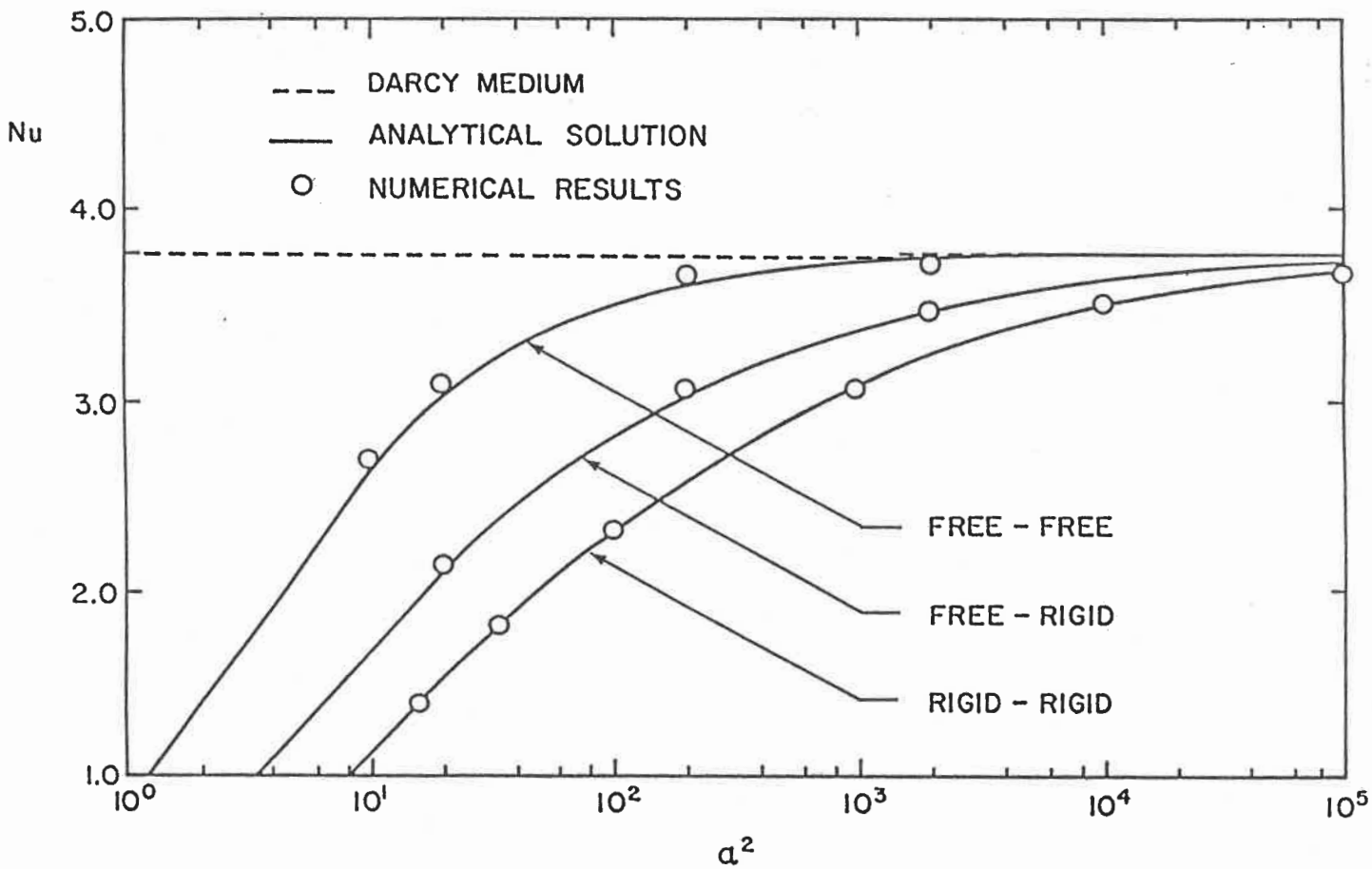

3.8: Comparison of Brinkman (present) and Darcy models for R = 100 for bottom heating.

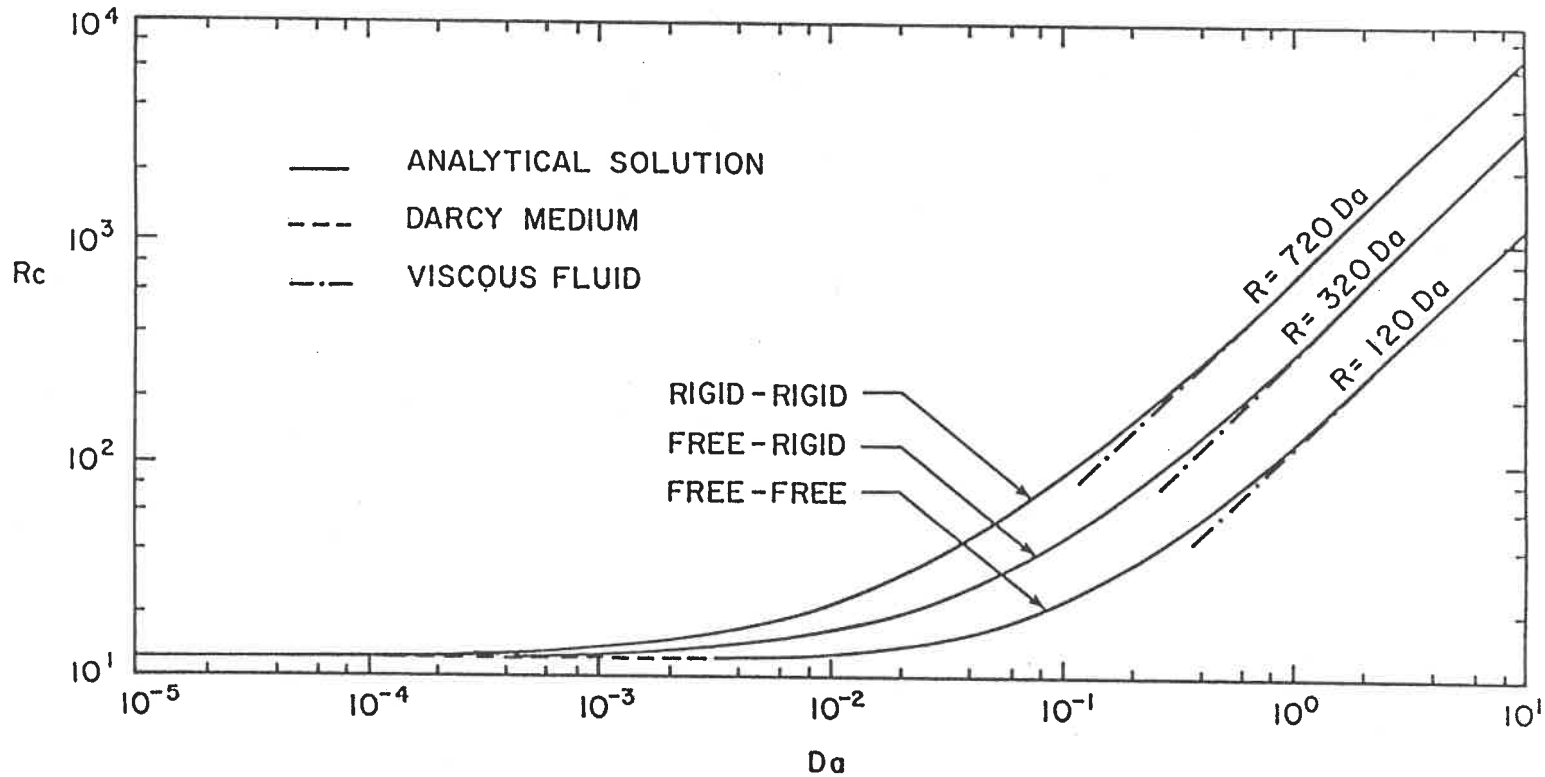

3.9: Critical Darcy-Rayleigh number R_c as a function of Darcy number Da for bottom heating

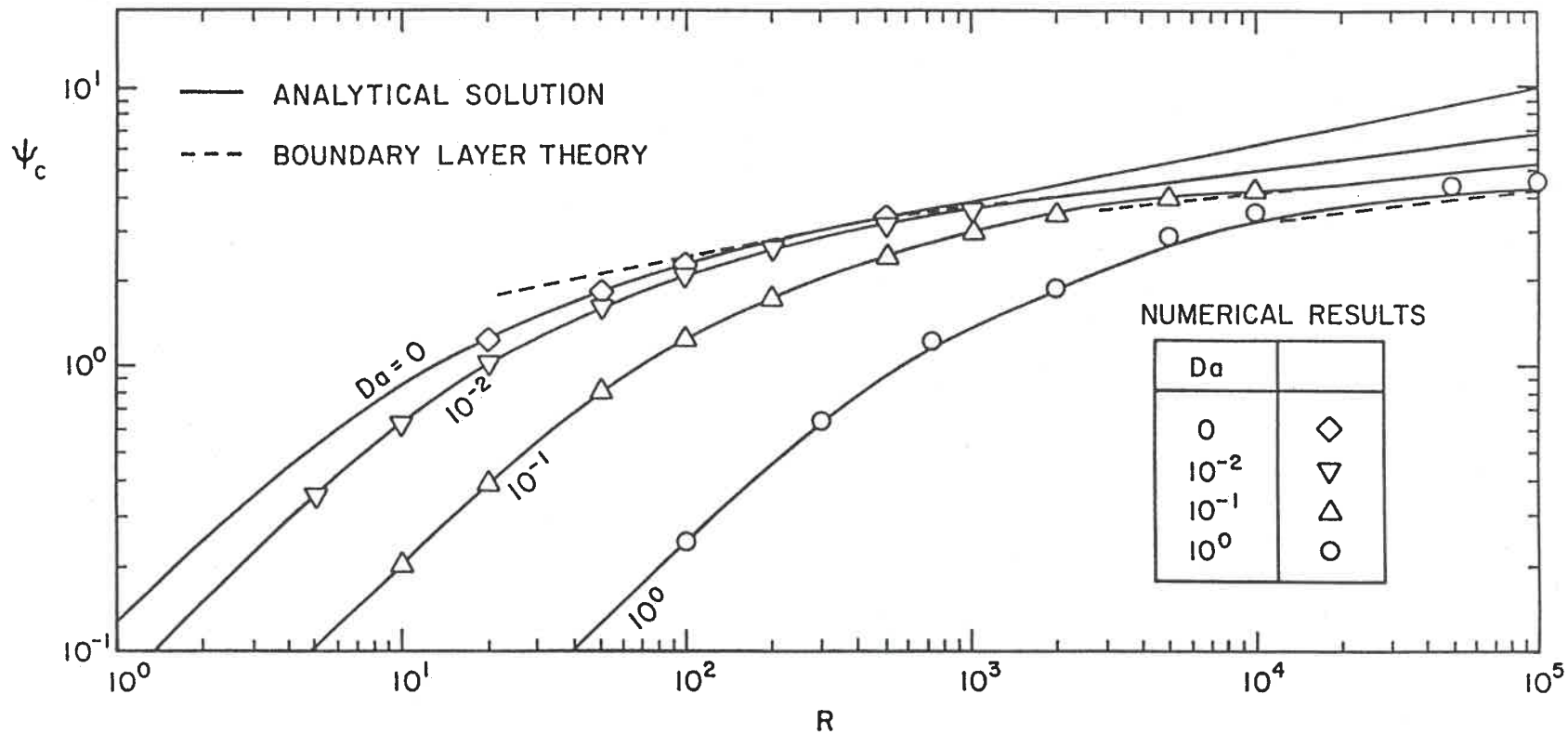

3.10: Stream function at center of layer Ψ_c as a function of Rayleigh number R and Darcy number Da.

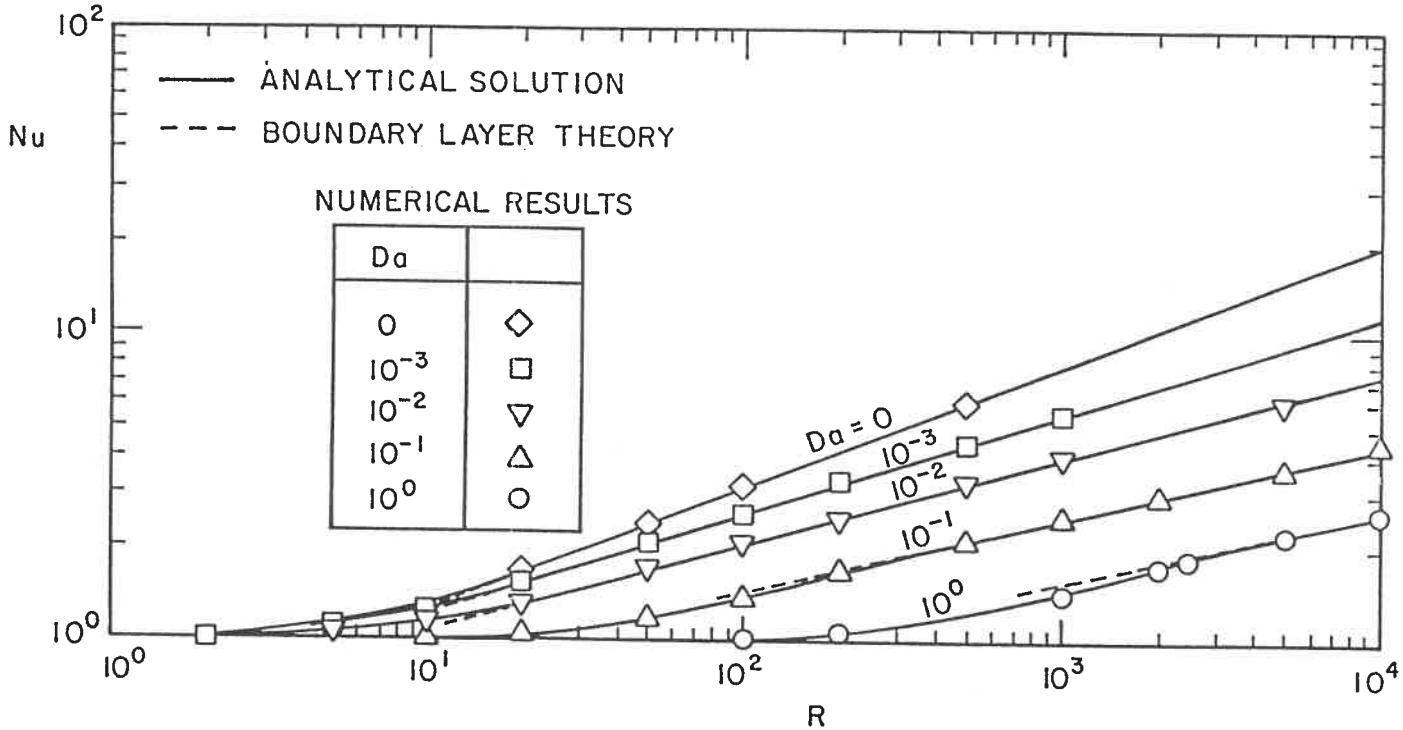

3.11: Nusselt number Nu as a function of Rayleigh number R and Darcy number Da.

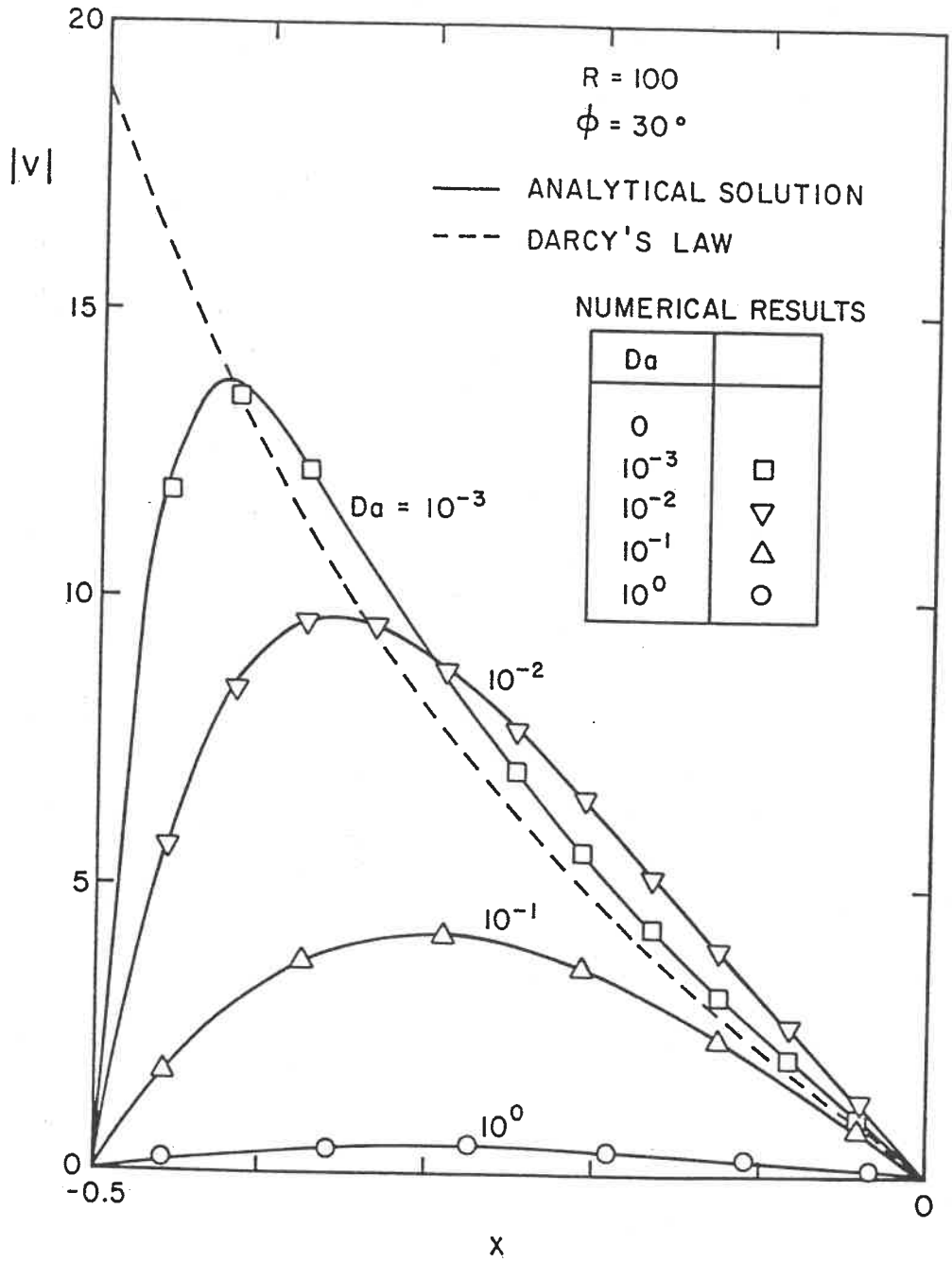

a

3.12: Velocity profile at mid-height of the enclosure, y = 0, as a function of Darcy number Da for R = 100 and (a) $\varphi = 30^0$, (b) $\varphi = 90^0$, $\varphi = 120^0$.

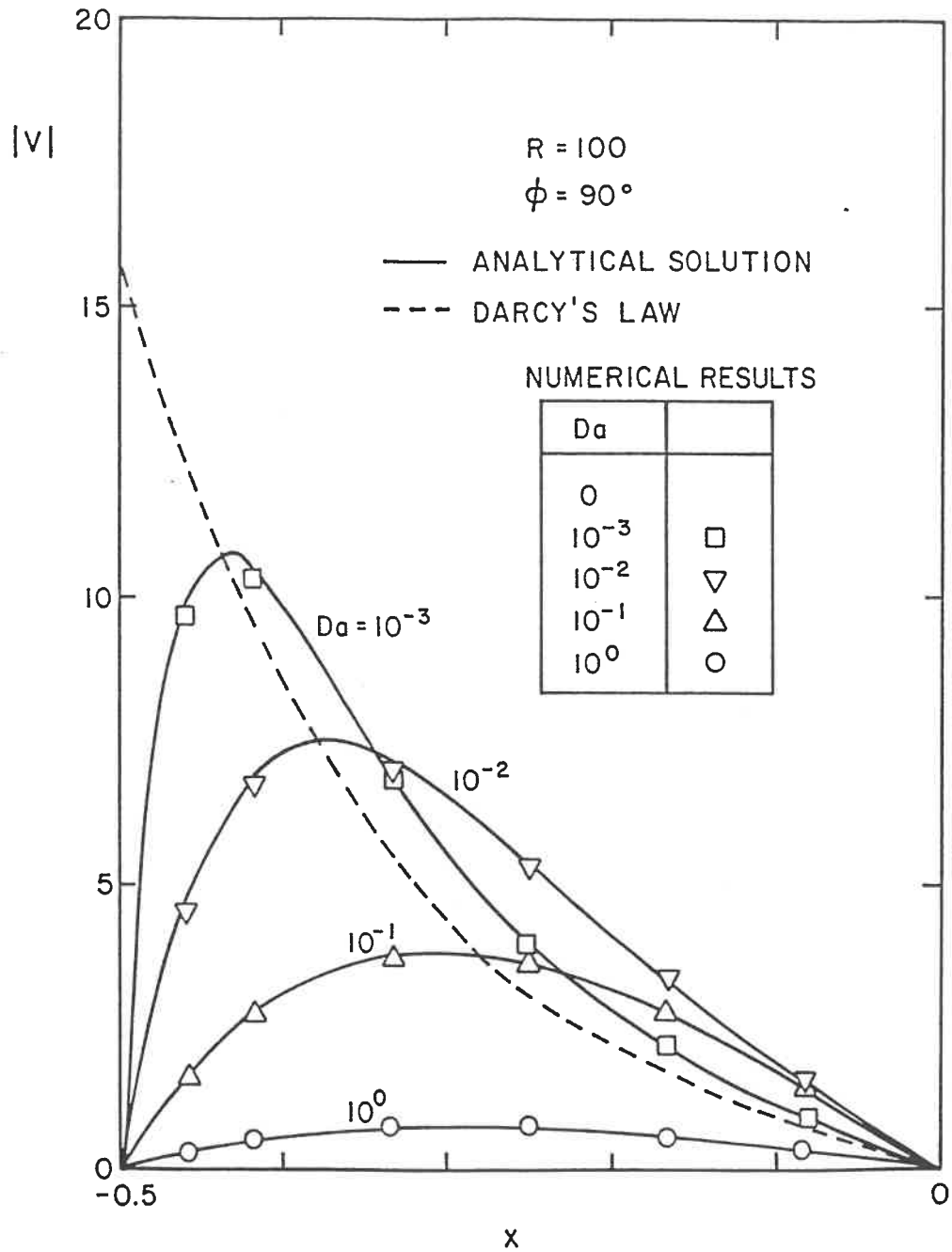
20
15
10
5
0
|V|
R = 100
ϕ = 90°
ANALYTICAL SOLUTION
DARCY'S LAW
NUMERICAL RESULTS
Da
0
10^-3
10^-2
10^-1
10^0
Da = 10^-3
10^-2
10^-1
10^0
-0.5
0
x

b

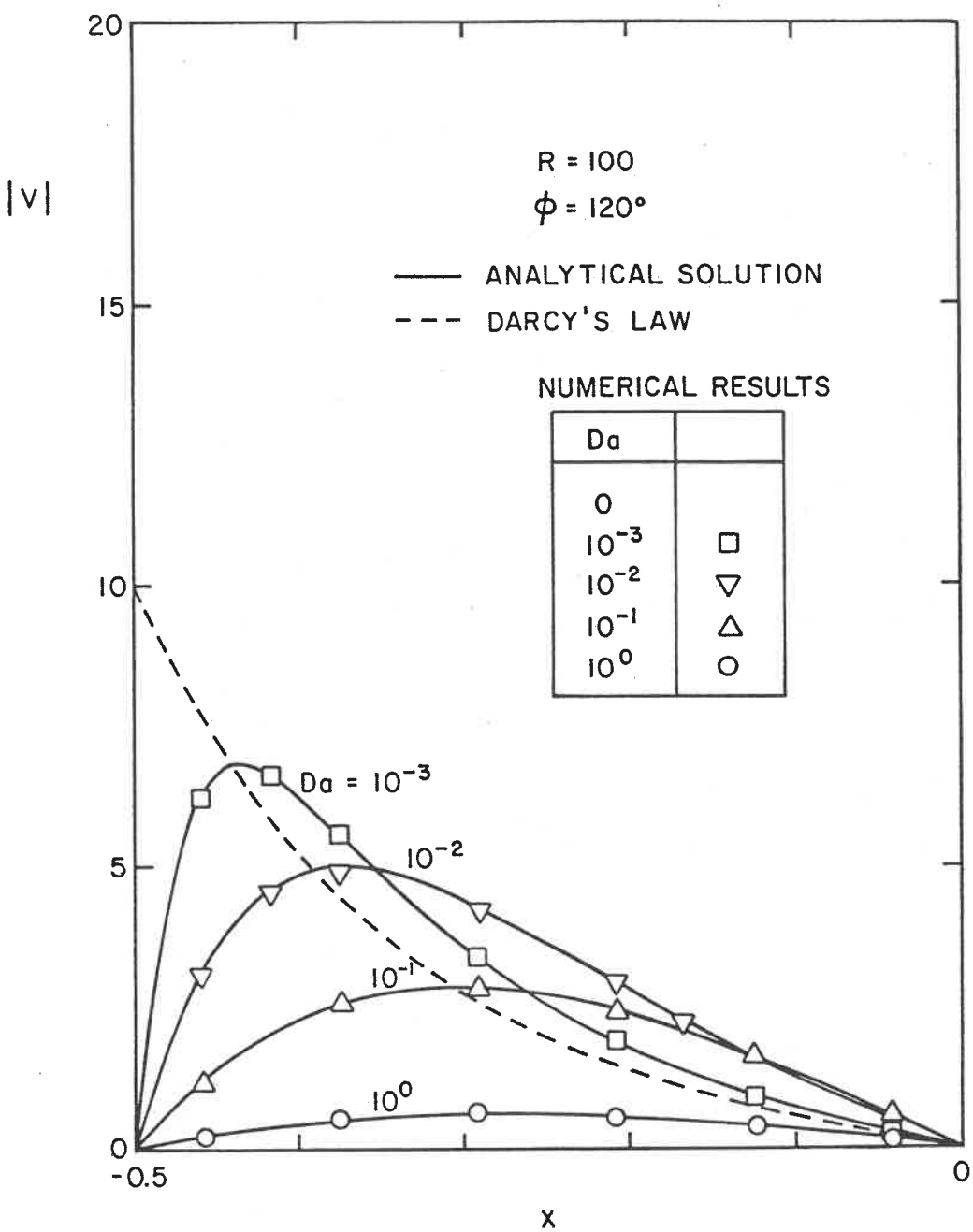
20
15
10
5
0
|V|
R = 100
ϕ = 120°
ANALYTICAL SOLUTION
DARCY'S LAW
NUMERICAL RESULTS
Da
0
10^{-3}
10^{-2}
10^{-1}
10^{0}
Da = 10^{-3}
10^{-2}
10^{-1}
10^{0}
-0.5
0
X

C

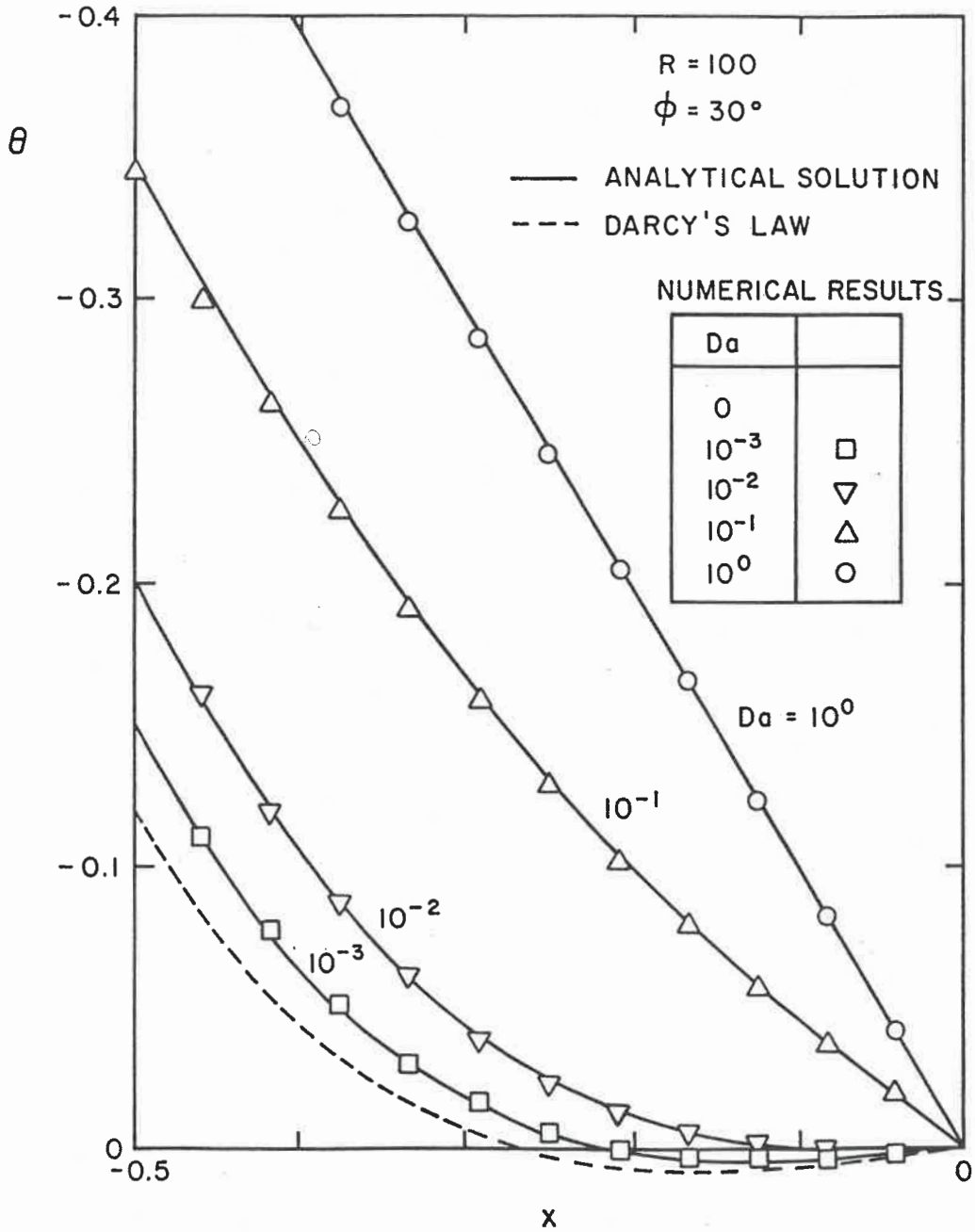

a

3.13: Temperature profile at mid-height of the enclosure, y = 0, as a function of Darcy number Da for R = 100 and (a) $\varphi = 30^0$, (b) $\varphi - 90^0$, $\varphi = 120^0$.

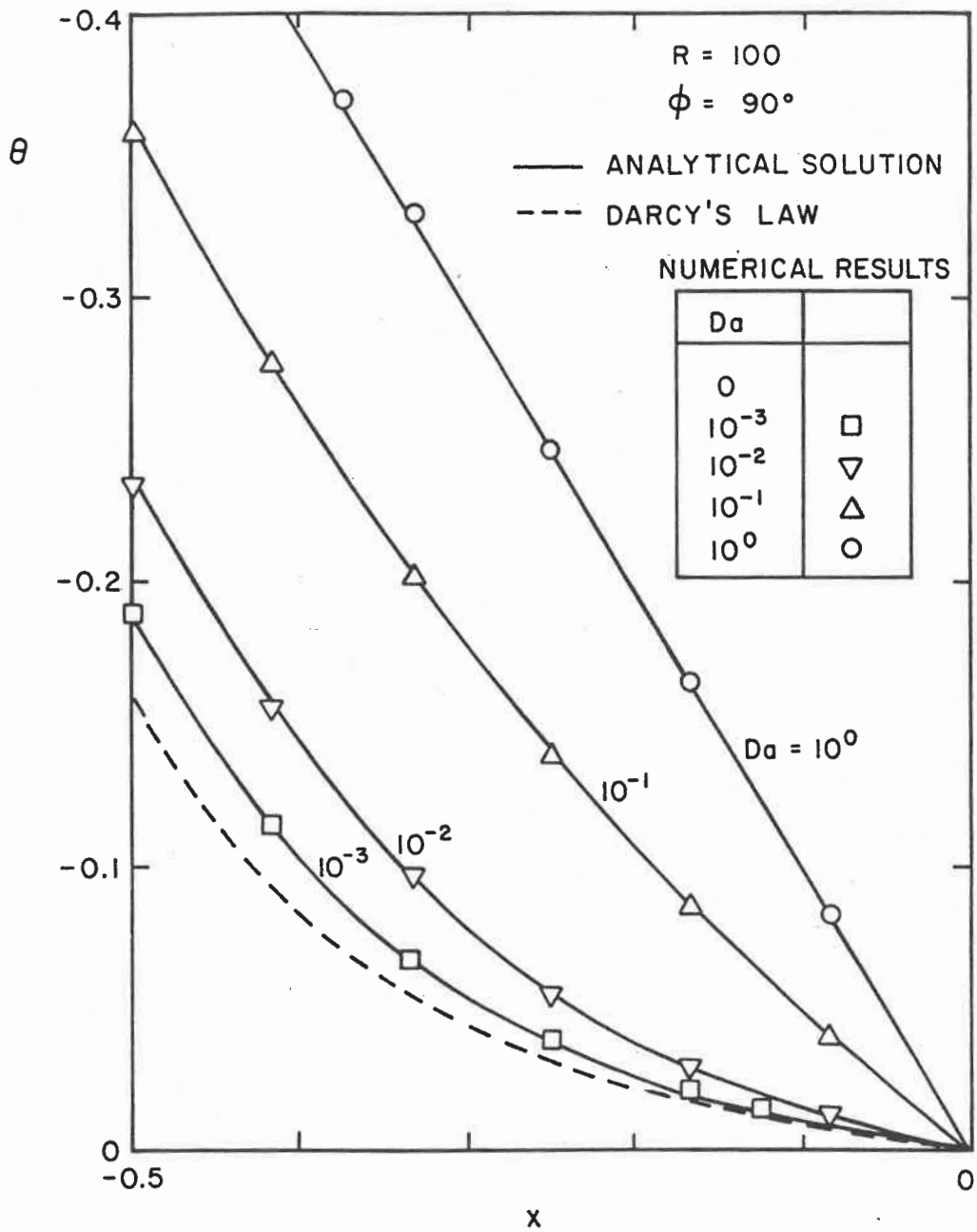
R = 100
ϕ = 90°
ANALYTICAL SOLUTION
DARCY'S LAW
NUMERICAL RESULTS
Da
0
10^{-3}
10^{-2}
10^{-1}
10^{0}
Da = 10^{0}
10^{-1}
10^{-2}
10^{-3}
θ
-0.4
-0.3
-0.2
-0.1
0
-0.5
0
x

b

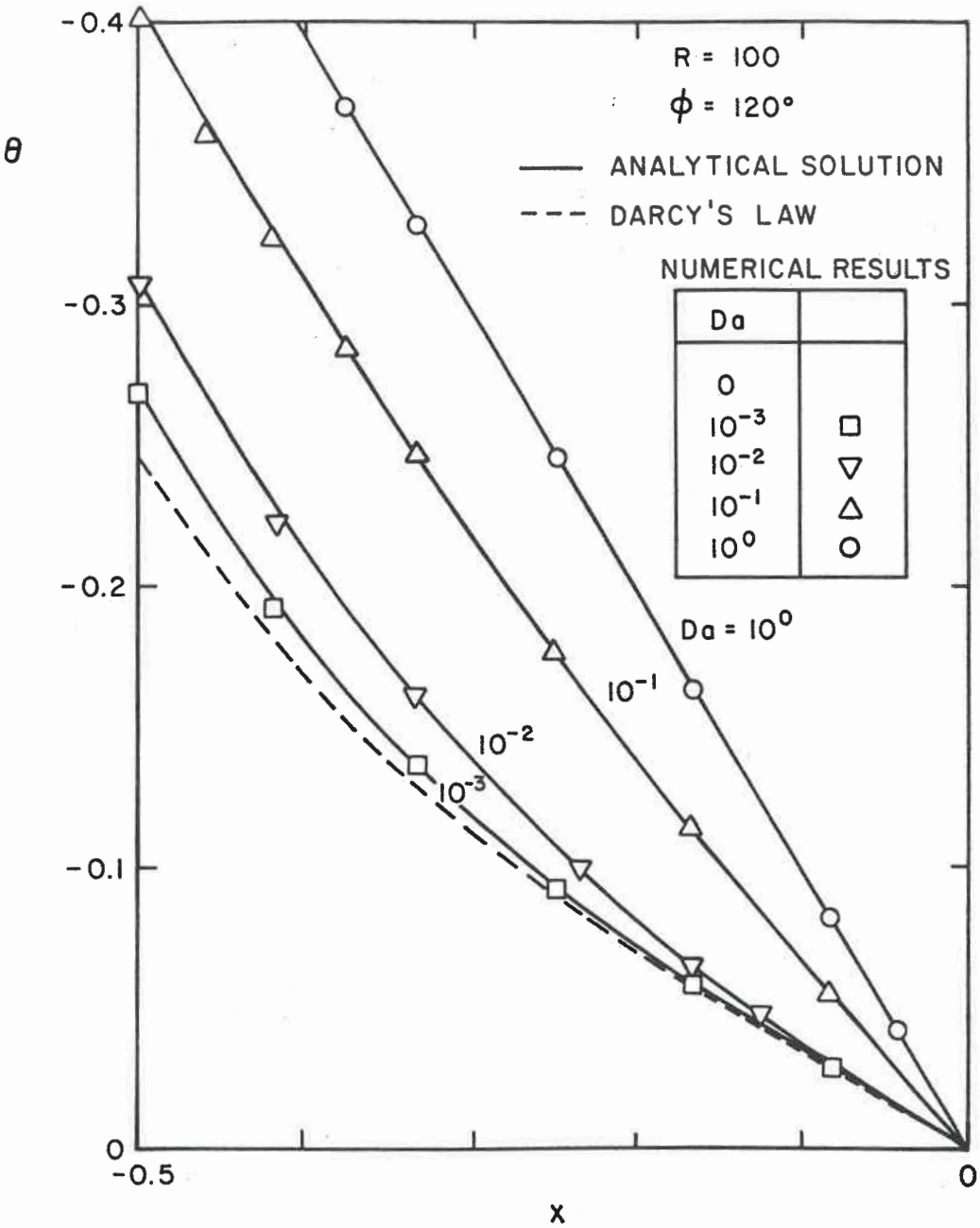
R = 100
ϕ = 120°
ANALYTICAL SOLUTION
DARCY'S LAW
NUMERICAL RESULTS
Da
0
10^-3
10^-2
10^-1
10^0
Da = 10^0
10^-1
10^-2
10^-3
θ
-0.4
-0.3
-0.2
-0.1
0
-0.5
0
x

C

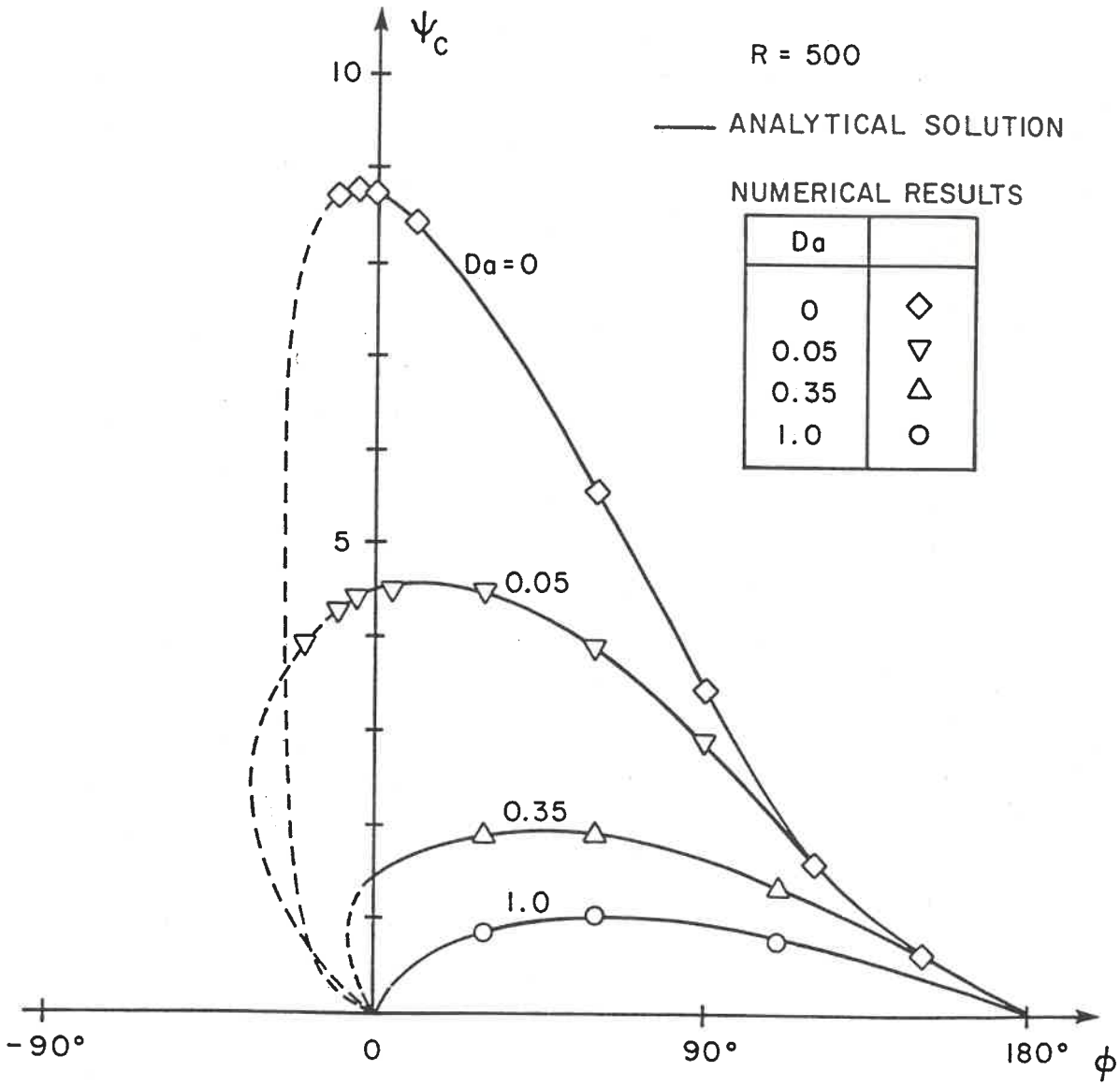

3.14: Variation of sdtream function at center of layer, Ψ_c, as a function of tilt angle φ for various values of Da for R = 500.

Page 188 manquante

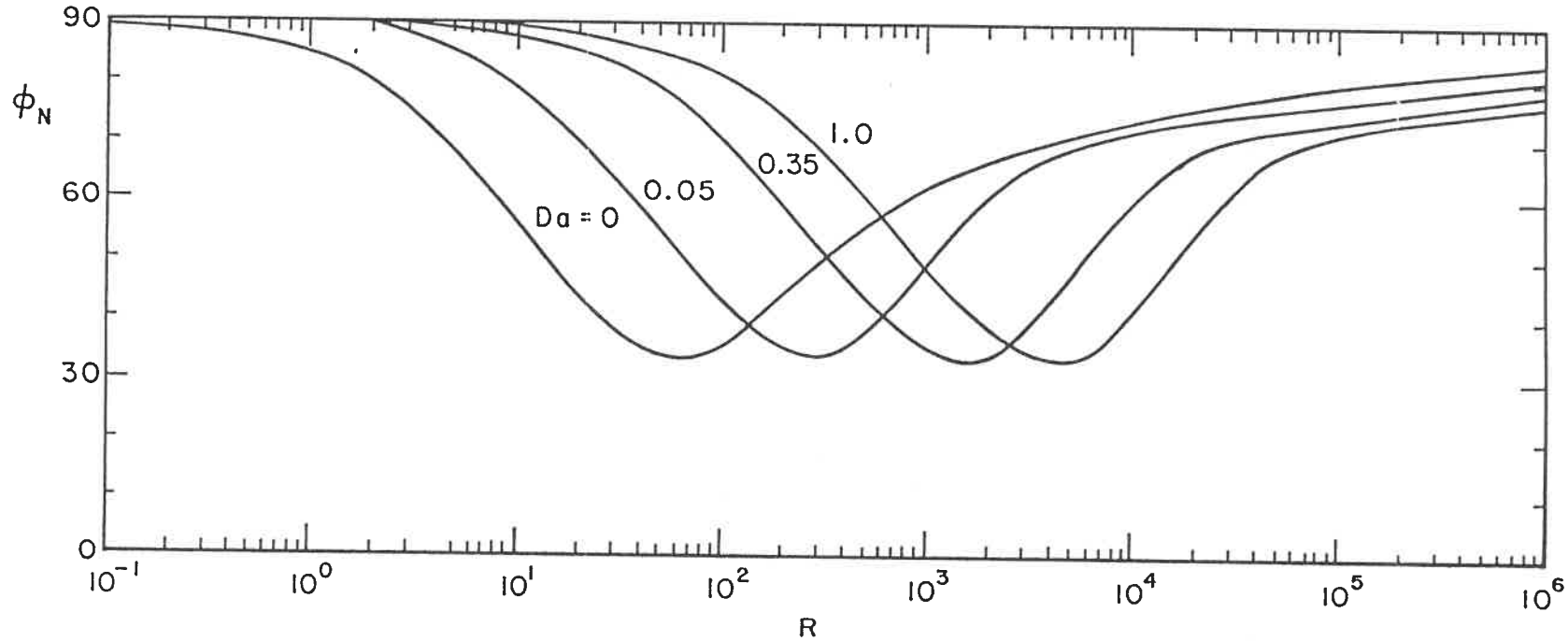

3.16: Tilt angle for maximum Nusselt number, φ_N, as a function of Rayleigh number R and Darcy number Da.

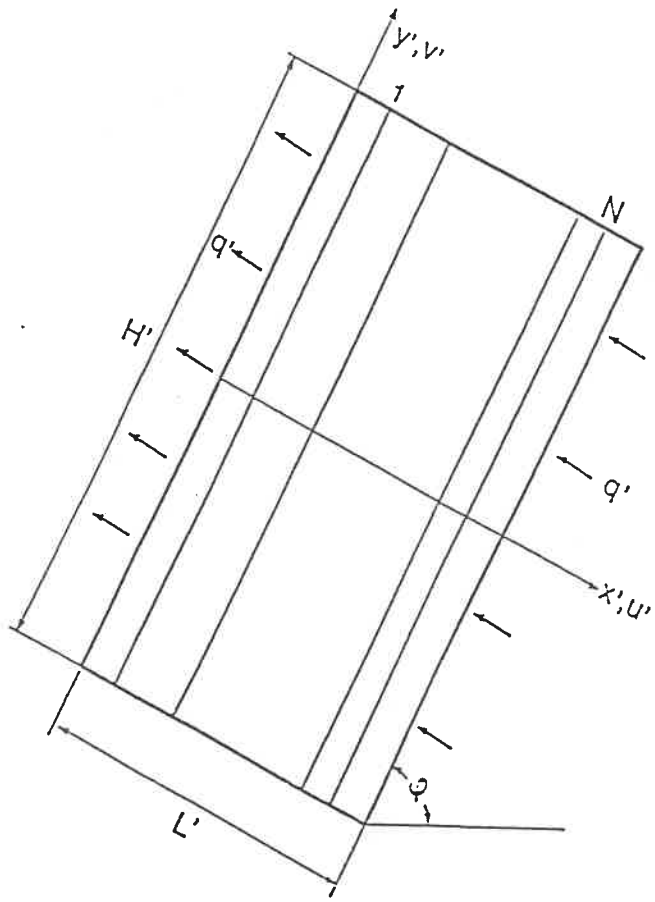

4.1: Schematic diagram of the partitioned inclined porous layer.

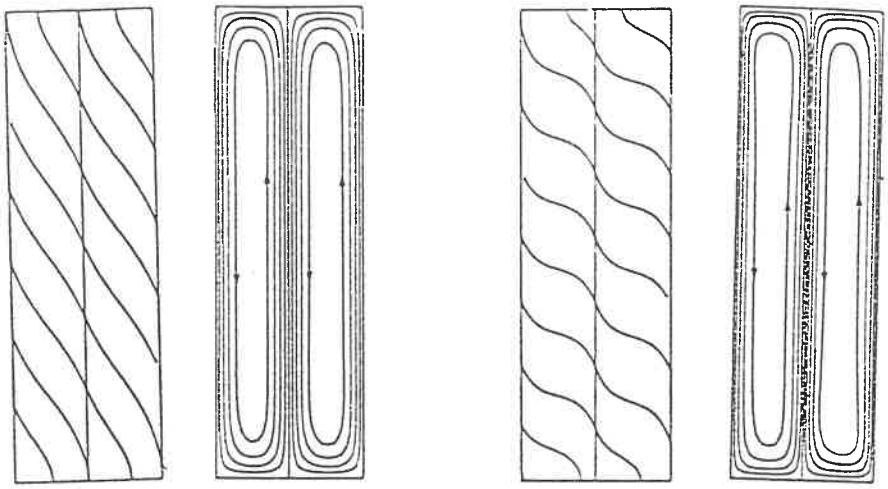

a b

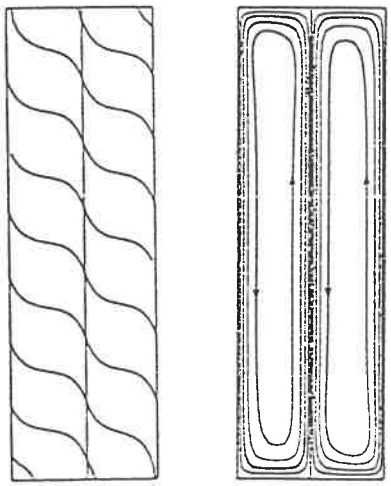

c

4.2: Isotherms and streamlines for

(a) R=50, η=0.5, φ=90^0
(b) R=300, η=0.5, φ=90^0
(c) R=500, η=0.5, φ=90^0
(d) R=500, η=0.2, φ=90^0
(e) R=500, η=0.5, φ=60^0
(f) R=500, η=0.5, φ=0^0

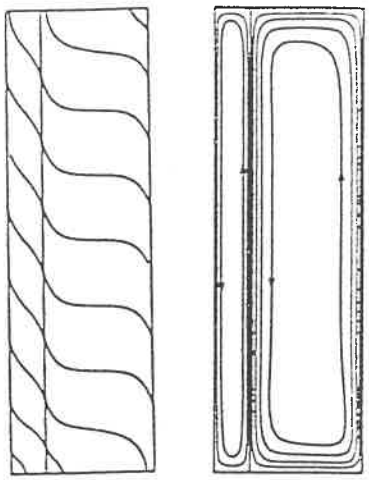

d

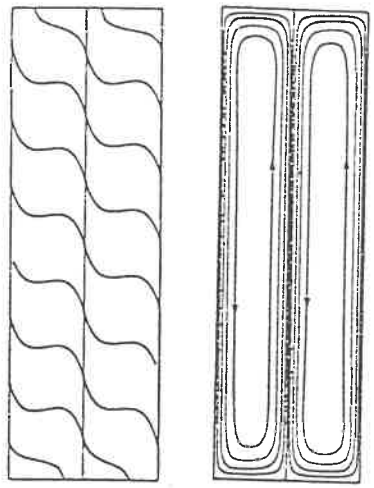

e

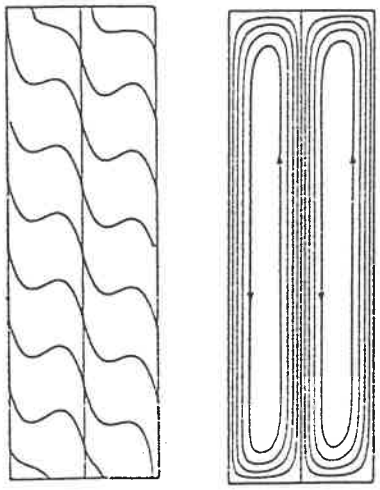

f

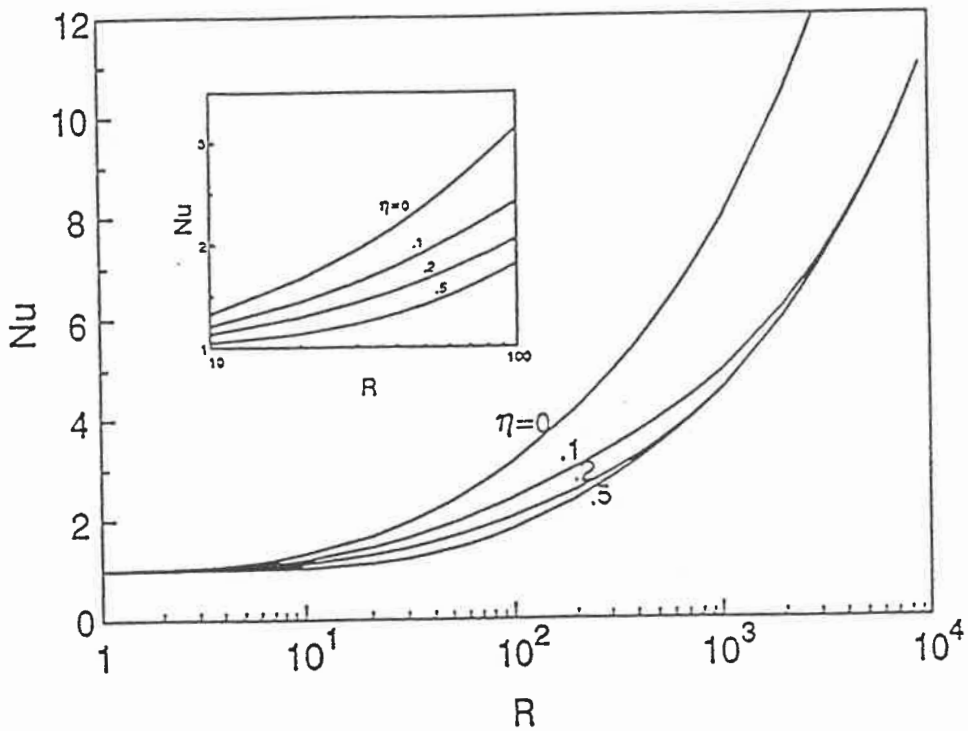

4.3: Heat transfer through a vertical porous layer with a single partition: effect of the partition position.

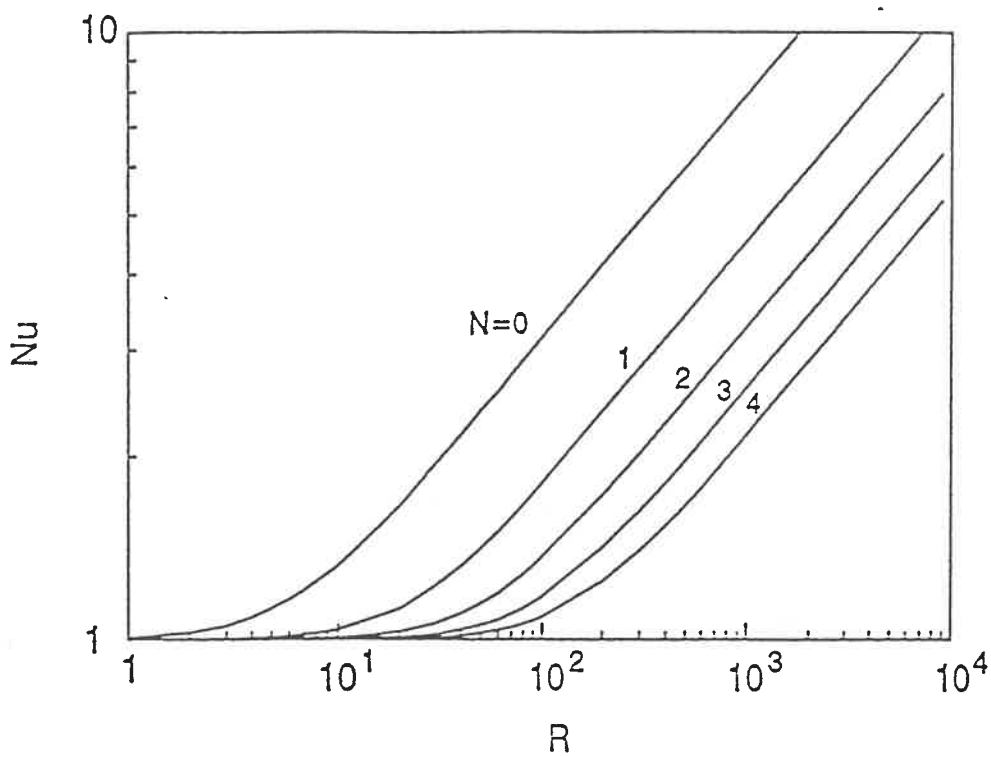

4.4: Heat transfer through a vertical porous layer with N equally spaced partitions.

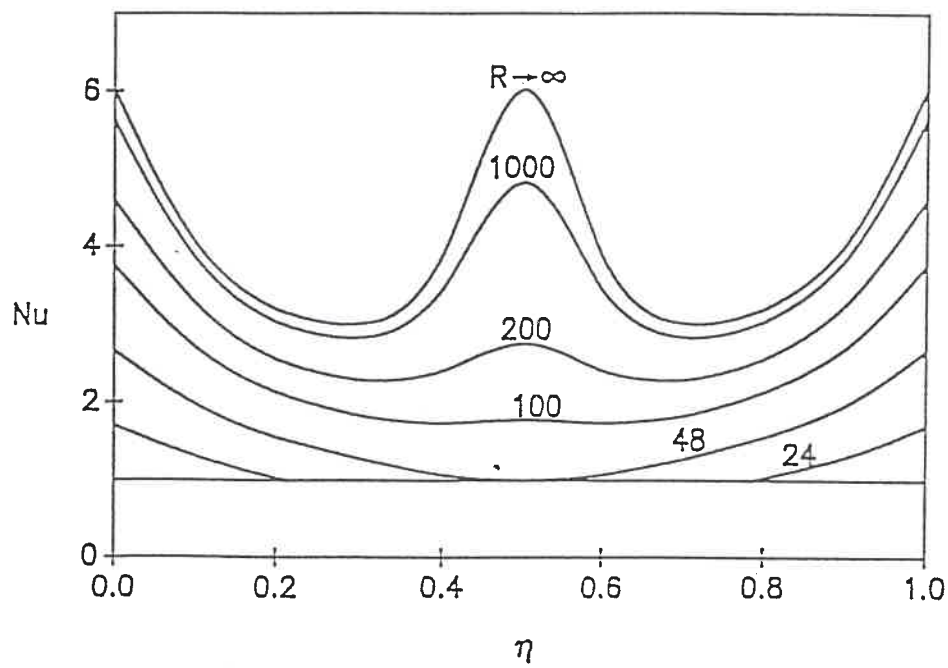

4.5: Heat transfer through a horizontal porous layer with a single partition: effect of the partition position.

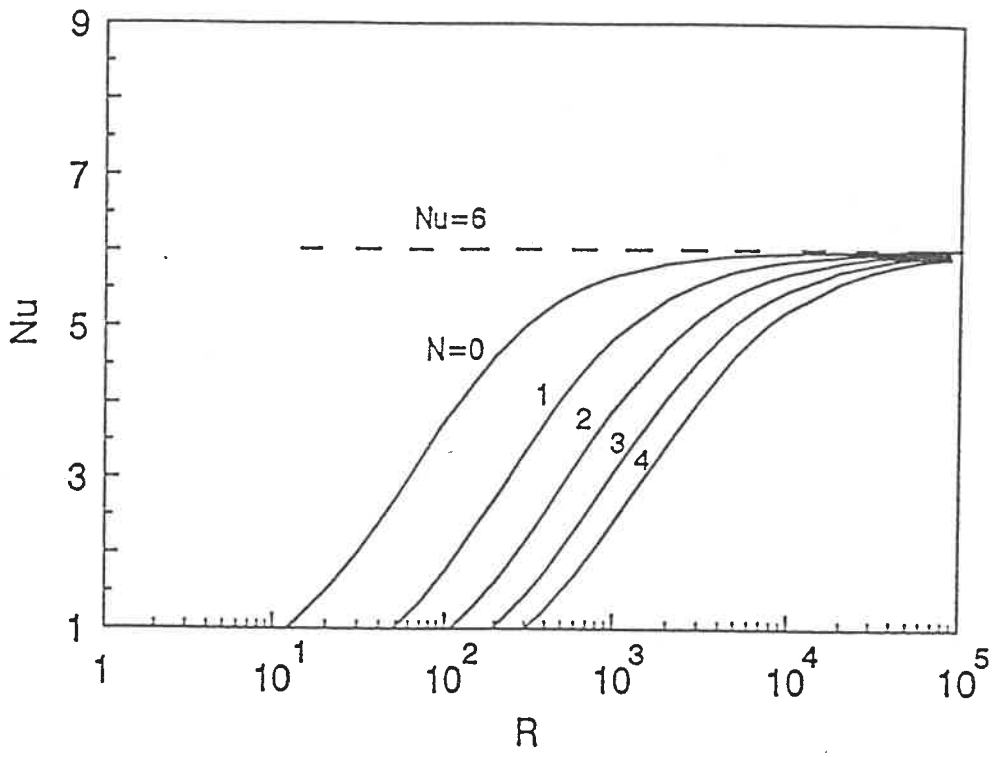

4.6: Heat transfer through a horizontal porous layer with N equally spaced partitions.

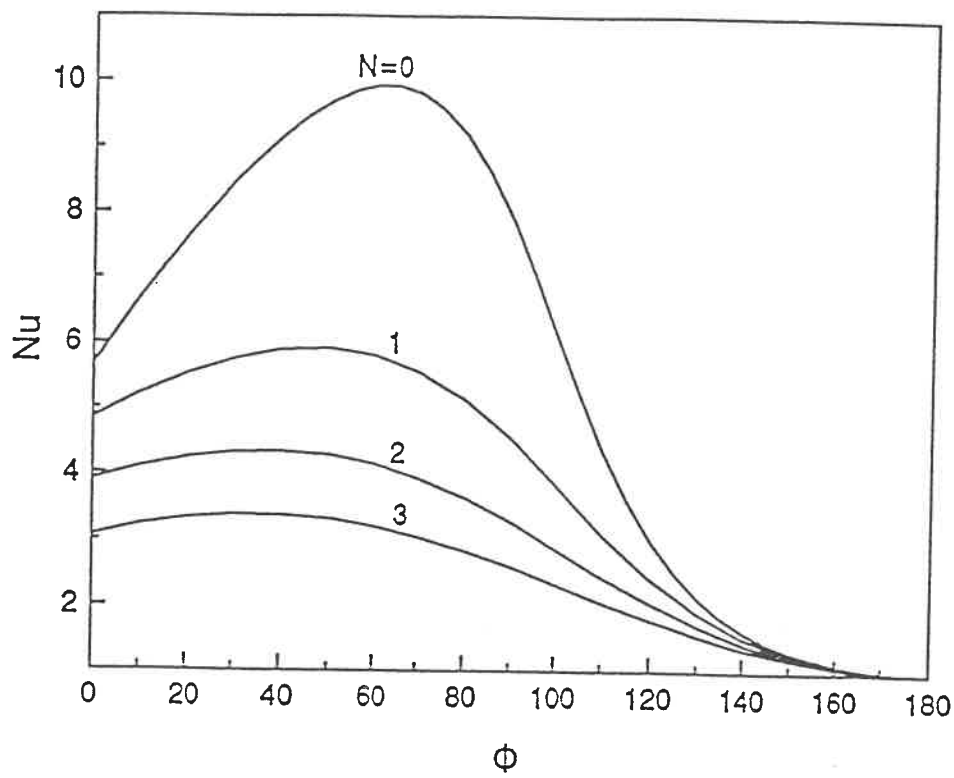

4.7: Effects of inclination angle φ or heat transfer through a porous layer with N equally spaced partitions, R = 1000.

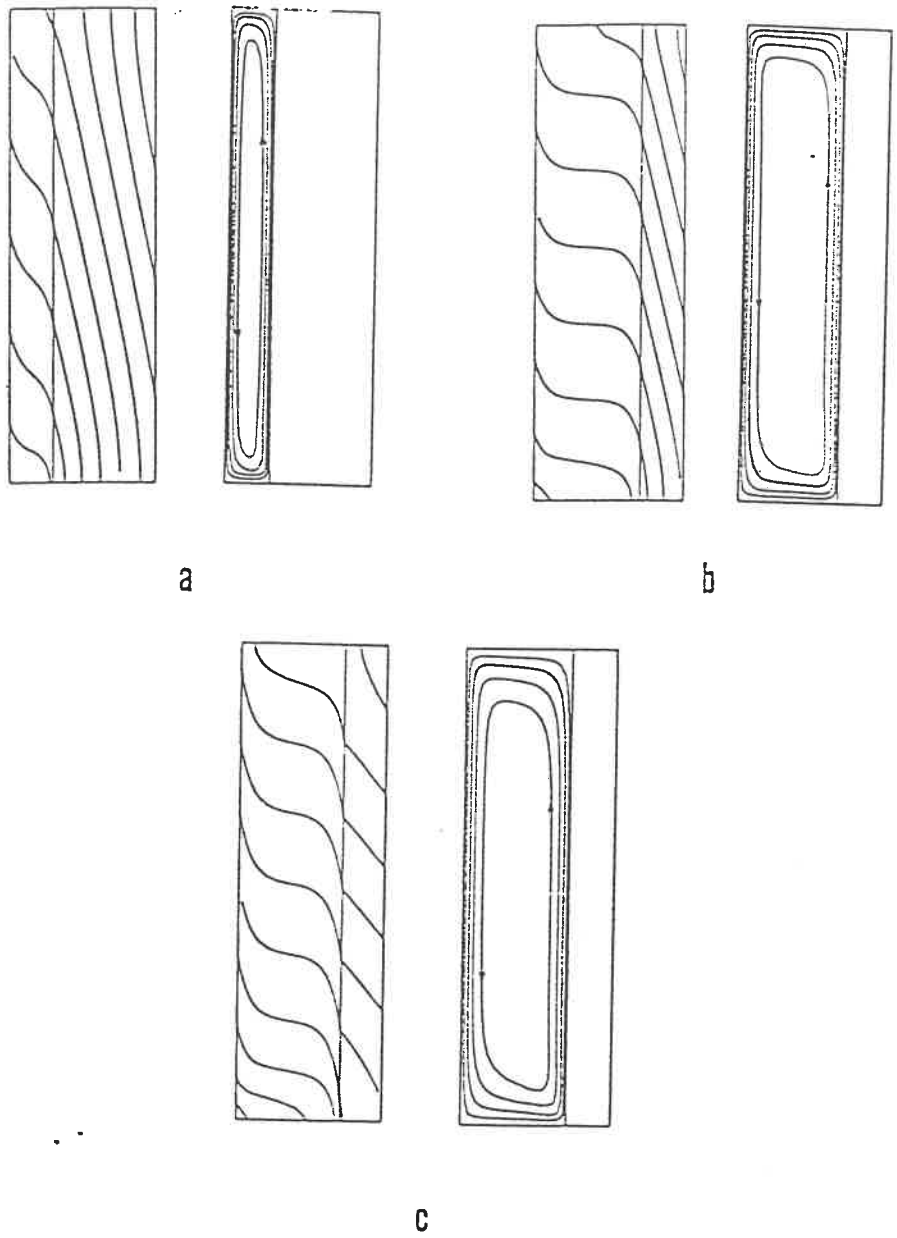

4.8: Isotherms and streamlines for a vertical porous layer borded by a solid slab.

(a) R=800, η=0.3, K^*=1
(b) R=800, η=0.7, K^*=1
(c) R=800, η=0.7, K^*=5

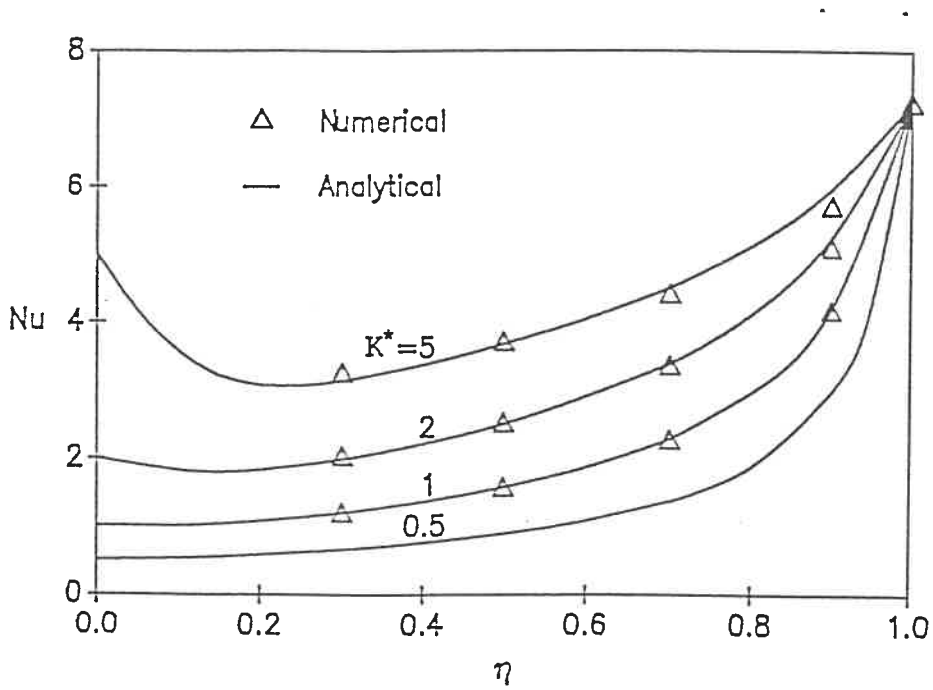

4.9: Heat transfer through a vertical porous layer of extension η borded by a solid slab: effect of K^*, R = 800.

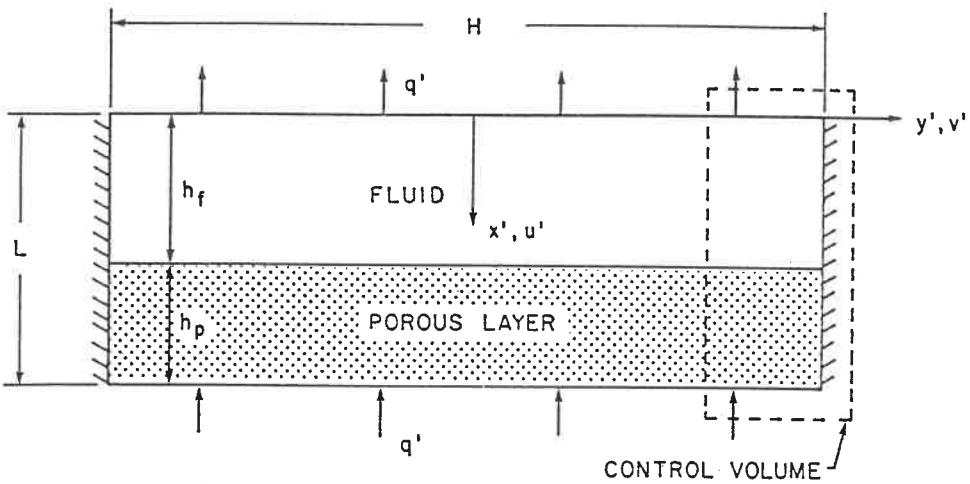

5.1: Physical model and coordinate system.

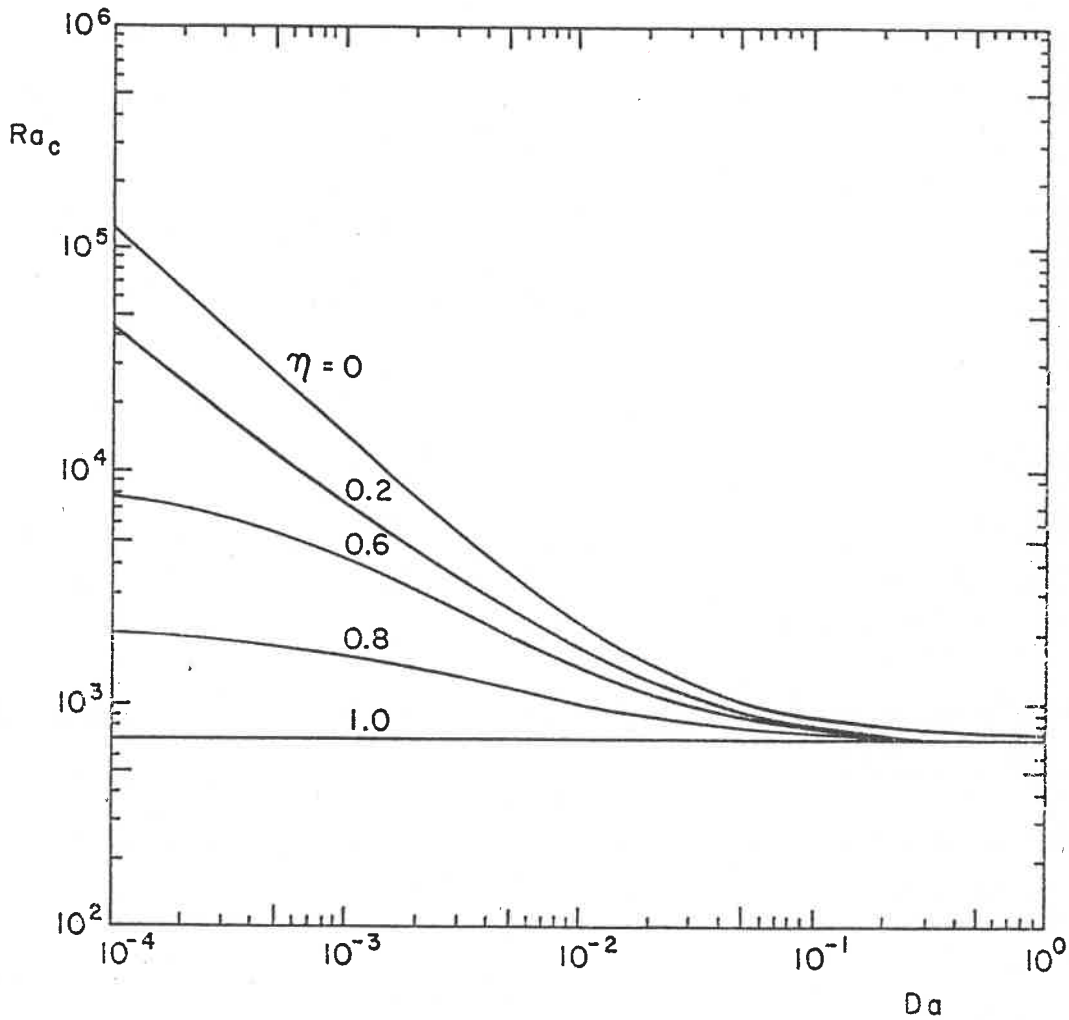

5.2: The effect of Da and η on the critical Rayleigh number Ra_c for a fluid-porous bed system with rigid upper surface ($G = 1$, $\gamma = 1$).

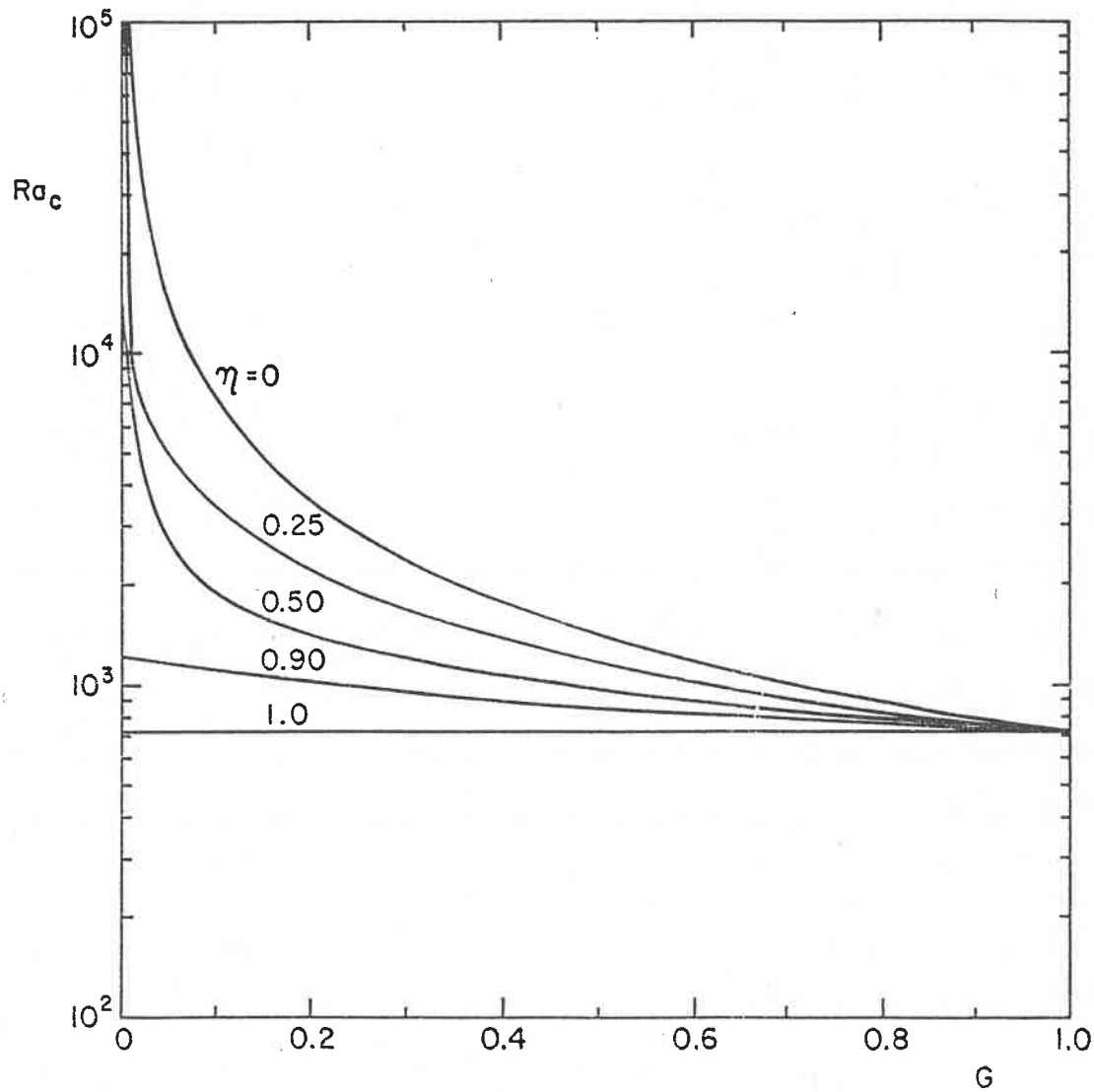

5.3: The effect of G and η on the critical Rayleigh number Ra_c for a fluid-fluid system with rigid upper surface (γ = 1).

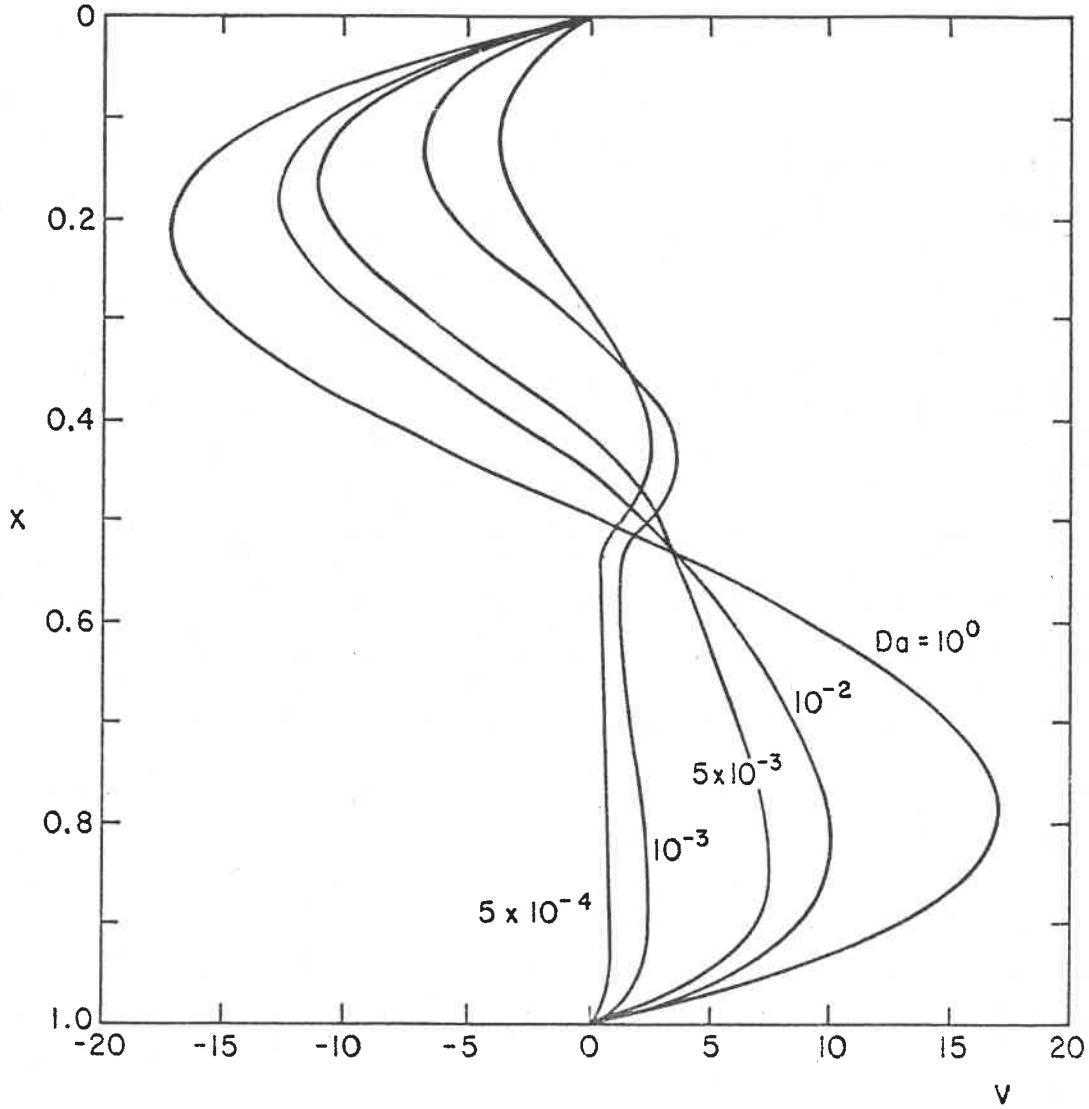

5.4(a): The effect of Da on the temperature distribution for a fluid-porous bed system with rigid upper surface ($G = 1$, $\gamma = 1$, $\eta = 0.5$, $Ra = 10^4$).

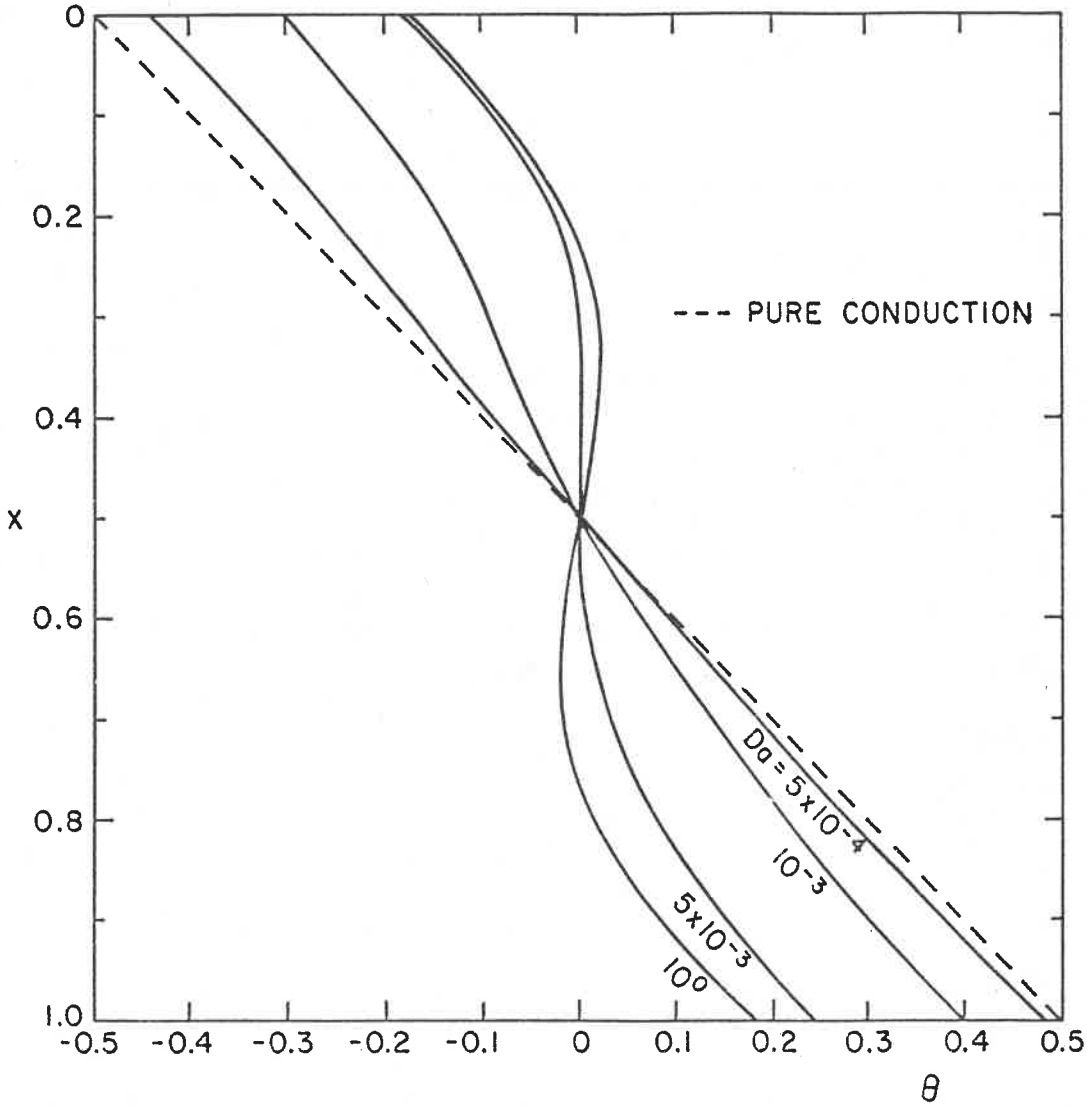

5.4(b): The effect of Da on the temperature distribution for a fluid-porous bed system with rigid upper surface ($G = 1$, $\gamma = 1$, $\eta = 0.5$, $Ra = 10^4$).

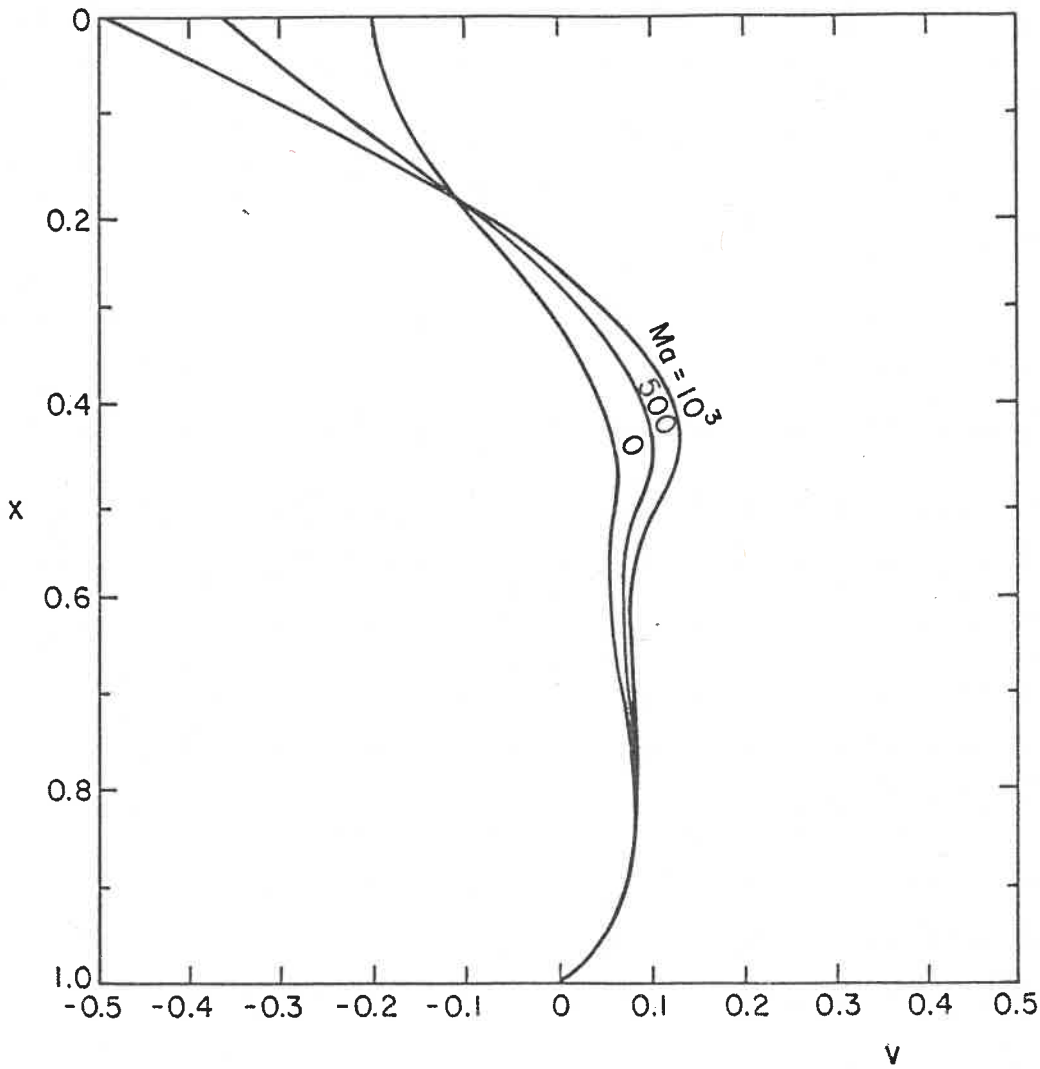

5.5(a): The effect of Ma on the velocity distribution for a fluid-porous bed system with free upper surface ($G = 1$, $\gamma = 1$, $\eta = 0.5$, $Ra = 10^4$).

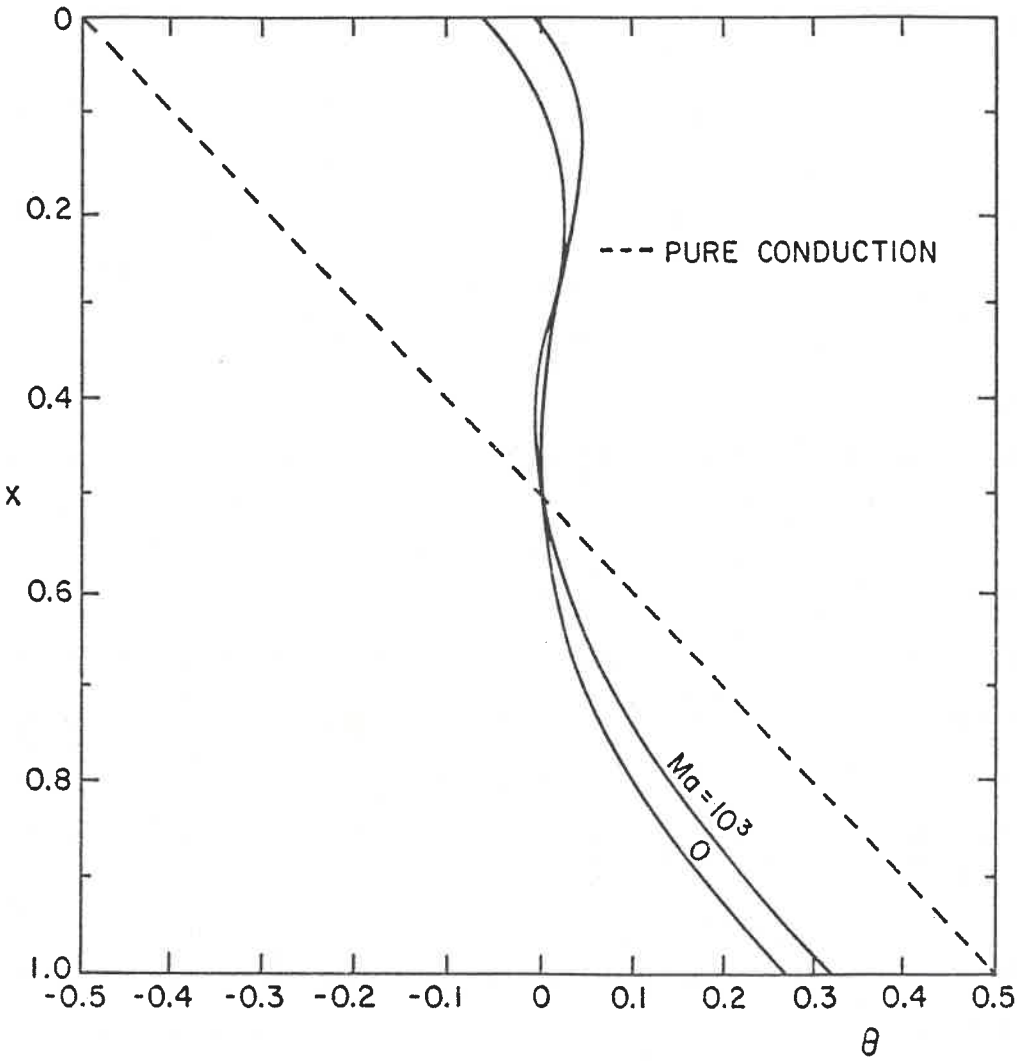

5.5(b): The effect of Ma on the temperature distribution for a fluid-porous bed system with free upper surface (G = 1, γ = 1, η =0.5, Ra = 10^4).

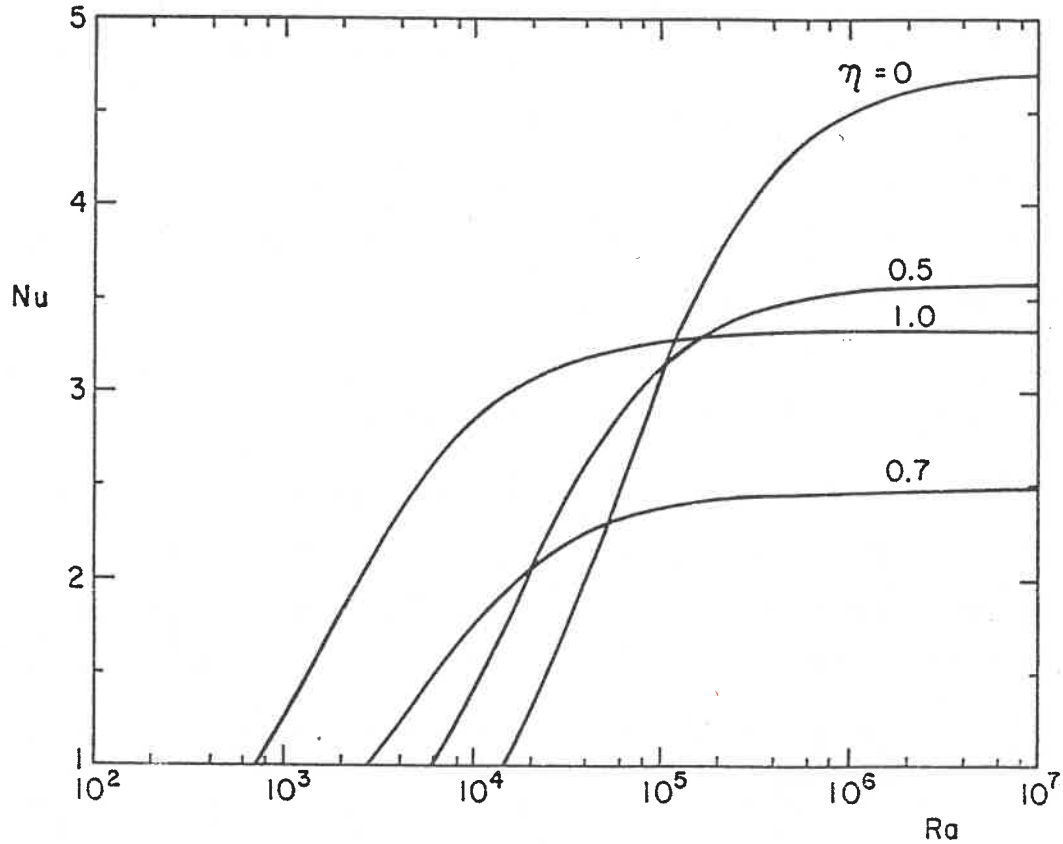

5.6(a): The effect of η and Ra on the Nusselt number for a fluid-porous bed system with rigid upper surface ($G = 1$, $\gamma = 1$, $Da = 10^{-3}$).

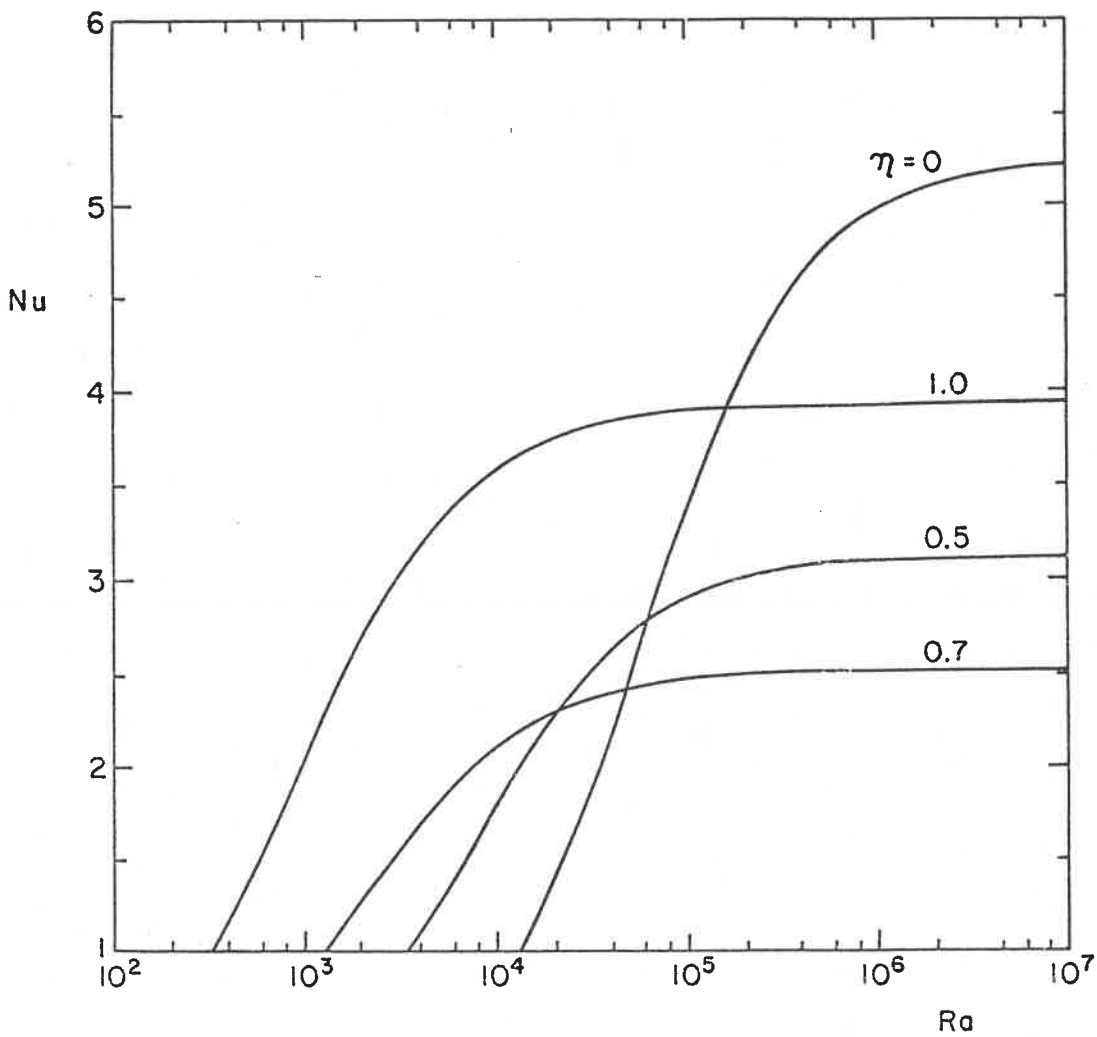

5.6(b): The effect of η and Ra on the Nusselt number for a fluid-porous bed system with free upper surface ($G = 1$, $\gamma = 1$, $Ma = 0$, $Da = 10^{-3}$).

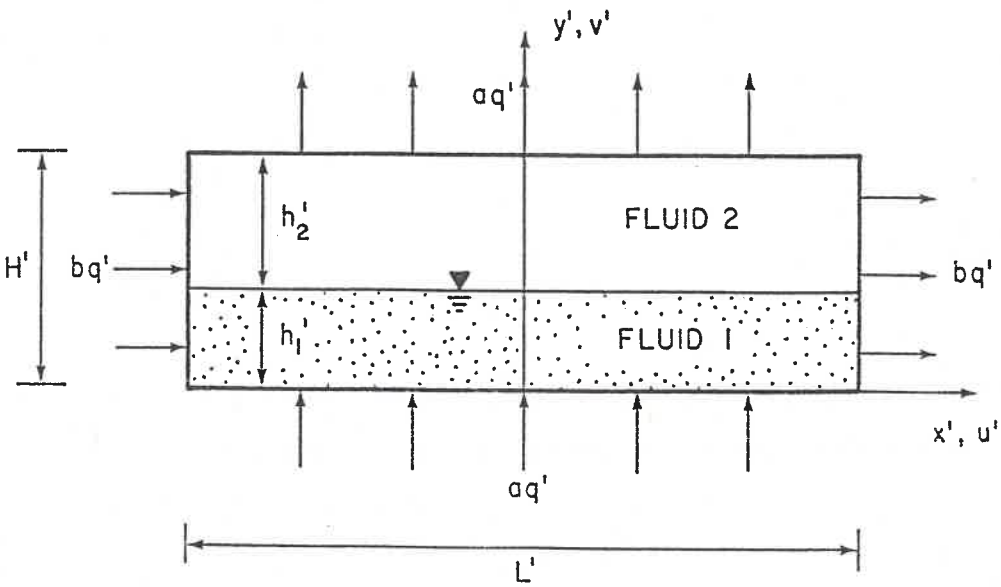

6.1: Schematic representation of two-layer geometry.

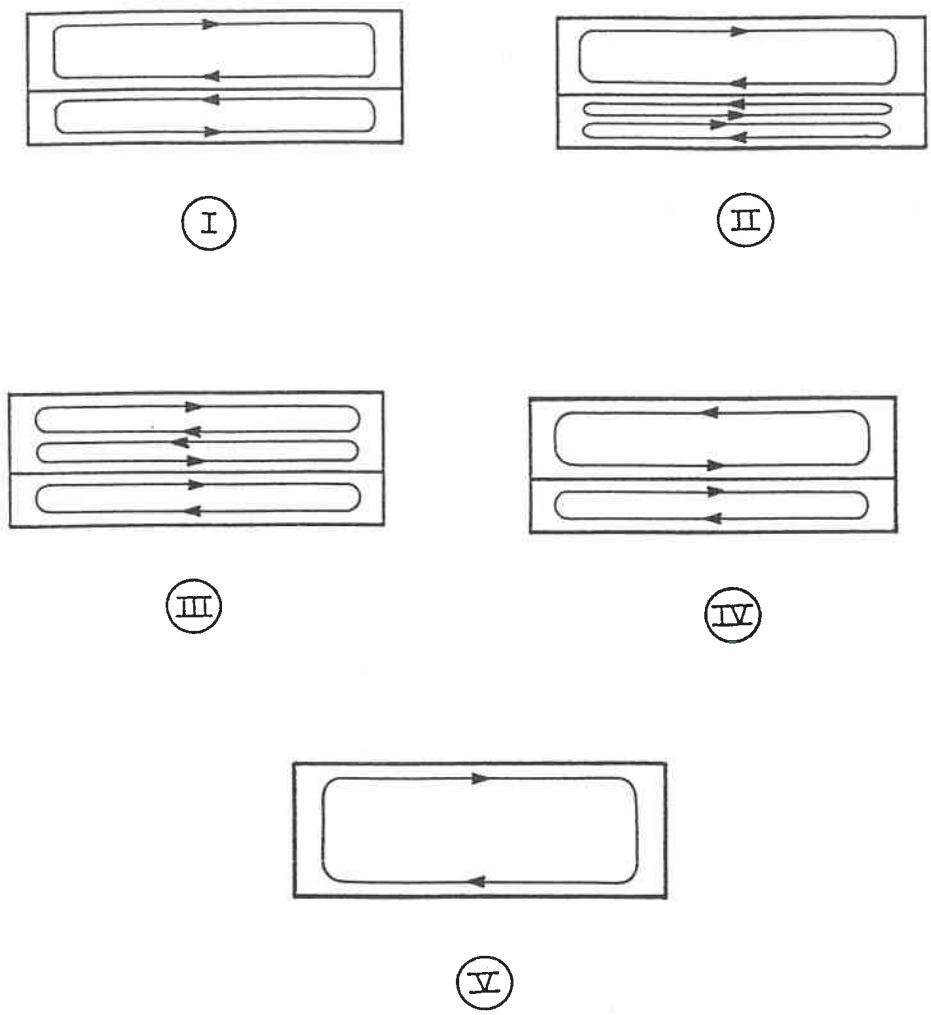

6.2: Flow structures in the two layers.

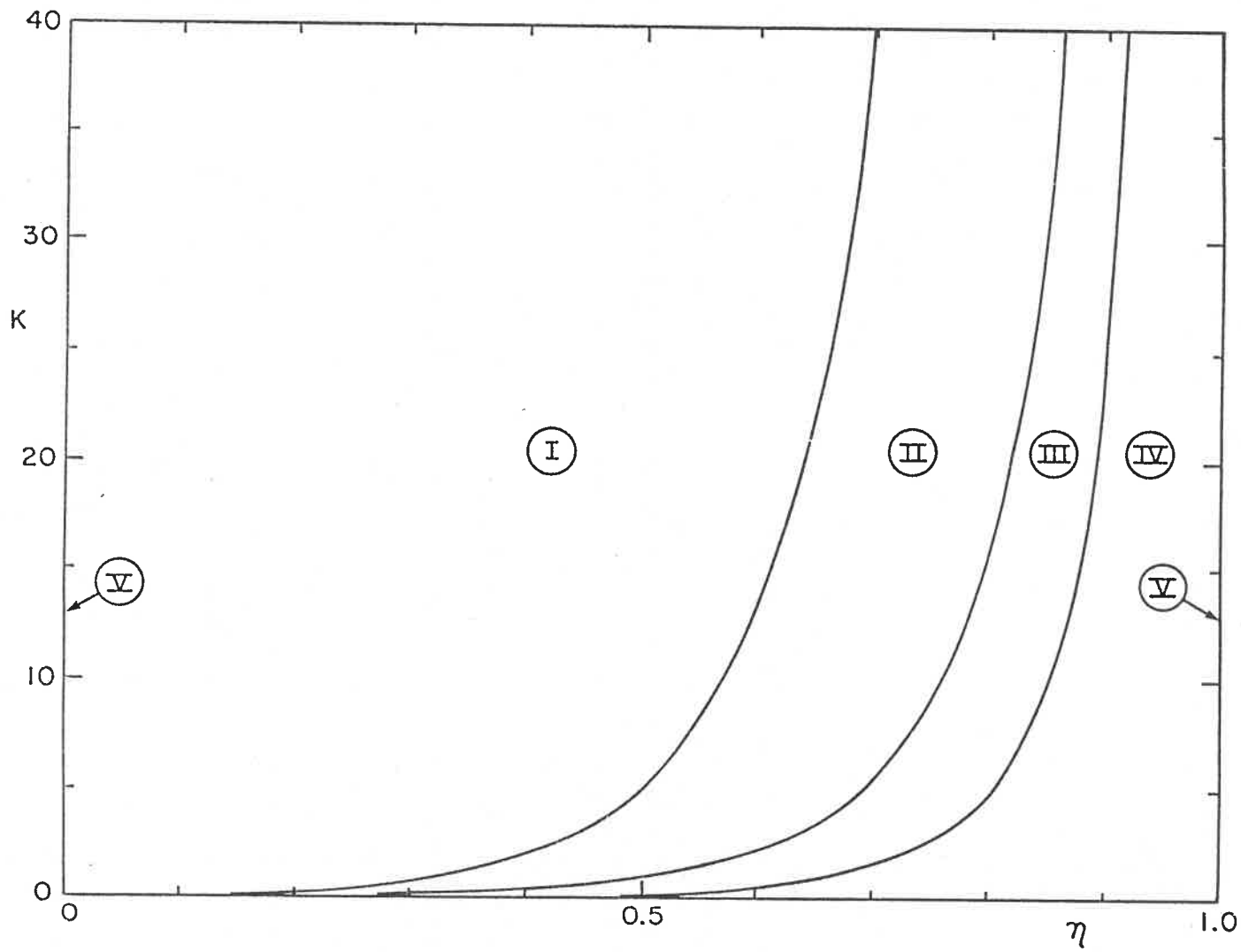

a

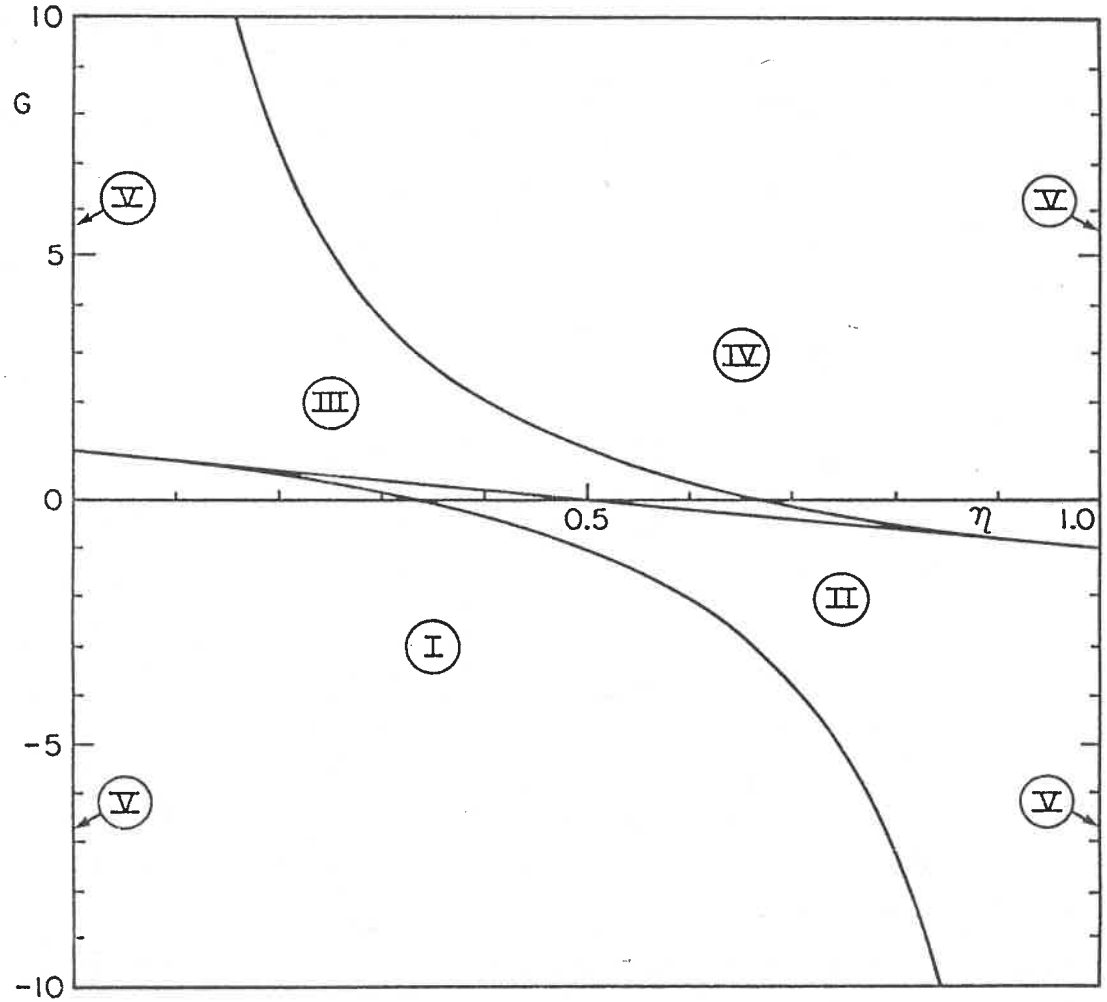

b

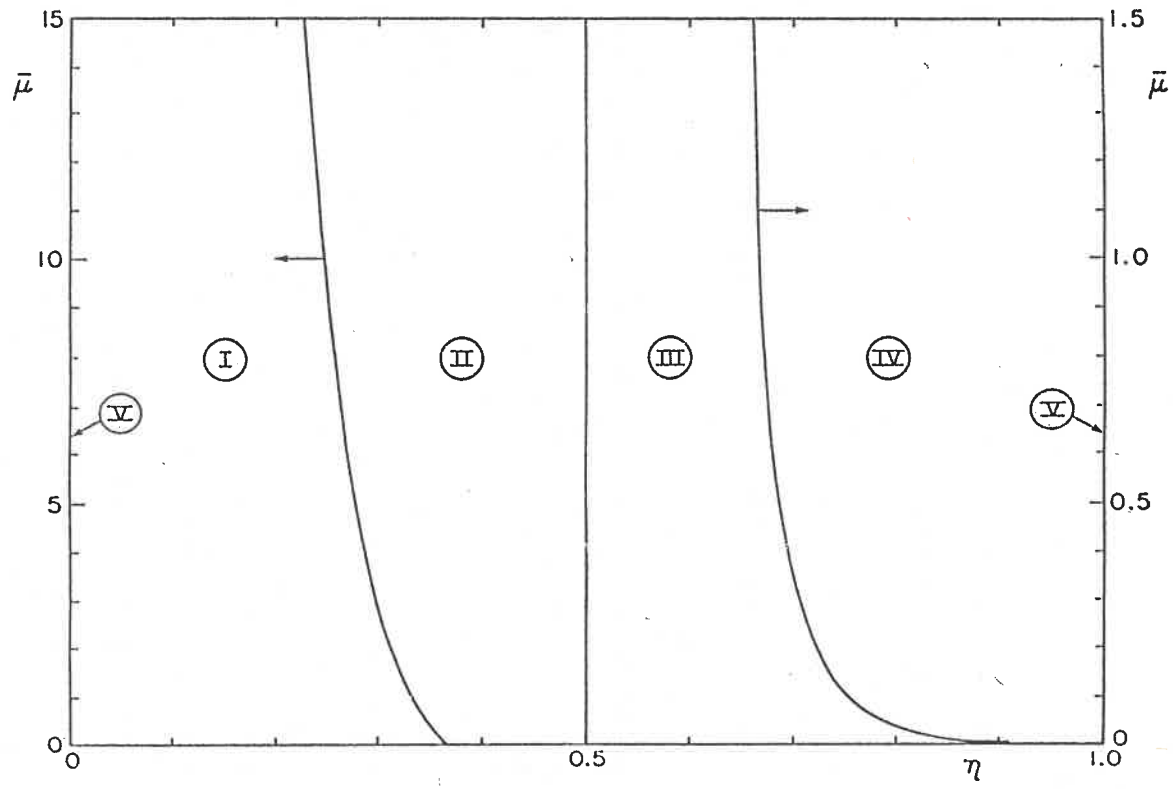

C

6.3: Effect on the flow structures in a two-layer system of (a) K with G = 0, μ = 1; (b) G with K = 1, μ = 1; (c) μ with G = 0, K = 1.

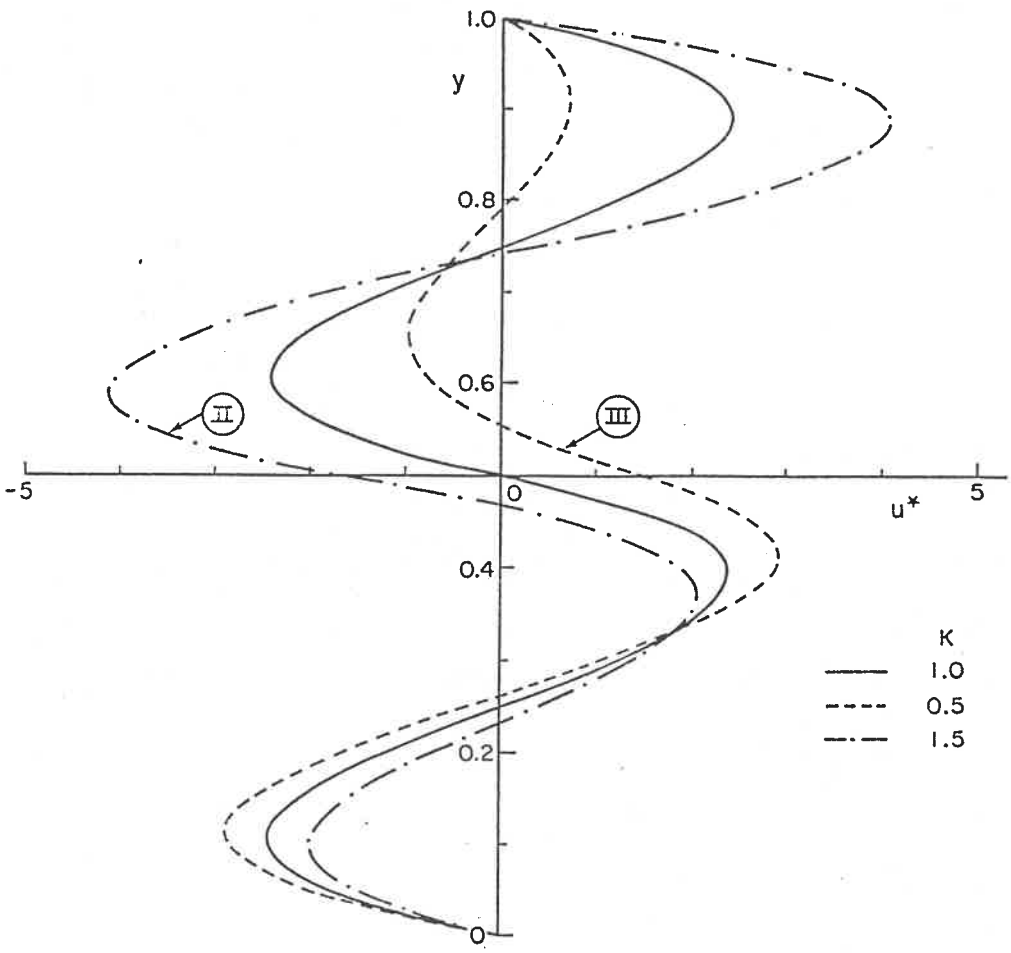

a

5.4: Distribution of horizontal velocity. Effect of (a) K with η = 0.5, μ = 1, G = 0; (b) G with η = 0.5, μ = 1, K = 1; (c) μ with η = 0.5, G = 0, K = 1.

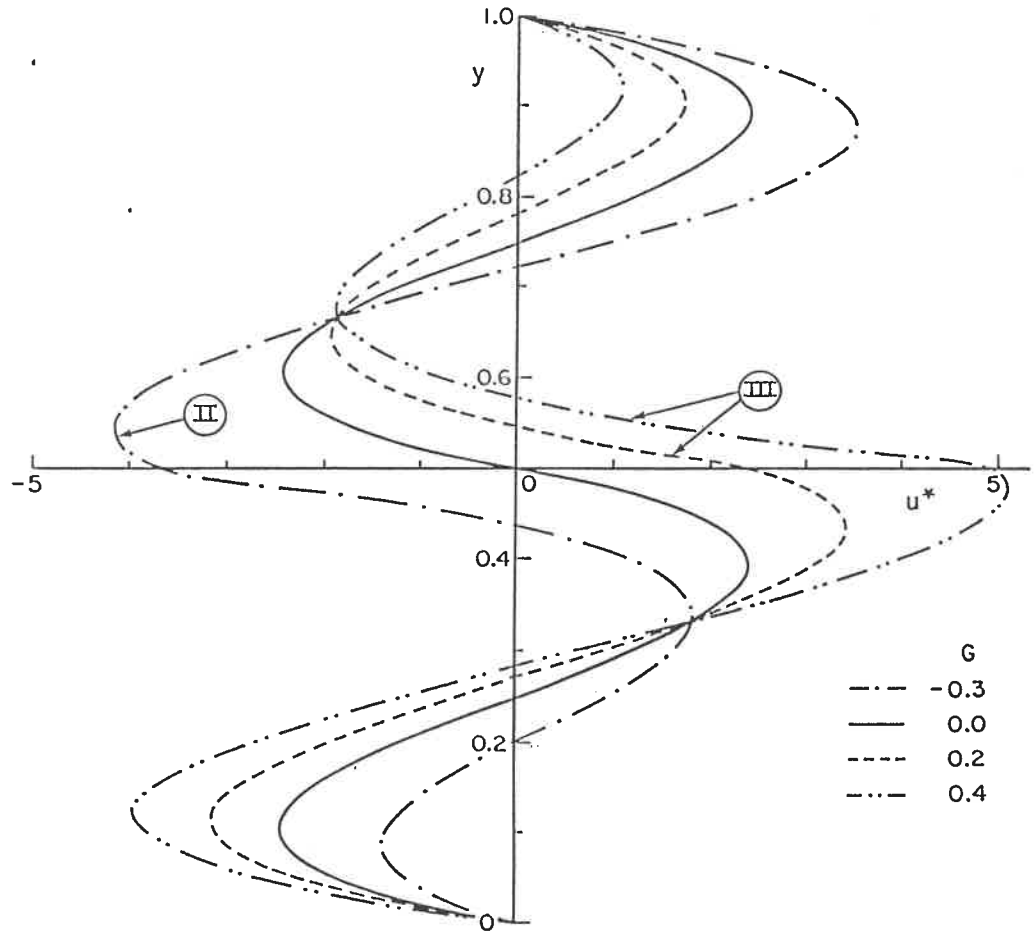

b

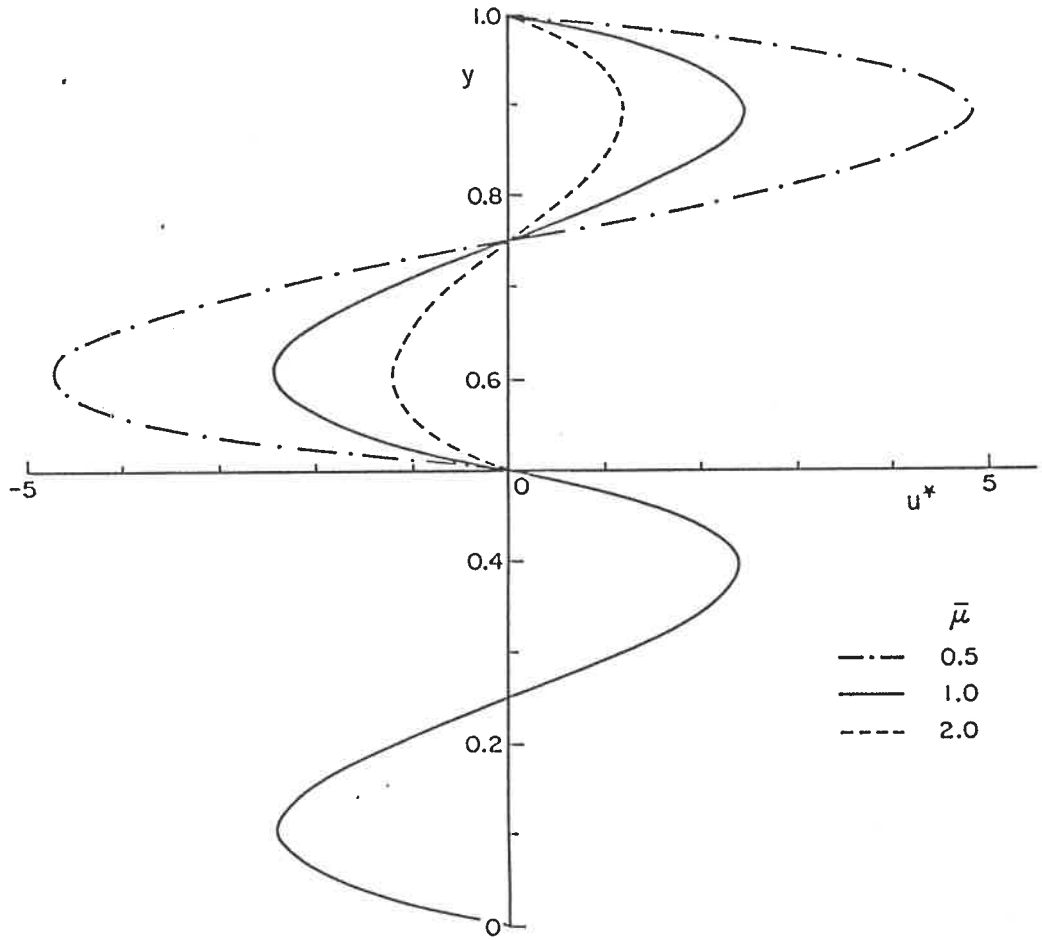

C

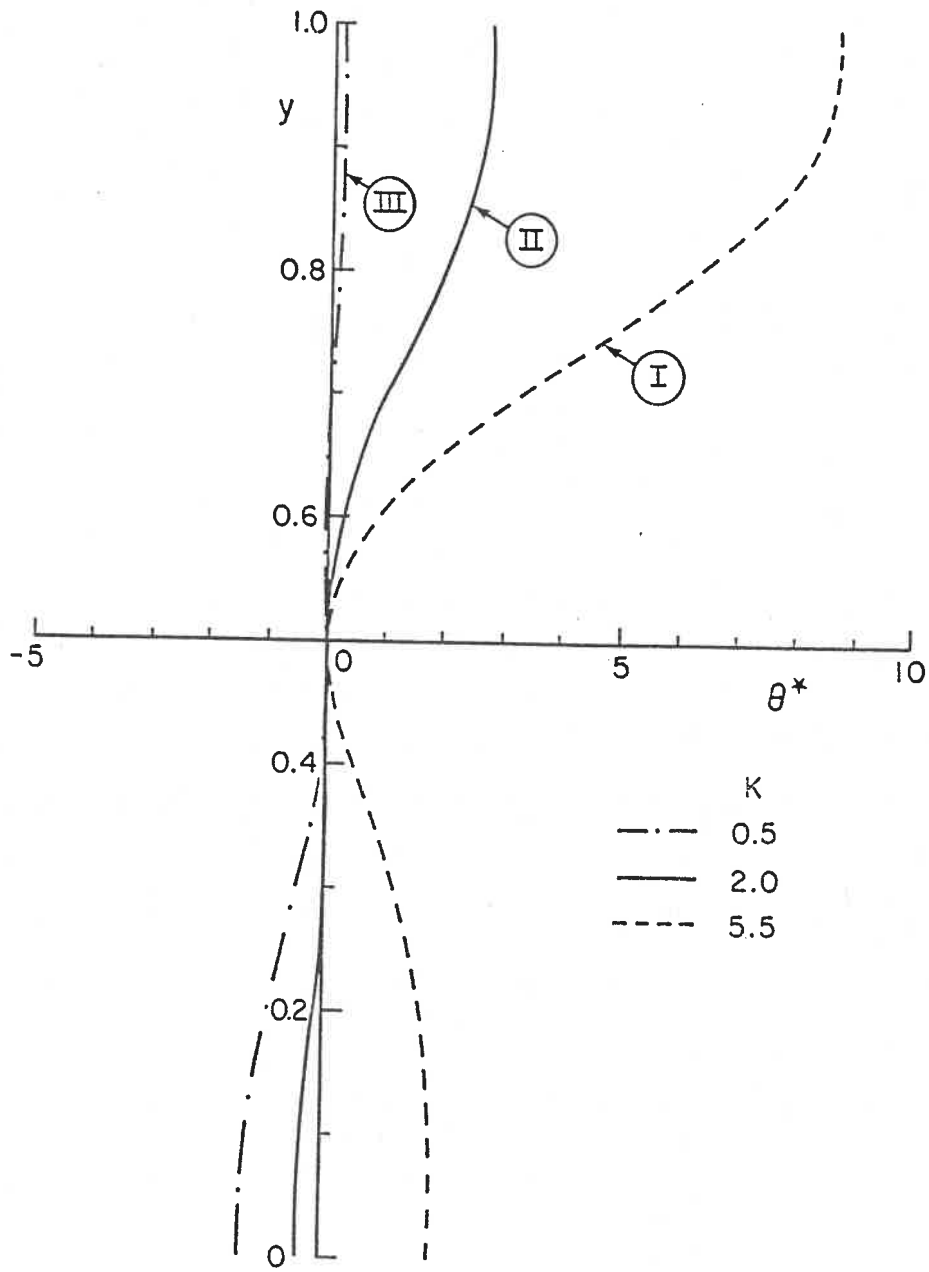

a

6.5: Vertical temperature distributions for a system heated from the side. Effect of (a) K with η = 0.5, G = 0, μ = 1; (b) G with η = 0.5, K = 1, μ = 1; (c) μ with η =0.5, G = 0, K = 1.

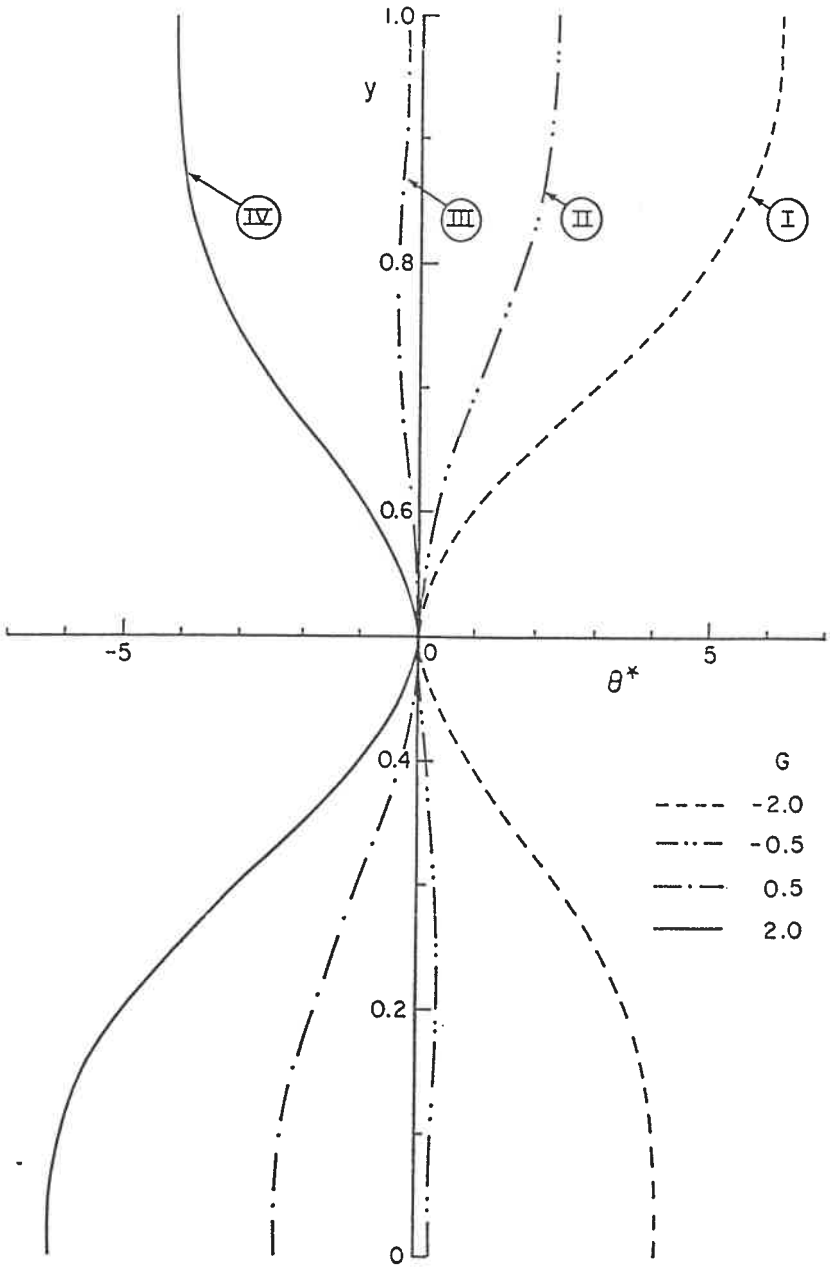

b

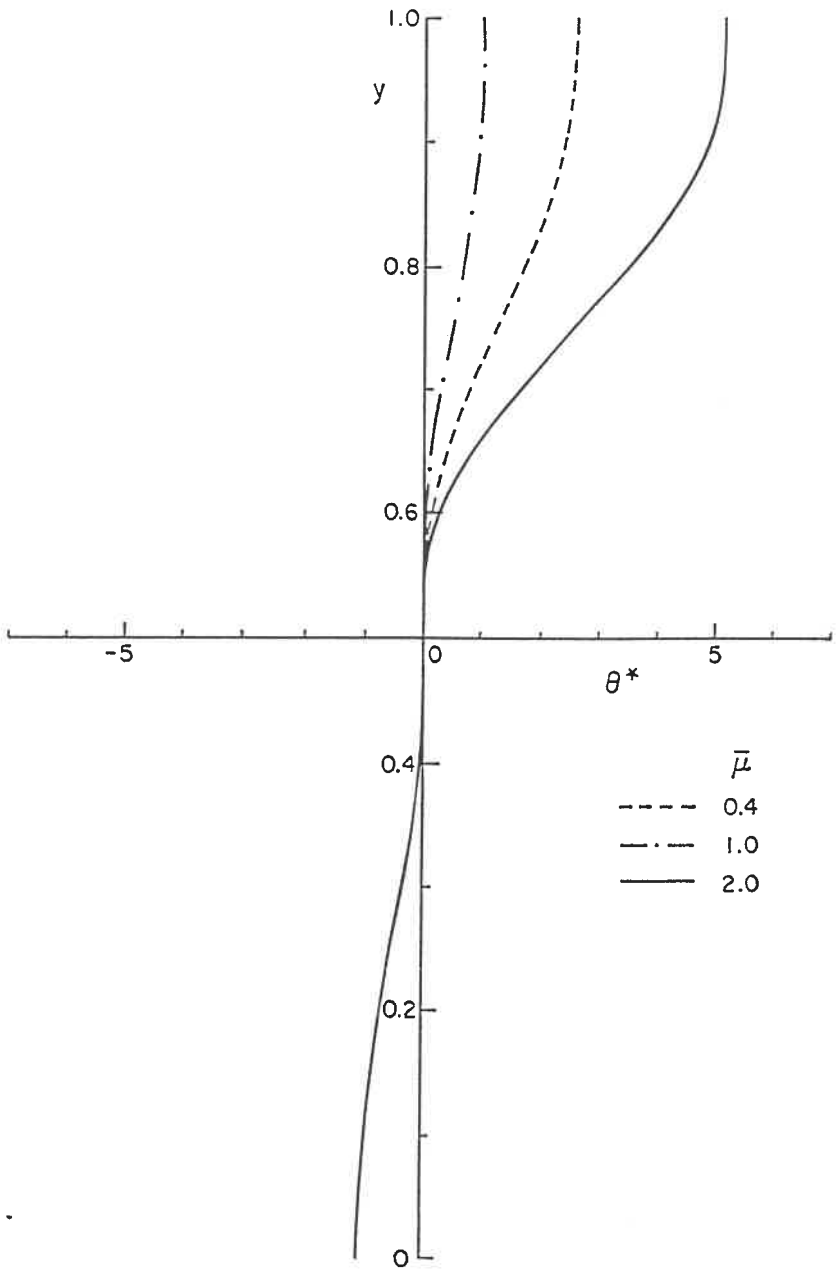

C

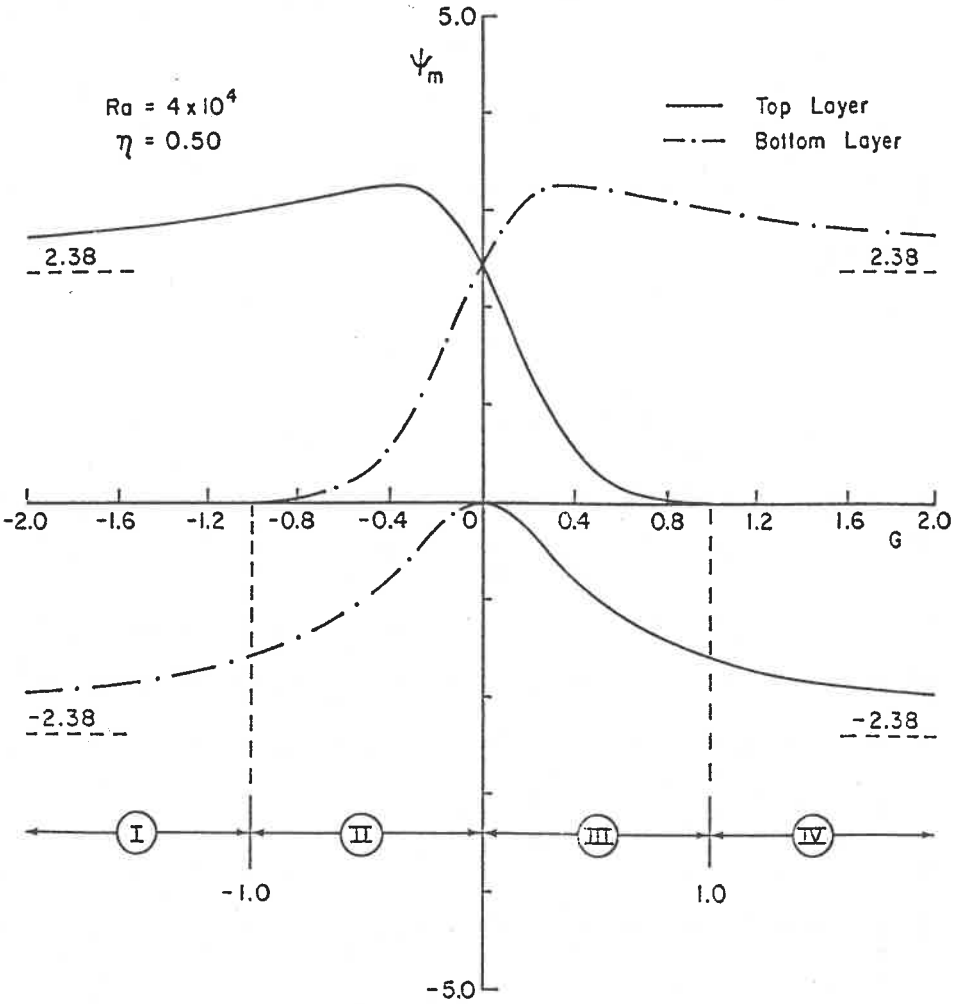

a

6.6: Maximum stream function Ψ_m in each fluid layer for a system heated from the bottom as a function of G with $Ra_1 = 4x10^4$, $\mu = 1$, K = 1 and (a) $\eta = 0.5$; (b) $\eta = 0.45$; (c) $\eta = 0.55$.

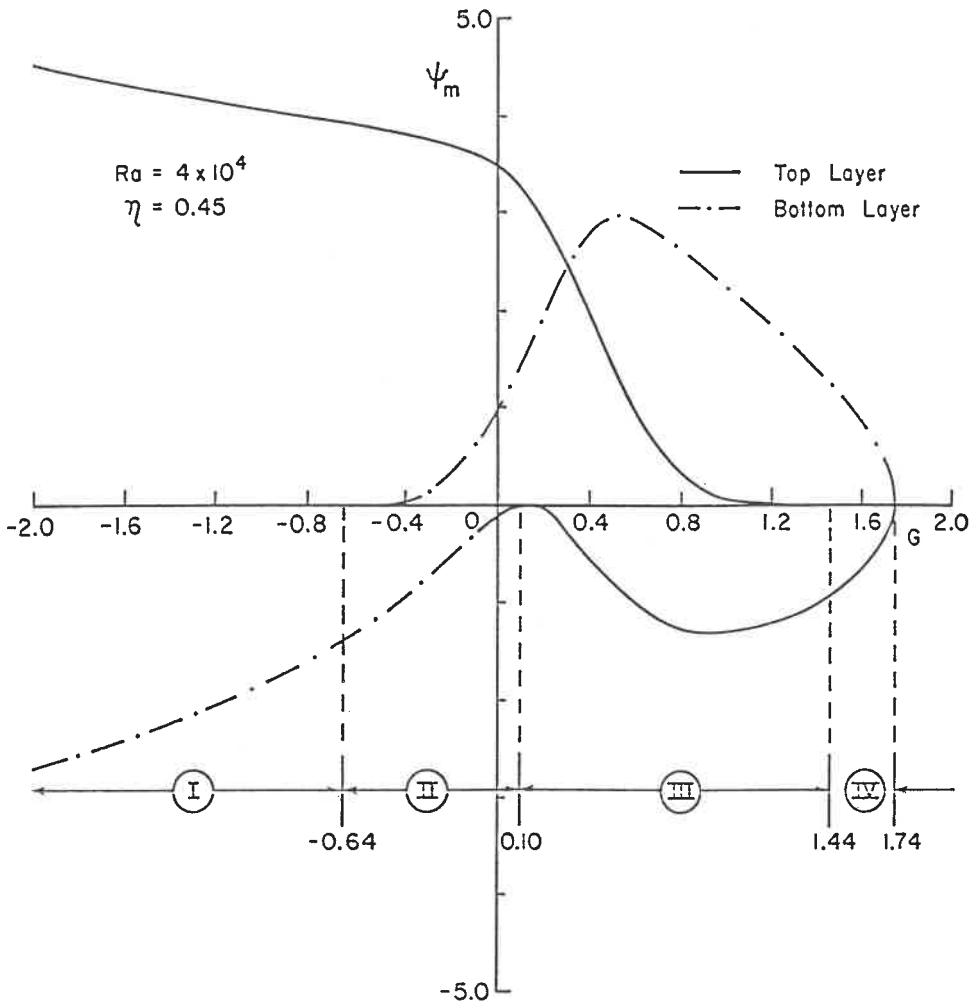
5.0
ψ_m
Ra = 4 x 10^4
η = 0.45
Top Layer
Bottom Layer
-2.0
-1.6
-1.2
-0.8
-0.4
0
0.4
0.8
1.2
1.6
G
2.0
I
II
III
IV
-0.64
0.10
1.44
1.74
-5.0

b

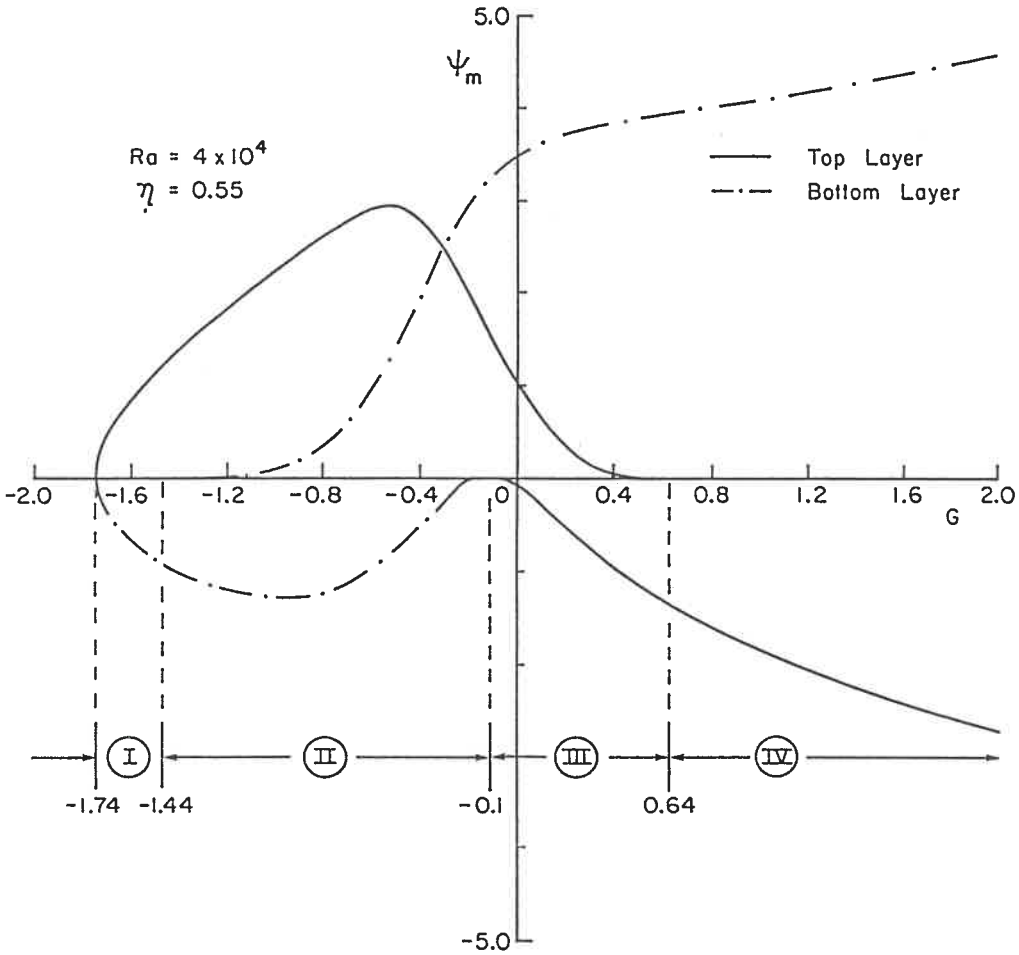
5.0
Ψ_m
Ra = 4 x 10^4
η = 0.55
Top Layer
Bottom Layer
-2.0
-1.6
-1.2
-0.8
-0.4
0
0.4
0.8
1.2
1.6
2.0
G
I
II
III
IV
-1.74
-1.44
-0.1
0.64
-5.0

C

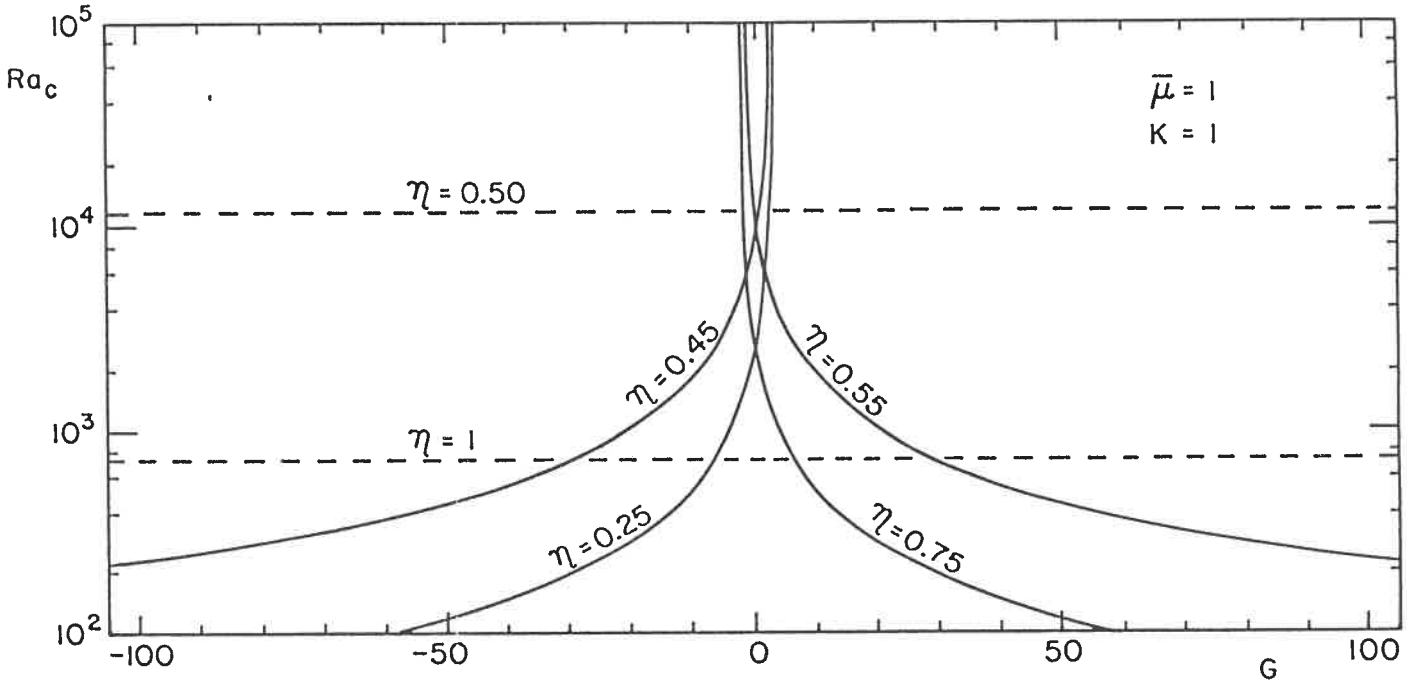

6.7: The effect of G and η on the critical Rayleigh number Ra_c for bottom heating with $\mu = 1$, K = 1.

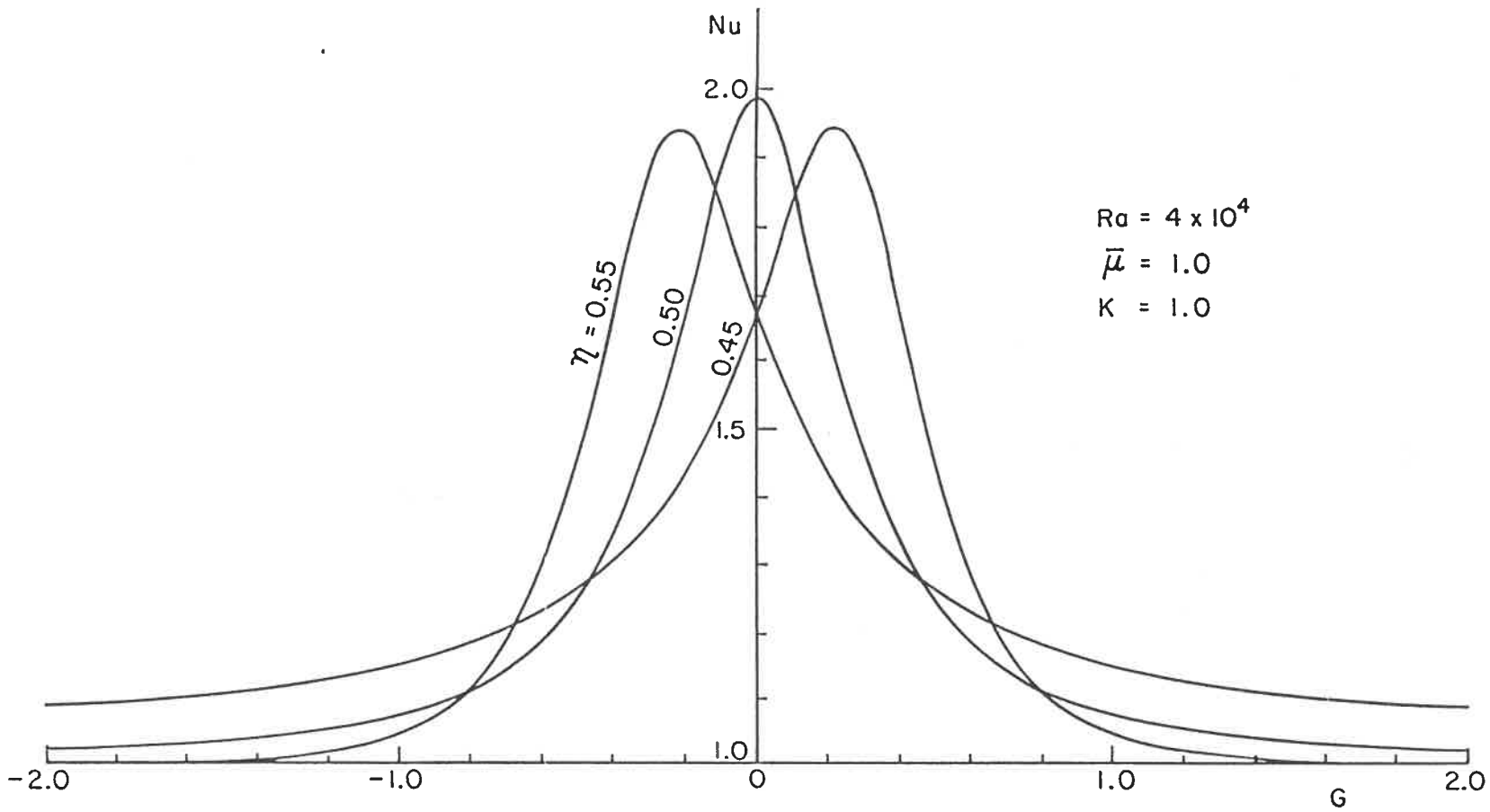

a

6.8: The effect on the Nusselt number Nu for bottom heating with $\mu = 1$, $K = 1$ and (a) $Ra_1 = 4 \times 10^4$; (b) $\eta = 0.5$.

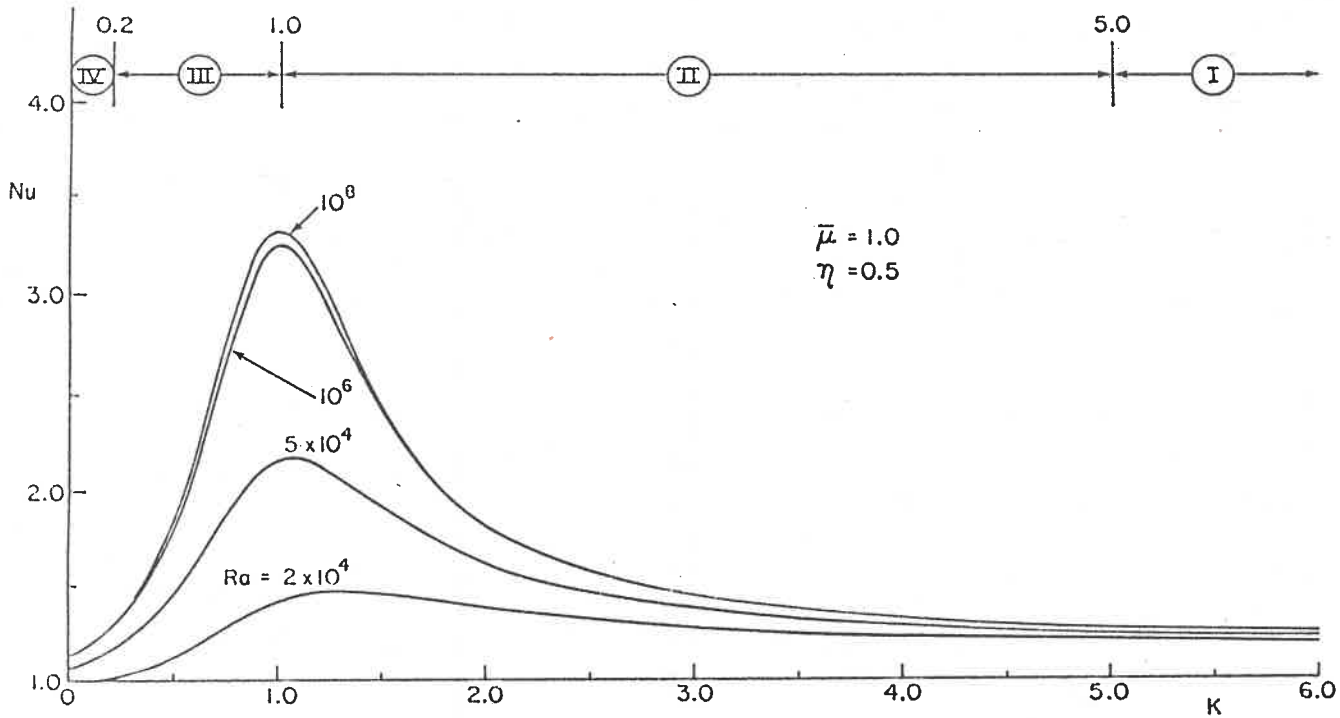
0.2
1.0
5.0
IV
III
II
I
4.0
Nu
3.0
2.0
1.0
10^8
10^6
5×10^4
Ra = 2×10^4
$\bar{\mu}$ = 1.0
η = 0.5
0
1.0
2.0
3.0
4.0
5.0
6.0
K

b

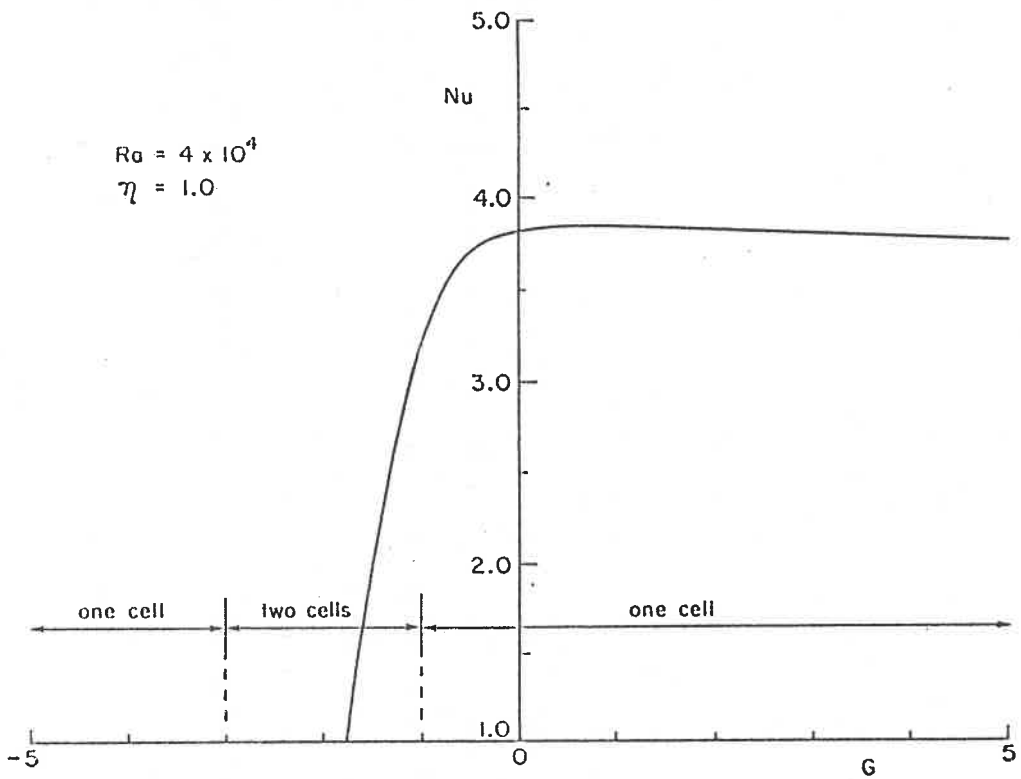

6.9: The effect of G on the Nusselt number Nu for a single layer of fluid with an upper free surface and bottom heating.

	Da = 5 × 10^{-4}		Da = 5 × 10^{-3}		Da = 5 × 10^{-2}	
R	Nu	ψ_c	Nu	ψ_c	Nu	ψ_c
100	3.444 (3.459)	3.595 (3.602)	3.055 (3.003)	3.334 (3.332)	2.148 (2.097)	2.182 (2.155)
200	4.169 (4.228)	5.262 (5.279)	3.707 (3.672)	4.913 (4.906)	2.840 (2.779)	3.393 (3.371)
300	4.482 (4.566)	6.510 (6.539)	2.986 (3.966)	6.092 (6.092)	3.177 (3.116)	4.275 (4.252)

3.1: Analytical and Numerical (in parentheses) Nusselt Number and Streamfunction at Center for a Cavity with a Free Upper Surface and Bottom Heating

	Da = 5 × 10^{-4}		Da = 5 × 10^{-3}		Da = 5 × 10^{-2}	
R	ΔT	ψ_c	ΔT	ψ_c	ΔT	ψ_c
100	0.381 (0.374)	2.618 (2.612)	0.378 (0.380)	2.487 (2.508)	0.414 (0.417)	1.914 (1.925)
200	0.327 (0.316)	3.408 (3.396)	0.323 (0.324)	3.237 (3.272)	0.368 (0.371)	2.545 (2.567)
300	0.296 (0.283)	3.952 (3.936)	0.292 (0.291)	3.748 (3.798)	0.336 (0.339)	2.971 (3.005)

3.2: Analytical and Numerical (in parentheses) Nusselt Number and Streamfunction at Center for a Cavity with a Free Upper Surface and Side Wall Heating

	Da = 5×10^{-4}		Da = 5×10^{-2}	
R	Nu	ψ_c	Nu	ψ_c
100	0.379 (0.373)	2.650 (2.641)	0.397 (0.401)	2.291 (2.306)
300	0.294 (0.281)	3.991 (3.973)	0.309 (0.311)	3.459 (3.156)

3.3: Analytical and Numerical (in parentheses) Temperature Difference and Streamfunction at Center for a Cavity with Both Boundaries Free and Bottom Heating

	Da = 5×10^{-4}		Da = 5×10^{-2}	
R	Nu	ψ_c	Nu	ψ_c
100	3.695 (3.726)	3.702 (3.700)	3.098 (3.016)	3.013 (2.978)
300	4.836 (4.965)	6.677 (6.695)	4.373 (4.292)	5.557 (5.525)

3.4: Analytical and Numerical (in parentheses) Temperature Difference and Streamfunction at Center for a Cavity with Both Boundaries Free and Side Wall Heating

R	Nu	
	Analytical	Numerical
50	1.42	1.41
100	1.81	1.80
200	2.36	2.36
300	2.80	2.79
500	3.44	3.42

4.1: Analytical and Numerical Nusselt number for a vertical layer ($\varphi = 90^0$) with a central partition.

R	Nu	
	Analytical	Numerical
100	1.76	1.74
200	2.73	2.67
300	3.33	3.25
500	4.05	3.95
800	4.61	4.51

4.2: Analytical and Numerical Nusselt number for an horizontal porous layer ($\varphi = 0^0$) with a central partition.

ϕ	Nu	
	Analytical	Numerical
0	3.33	3.25
20	3.61	3.53
40	3.66	3.59
60	3.48	3.43
90	2.80	2.79

4.3: Analytical and Numerical Nusselt number for an inclined porous layer with a central partition, R = 300.

G	Da			
	5×10^{-4}	10^{-3}	10^{-1}	1
0	23,040	23,040	23,040	23,040
0.01	12,793	10,689	7,390	7,351
0.1	9,965	7,060	1,986	1,919
1	8,790	5,906	805	729
2	8,540	5,722	591	504
5	8,231	5,533	398	296
10	8,004	5,418	313	204

5.1: The effect of G and Da on the critical Rayleigh number Ra_c for a fluid-porous bed system with rigid upper surface: $\gamma = 1$, $\eta = 0.5$.

η	0.2		0.4		0.6		0.8	
Da	A	B	A	B	A	B	A	B
5×10^{-4}	703.0	9,028.7	466.3	7,568.7	187.3	2,781.2	85.0	817.1
10^{-3}	432.0	5,022.3	364.2	4,617.6	171.0	2,262.6	81.1	749.9
10^{-2}	115.3	977.6	116.0	894.1	93.7	774.4	61.0	458.2
10^{-1}	57.2	398.0	56.3	382.3	54.5	374.1	49.9	338.1
1	49.0	328.0	48.9	326.3	48.7	325.5	48.2	321.9
10	48.1	320.8	48.1	320.6	48.1	320.6	48.0	320.2
10^2	48.0	320.1	48.0	320.1	48.0	320.1	48.0	320.0

5.2: The effect of Da and η on the critical Rayleigh Ra_c and Marangoni Ma_c numbers for a fluid-porous bed system with free upper surface, $G = \gamma = 1$.

η	0.2		0.4		0.6		0.8	
G	A	B	A	B	A	B	A	B
0.1	159.7	1,942.2	105.8	1,043.8	106.0	974.2	80.3	720.4
0.2	124.7	1,231.8	82.6	747.1	80.6	660.2	71.6	589.6
0.5	77.7	594.5	61.9	479.4	58.5	425.5	57.7	418.1
1	48.0	320.0	48.0	320.0	48.0	320.0	48.0	320.0
2	27.3	166.4	34.3	196.0	39.9	238.6	40.7	254.1
5	11.9	68.2	18.8	91.4	29.5	146.6	34.5	199.0
10	6.1	34.4	10.7	48.4	21.2	91.2	31.0	166.4

5.3: The effect of G and η on the critical Rayleigh Ra_c and Marangoni Ma_c numbers for a fluid-fluid system with free upper surface, $\gamma = 1$.

	|C|	
Ra_1	Side wall heating	Bottom heating
10^3	0.990	-
10^4	0.672	-
1.15×10^4	0.635	0
10^5	0.195	0.267
10^6	0.045	0.089
10^7	0.010	0.028

6.1: The effect of Rayleigh number Ra_1 on axial temperature gradient C, with $\eta = 0.5$, $K = 1$, $G = 0$, $\mu = 1$.

	|C|	
K	Side wall heating	Bottom heating
0	0.304	0.172
0.5	0.352	0.329
1	0.338	0.379
5	0.122	0.140
10	0.075	0.091

6.2: The effect of parameter K on axial temperature gradient C, with $\eta = 0.5$, $G = 0$, $\mu = 1$, $Ra_1 = 10^5$.

	|C|	
G	Side wall heating	Bottom heating
0	0.337	0.379
0.5	0.258	0.240
1	0.189	0.143
5	0.071	0.031
10	0.045	0.015

6.3: The effect of parameter G on axial temperature gradient C, with $\eta = 0.5$, $K = 1$, $\mu = 1$, $Ra_1 = 10^5$.

	|C|	
$\overline{\mu}$	Side wall heating	Bottom heating
0	0	0
0.5	0.258	0.313
1	0.338	0.379
5	0.405	0.348
10	0.408	0.323

6.4: The effect of parameter μ on axial temperature gradient C, with $\eta = 0.5$, $K = 1$, $G = 0$, $\mu = 1$, $Ra_1 = 10^5$.

ÉCOLE POLYTECHNIQUE DE MONTRÉAL
3 9334 00213567 9